CCMS-93-01
VPI-E-93-01

CENTER FOR COMPOSITE MATERIALS AND STRUCTURES

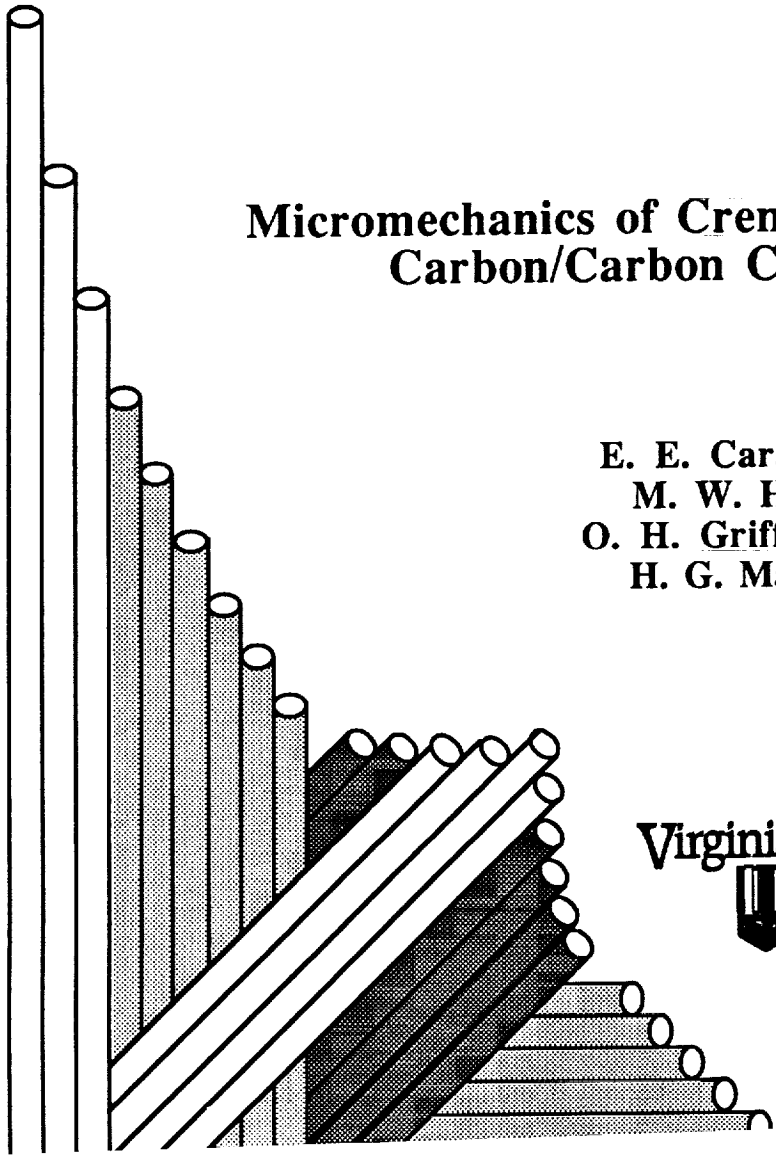

Micromechanics of Crenulated Fibers in Carbon/Carbon Composites

E. E. Carapella
M. W. Hyer
O. H. Griffin, Jr.
H. G. Maahs

Virginia Tech
VIRGINIA POLYTECHNIC INSTITUTE AND STATE UNIVERSITY

BLACKSBURG, VIRGINIA
24061

January 1993

College of Engineering
Virginia Polytechnic Institute and State University
Blacksburg, Virginia 24061

January 1993

CCMS-93-01
VPI-E-93-01

Micromechanics of Crenulated Fibers in Carbon/Carbon Composites

E.E. Carapella[1]
M.W. Hyer[2]
O.H. Griffin, Jr.[3]
H.G. Maahs[4]

Department of Engineering Science and Mechanics

NASA Grant NAG-1-343

Interim Report 92

The NASA-Virginia Tech Composites Program

Prepared for: Applied Materials Branch
National Aeronautics and Space Administration
Langley Research Center
Hampton, VA 23681-0001

---

1. Graduate Student, Department of Engineering Science and Mechanics, Virginia Polytechnic Institute and State University
2. Professor, Department of Engineering Science and Mechanics, Virginia Polytechnic Institute and State University
3. Associate Professor, Department of Engineering Science and Mechanics, Virginia Polytechnic Institute and State University
4. Head, Applied Materials Branch, NASA Langley Research Center, Hampton, VA

Abstract

The influence of crenulated noncircular fibers on the micromechanical stress states due to a transverse strain and to a temperature change in carbon/carbon composites is examined using the finite element method. Stresses at the interface of both fully bonded and fully disbonded fibers having two crenulation amplitudes and with two fiber volume fractions are presented. In each case, these interface stresses are compared to stresses at the interface of circular fibers which have the same degree of disbond and fiber volume fraction and are under the same loading conditions. For the disbonded cases, deformed meshes showing locations of fiber/matrix contact are also included. In addition to the interface stress states, selected composite properties are also computed and compared in each case examined. Interest in studying noncircular fibers stems from a desire to increase the transverse properties of carbon/carbon by introducing a mechanical interlocking between the fiber and the matrix. Results presented here indicate that this interlocking does in fact occur. Evidence from the interface stress data suggests, however, that any possible advantage of this interlocking may be outweighed by the disadvantage of stress concentrations which arise at the interface due to the crenulated geometry of the fibers.

Acknowledgments

This study was supported by the Applied Materials Branch of the NASA-Langley Research Center through the NASA-Virginia Tech Composites Program under Grant NAG 1-343. This financial support has been greatly appreciated.

Table of Contents

List of Illustrations

List of Tables

1.0 Introduction and Literature Review

1.1 Introduction

Since their development began in the late 1950's, carbon-carbon composites have become increasingly important in a wide variety of applications. Properties which include low density, good retention of mechanical properties at high temperatures (>1600 ^{o}C), good frictional characteristics, and low coefficient of thermal expansion have made carbon-carbon materials excellent candidates for many applications, particularly in the aerospace industry. Currently, carbon-carbon materials are being used for aircraft brakes, rocket nozzles and throats, missile nose cones, turbine engine components, and spacecraft radiators and thermal shields such as the wing leading edges of the space shuttle vehicles. Certain undesirable properties have limited the use of carbon-carbon composites in other applications, however, and much research is directed toward improving these properties. Among the disadvantages are rapid oxidation at temperatures above 370 ^{o}C, low strain to failure, poor fiber/matrix bonding, and low strength perpendicular to the direction of the fiber reinforcement. Processing drawbacks are also a factor, including high cost, long fabrication times, and inadequate reproducibility.

The work presented here focuses on the problem of low transverse strength in carbon-carbon composites. The use of noncircular fibers, which provide an increased surface area for fiber/matrix bonding, may help to improve this low transverse strength. More importantly, a mechanical interference between the fiber and matrix is possible with the use of noncircular fibers. This type of physical interlocking could serve to increase transverse composite properties. The objective of this research is to investigate the effect of noncircular fibers on the stress states in carbon-carbon composites. Stresses are determined on the micromechanics level using finite element analysis. Two loading conditions will be discussed, cooling of the composite by $1^{o}F$, and the application of a uniform transverse tensile strain of 1000 μin/in. As stated, the strength of fiber/matrix bonding in carbon-carbon is low. Here both fully bonded fiber and matrix and fully disbonded fiber and matrix cases are considered. By fully disbonded it is meant that the fiber is disbonded from the matrix at all circumferential locations around the fiber. The results of the fully bonded and fully disbonded cases are believed to bracket the stress states in an actual carbon-carbon composite, where the bonding that exists is somewhere between fully bonded and fully disbonded.

The fully disbonded case will be considered from two viewpoints. First, as an extreme case, if the disbond results in a large gap between the fiber and matrix, the matrix behaves as if there is no fiber present whatsoever. This no-fiber case will be considered in this work. The second case, and the one of interest, is the existence of a gap that, despite being fully disbonded, is small enough that when the carbon-carbon is loaded, the fiber and matrix contact at locations determined by the size of the gap, the geometry of the fiber, and the direction of the loading.

Noncircular pitch-based carbon fibers have been made in a variety of shapes by meltspinning and extrusion through a noncircular spinnerette. The particular noncircular fiber

geometry chosen for this analysis is the crenulated fiber shown in Figure 1. To model the crenulation the fiber outer radius is assumed to be described by a cosine function. With this assumption, the frequency and depth of the fiber crenulation can be easily changed. The crenulated fiber is also close enough in geometry to a circular fiber that comparison of stress states around these two geometries may be carried out. In this study such comparisons will be made. In addition, a crenulated fiber is symmetric about both the x and the y axes, a factor which allows for simplification in analysis.

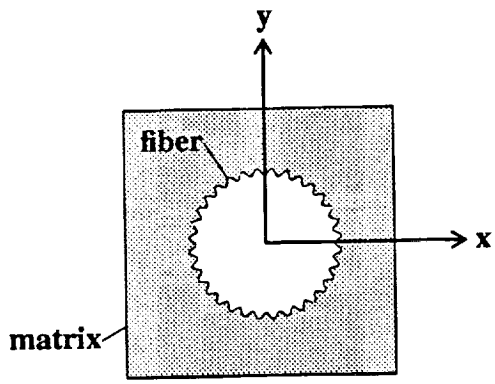

Figure 1. Cross Section of Crenulated Fiber and Surrounding Matrix

In Chapter 2 an overview of the factors involved in modeling the crenulated geometry will be presented. A discussion of features which are common to the modeling of both loading conditions and the varying degrees of fiber/matrix disbond that will be considered is also given. In Chapter 3 the thermally induced stress state around a perfectly bonded crenulated fiber will be presented and compared to the stress state around a similarly loaded circular fiber. This comparison will also be made for the case of transverse tensile loading of the perfectly bonded crenulated fiber in Chapter 4. Analysis of fully disbonded noncircular fibers under transverse tension is presented in Chapters 5 and 6. Chapter 5 contains results for the aforementioned case of disbonding to the point of no interference between the fiber

and the matrix. This situation is considered by modeling the matrix alone containing a void in the shape of the crenulated fiber. In Chapter 6 disbonds which result in gaps between the fiber and matrix that are small enough to allow interference to occur between the two materials when transverse tensile strains are applied are analyzed. Two gap magnitudes are considered. In each of the above analyses (Chapters 3-6) the effect on the stress states of several crenulation amplitudes and fiber volume fractions are considered and compared. Conclusions regarding the effect of the noncircular fibers on the micromechanical stress states in carbon-carbon will be presented in Chapter 7, along with recommendations for future work.

1.2 Literature Review

1.2.1 Noncircular Fibers

Noncircular synthetic fibers which are melt spun from polymers such as nylon and polyester have been produced commercially for over twenty-five years. The first report of noncircular carbon fibers, however, was that of Harrison, Fain, and Edie (1986). In this work pitch based carbon fibers, which are also melt spun, were made into C-shaped and hollow circular fibers by altering the geometry of the spinnerette through which the melt was extruded. Due to the extrusion process, these fibers were found to contain preferential alignment of the aromatic carbon rings which resulted in a higher tensile strength than similarly manufactured solid circular fibers. However, these noncircular fibers had larger cross sections and lower moduli than the circular carbon fibers.

In the same year, Edie et. al. (1986) produced trilobal shaped fibers by the melt-spinning

process and subjected these to single filament testing. These fibers were determined to have both higher strength and higher modulus than comparable circular fibers. It was deduced that the increased surface area of the noncircular fibers could increase wetting of the fiber and therefore fiber/matrix bonding. In addition, octolobal-shaped fibers were also successfully produced, and it was stated that nearly any shaped fiber could be similarly made.

Manocha, Bahl, and Singh (1989) compared performance of carbon-carbon composites containing irregularly shaped fibers produced from a rayon precursor, and bean-shaped and circular fibers produced form a PAN precursor. They found the morphology of the fiber surface greatly influenced the microstructure of the matrix surrounding it in the composite. The irregularly shaped fibers led to better fiber/matrix adhesion than the smoother bean shaped and circular fibers but the sharp corners of the irregularly shaped fibers caused kinking in the graphitic layers of the matrix which surrounds the fiber. This led to high stress concentrations in the matrix.

Several papers presented at the International Symposium on the Development of Carbon Fibers and Their Applications in Seoul, Korea in March of 1990 discussed possible advantages of noncircular fibers. Rhee (1990) produced C-shaped and hollow carbon fibers by melt spinning a coal-tar pitch and found them to possess higher moduli than circular fibers. The noncircular fibers were also determined to have a higher flexible strength than the circular fibers which facilitates processing. In two papers, Edie et. al. (1990) and Stoner, Edie, and Kennedy (1990) determined that trilobal and circular fibers of the same cross sectional area could be produced with comparative ease but the trilobal shaped fibers had a tensile strength which was about 27% higher than that of the circular fibers. Trilobal fibers of larger cross sections could also be produced at an increased rate of spinning. This

could lower production costs. These larger fibers still maintained stiffness comparable to the smaller circular fibers.

As shown, much work has been published on the manufacture and testing of noncircular fibers with focuses on their tensile strength, moduli, and processibility. No work has been published on the particular fiber geometry chosen for this analysis, however, and little information is available on the actual effect noncircular fiber shapes have on the micromechanical stress states in composite materials. This work will present such a detailed analysis.

1.2.2 Micromechanical Modeling

A vast array of literature is available on micromechanical modeling. A number of papers which deal with the determination of transverse properties or stresses in continuous fiber reinforced composites are briefly reviewed here. One of the early papers on micromechanics which considered the transverse strength of a composite material is that of Adams and Doner (1967). In this work a rectangular array of elastic fibers in an elastic matrix subjected to a transverse normal stress was analyzed. A condition of plane strain was assumed, and solutions to stress-displacement and equilibrium equations were found using a finite-difference method. Maximum normal stresses around elliptical fibers of two axes ratios were also presented and compared to those around a circular fiber.

Adams and Crane (1984) presented an analysis which used finite element methods to determine stresses and strains on the fiber/matrix level. A square packed array of transversely isotropic fibers in a fully isotropic matrix and generalized plane strain conditions

were assumed. The method was able to compute fiber and matrix stress fields due to a temperature or moisture change and due to a mechanical loading. Correlation with experimental measurements was found to be reasonable.

Chamis (1987) devised a set of simple theoretical equations for the prediction of stresses in the fiber, matrix, and at the interface of a three-dimensional composite based on known ply level stresses. The equations were derived from elementary mechanics of materials theory and could be used to predict stresses due to longitudinal or transverse loads, as well as temperature and moisture changes.

Aboudi (1989) devised a method of predicting behavior of a composite from known fiber and matrix material properties by application of continuity of displacements and tractions and equilibrium equations to basic repeating cell units in the composite. In this analysis, fibers were assumed to be have square cross sections. This method was used to predict effective moduli, coefficients of thermal expansion, strength, and fatigue failure for composites in general, as well as effective creep and relaxation functions of viscoelastic composites, and yield surfaces of metal matrix composites.

Bowles (1990) used finite element analysis and the closed form composite cylinder model to determine thermally induced stress fields in the fiber and matrix of a carbon fiber/epoxy composite. Matrix stresses were shown to increase with increasing fiber volume fraction and increasing ply angle in multidirectional laminates. Failure of the matrix due to thermal stresses was predicted based on maximum normal interface stresses and was found to correlate well with experimental data.

A number of works have also been published on the modeling of imperfect bonding

between the fiber and matrix on a micromechanics level. For example, Adams (1987) used a two-dimensional finite element analysis to predict micromechanical response of a composite to transverse tensile loading. The element mesh used included an interface zone. The strength of this zone could be varied to model varying degrees of bonding. By changing the interface strength and comparing finite element results to experimental transverse strength measurements, an idea of the level of disbond in an actual fiber composite could be determined.

Aboudi (1987) modeled the fiber-matrix bond as a "flexible film" in which the shear stress and normal stress were proportional to the relative displacements of the fiber and matrix at the interface. This model was used to predict the shear moduli, Young's moduli, Poisson's ratios, and coefficients of thermal expansion of composites containing imperfect bonding.

Takahashi and Chou (1988) used a mathematical model to determine transverse elastic properties of unidirectional composites containing perfectly bonded and completely disbonded fibers. In their "cavity formation model" the fiber and surrounding cavity, which opens due to transverse loading, was replaced by an imaginary inclusion which sustains only compressive loads. The effective elastic compliance was then derived based on analysis of the work done in applying a given load.

Achenbach and Zhu (1989) used boundary element methods to determine stress fields in the matrix, fiber, and interfacial zones of a perfectly bonded and partially disbonded transversely loaded composite. Analysis of initiation, propagation, and arrest of the interface cracks was conducted based on critical strain energy density considerations.

Sullivan, Cassin, and Rosen (1990) used finite element analysis to determine transversely

isotropic properties of unidirectional composites for circular fibers with varying degrees of disbond and for fully bonded "pac man" shaped fibers. The analysis assumed a hexagonal array of fibers and generalized plane strain conditions. One-dimensional gap elements and a nonlinear iterative analysis was used to model the disbond. It was determined that the degradation of transverse properties increased as the degree of disbond increased and that the degradation is more severe at higher fiber volume fractions.

Nimmer et. al. (1991) also used finite element methods in the analysis of a square array of circular fibers under transverse tensile strain. Behavior was predicted for a composite containing perfectly bonded fibers and for one with complete disbond between the fiber and the matrix. Again, the transverse tensile modulus was found to be severely reduced by the presence of fiber/matrix disbond.

As can be seen, there is literature available which deals with noncircular fibers, micromechanical modeling, and disbond modeling. In the next chapter, modeling issues for the particular noncircular fiber investigated here, namely the crenulated fiber, will be discussed.

2.0 Common Geometric and Modeling Issues

The specific problem to be addressed is shown in Figure 2. In this figure a square packed array of crenulated fibers is illustrated. The x-y-z coordinate system used throughout the analysis is also shown. The array in Figure 2 will be subjected to a uniform temperature change, ΔT, and a known applied overall uniform transverse strain in the x direction, $\bar{\varepsilon}_x$. Though crenulated fibers are shown in the figure, circular fibers in similar situations will also be discussed. As indicated in the figure, due to the symmetry of the square packed array, attention can be focused on a single unit cell. For the loading conditions considered in this analysis, only a quarter of the unit cell, as indicated by the outlined region, need be considered. There are several issues related to the geometry of the crenulated fiber which deserve special attention. These issues will be discussed in this chapter.

2.1 Geometric Considerations

The parameters which define the crenulated fiber geometry are illustrated in Figure 3. As stated, the radius of the crenulated fiber $\bar{r}$, is described by a simple cosine function involving the fiber mean radius r_o, the wavelength of crenulation λ, the amplitude of crenulation α, and the integer m, which represents the number of crenulation cycles around the entire

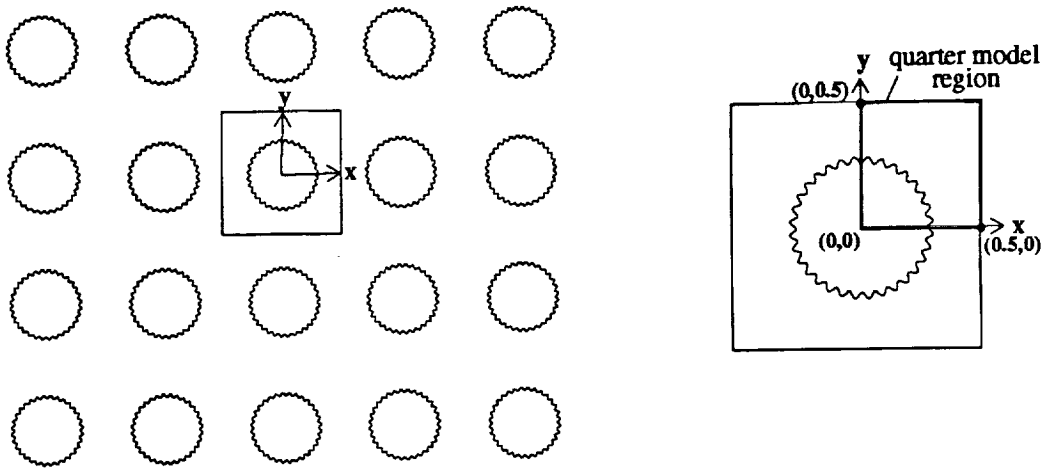

Figure 2. Square Packed Array and Unit Cell Geometry

fiber. Specifically, referring to Figure 3,

$$\bar{r} = r_0 (1 - \alpha\cos(m\theta)) \cos\theta\hat{i} + r_0 (1 - \alpha\cos(m\theta)) \sin\theta\hat{j} , \qquad (1)$$

where $\hat{i}$ and $\hat{j}$ are unit vectors in the x and y directions respectively, and the origin of the x-y coordinate system is located at the center of the fiber as shown. The magnitude of $\bar{r}$ is given by

$$|\bar{r}| = r_0 (1 - \alpha\cos(m\theta)) . \qquad (2)$$

With this representation, the radius of the fiber is parameterized by the angle θ which describes circumferential location around the fiber relative to the x axis.

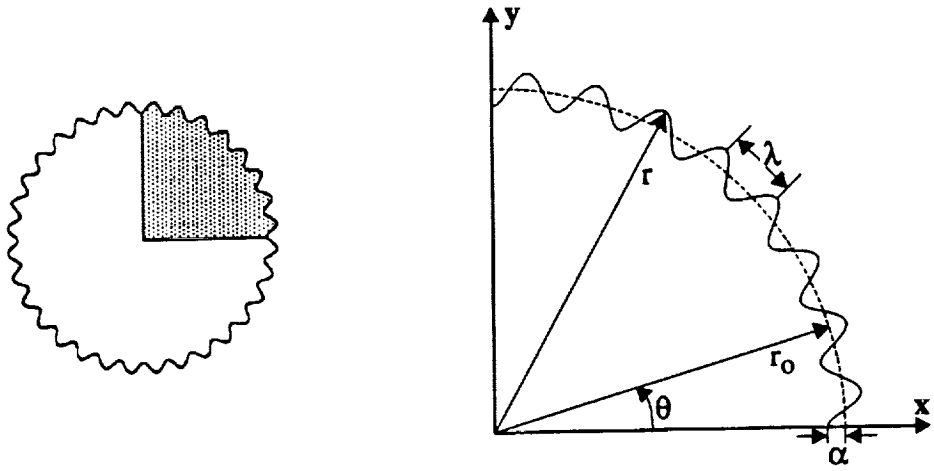

Figure 3. Crenulated Fiber Definitions

The stresses calculated by the finite element analysis, to be discussed shortly, are referenced to the x-y system. Since the stresses along the fiber/matrix interface are of interest in this study, it is necessary to transform the stresses referenced to this coordinate system into a system which is normal and tangential to the crenulated interface. Details of the crenulated fiber surface and the orientation of the two coordinate systems are shown in Figure 4. As can be seen in the figure, the angle β defines the orientation of one coordinate system relative to the other. In particular, β defines the angle between the x-direction and the normal to the fiber surface $\hat{n}$. This angle is important for defining the transformation relations and it can be calculated from the interface radius equation. Specifically, by definition, the unit tangent to the interface is given by

$$\hat{t} = \frac{\dfrac{d\bar{r}}{d\theta}}{\left|\dfrac{d\bar{r}}{d\theta}\right|} . \qquad (3)$$

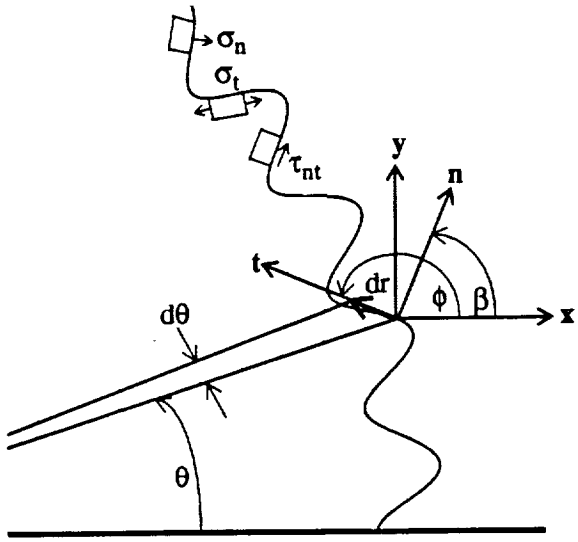

Figure 4. Interface Stress Nomenclature

Equation 3 can be written as

$$\hat{t} = t_x \hat{i} + t_y \hat{j}, \tag{4}$$

where

$$t_x = (m\alpha \sin(m\theta) \cos\theta - (1 - \alpha \cos(m\theta)) \sin\theta) / (\alpha m \sin(m\theta)) \tag{5a}$$

and

$$t_y = (m\alpha \sin(m\theta) \sin\theta + (1 - \alpha \cos(m\theta)) \cos\theta) / (\alpha m \sin(m\theta)). \tag{5b}$$

The angle ϕ between the unit tangent and the x axis is then given by

$$\phi = \tan^{-1}\left(\frac{t_y}{t_x}\right). \tag{6}$$

The unit normal is perpendicular to the unit tangent. Therefore,

$$\beta = \frac{\pi}{2} - \phi \ . \tag{7}$$

The normal stress σ_n, tangential stress σ_t, and shear stress τ_{nt} along the interface may then be calculated from the stresses in the x-y system using the following equations:

$$\sigma_n = \frac{\sigma_x + \sigma_y}{2} + \frac{\sigma_x - \sigma_y}{2}\cos(2\beta) + \tau_{xy}\sin(2\beta)$$

$$\sigma_t = \frac{\sigma_x + \sigma_y}{2} + \frac{\sigma_x - \sigma_y}{2}\cos(2\phi) + \tau_{xy}\sin(2\phi) \tag{8}$$

$$\tau_{nt} = -\left(\frac{\sigma_x - \sigma_y}{2}\right)\sin(2\beta) + \tau_{xy}\cos(2\beta).$$

Note that the normal and shear interface stresses, as shown in Figure 4, act directly on the interface and should, therefore, be continuous across the interface for a fully bonded fiber. For the fully bonded models stresses calculated by finite element analysis at the Gauss points closest to the interface in the fiber and in the matrix are therefore averaged across the interface in this analysis. Tangential stresses at the interface act within the fiber and the

matrix on either side of the interface and will therefore be different in each material due to differences in material properties. In general, none of the stress components will be continuous across the disbonded interface.

For each of the loading cases and degrees of disbond considered in the following chapters, the stresses σ_n, σ_t, and τ_{nt} will be presented for models having varying fiber volume fractions and crenulation amplitudes. Two values of fiber volume fraction, 40% and 60%, are considered for each case. This parameter is easily changed by varying the fiber mean radius r_o in equation 1. Circular fibers and fibers of two crenulation amplitudes, $\alpha = 0.02$ and $\alpha = 0.05$, are also considered for each case. The circular case is clearly equivalent to a crenulation amplitude $\alpha = 0.0$. The frequency of fiber crenulation m is related to the fiber crenulation wavelength λ by the following expression,

$$\lambda = \frac{2\pi r_o}{m} \quad . \tag{9}$$

This parameter is kept constant at a value of 32 for all cases considered but could be changed if studies on the effect on stress states of varying frequency of crenulation were of interest. Increasing the frequency of crenulation, however, would certainly increase difficulties in both processing and modeling of the crenulated fiber. With the given variations in r_o and α, a total of six separate stress states are examined for each loading condition and degree of disbond.

2.2 Characteristics of Stress Transformations

At this point it is important to note that the transformation of stresses from the x-y system to the $\hat{n}$-$\hat{t}$ system may lead to apparent variations in stress that could be wrongly interpreted as being due to crenulation geometry, material property differences, loading, etc. To investigate the effect this transformation has on the character of the interface stresses, consider a homogeneous isotropic material subjected to a uniform strain in the x direction. Let the strain in the y direction be controlled by Poisson's ratio. Recall, Figures 1 - 3 define the x and y directions. The stress state in this material is given by

$$\sigma_x = E\varepsilon_x = \sigma_o$$

$$\sigma_y = 0 \qquad (10)$$

$$\tau_{xy} = 0,$$

E being the Young's modulus of the material and σ_o being a constant. Now, consider an imaginary interface in the material having the shape of the crenulated fiber. The stress state at points on the imaginary interface and referenced to the x-y coordinate system, just like the stress state at any other point within the homogeneous isotropic body, is given by equation 10, a very simple condition. However, if the simple stress state is transformed in accordance with equation 8 to find the stresses acting in a system which is normal and tangential to the imaginary interface, the result is

$$\sigma_n = \frac{\sigma_o}{2} + \frac{\sigma_o}{2}\cos(2\beta)$$

$$\sigma_t = \frac{\sigma_o}{2} + \frac{\sigma_o}{2}\cos(2\phi) \qquad (11)$$

$$\tau_{nt} = -\left(\frac{\sigma_o}{2}\right)\sin(2\beta).$$

For comparison, the transformed stress state around a circular imaginary interface would be given by

$$\sigma_n = \frac{\sigma_o}{2} + \frac{\sigma_o}{2}\cos(2\theta)$$

$$\sigma_t = \frac{\sigma_o}{2} + \frac{\sigma_o}{2}\cos\left(2\left(\frac{\pi}{2} - \theta\right)\right) \qquad (12)$$

$$\tau_{nt} = -\left(\frac{\sigma_o}{2}\right)\sin(2\theta).$$

The variation of the normal, shear, and tangential interface stresses on the imaginary circular interface and the imaginary crenulated interface for values of $\alpha = 0.02$, $m = 32$ and a fiber volume fraction of 60% in a homogeneous material subjected to a unit stress σ_o are shown in Figures 5, 6, and 7, respectively. The stresses have been normalized with respect to σ_o. As shown, stresses for the noncircular case appear to vary a great deal relative to

those in the circular case, even though both cases are the same homogeneous material subjected to a simple force per unit area stress state in the x-y system. In fact, relative to the actual simple uniaxial stress state σ_o, the apparent variation for a crenulated fiber is substantial. With a larger amplitude of crenulation, the apparent variation of the normal, tangential, and shear stresses for the crenulated fiber will increase. Therefore, when examining interface stresses in composites containing crenulated fibers, it should be noted that much of the variation from the circular stress state is simply due to the transformation of the x-y stresses around the noncircular interface.

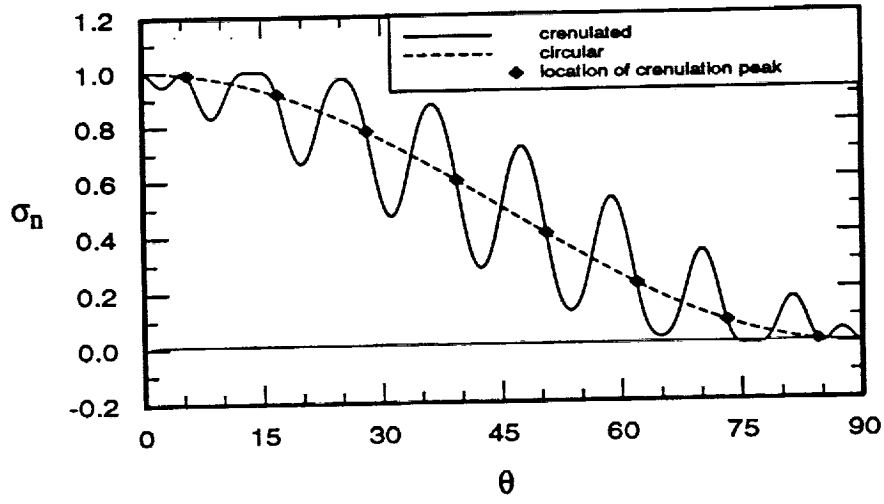

Figure 5. Normal Stresses on Imaginary Interface

The diamond shaped symbols shown in Figures 5 - 7 will also be used in similar figures in the chapters which follow. In the next four chapters, these diamond symbols will be included in each figure to indicate the circumferential locations, θ, of the maximum fiber radius, i.e., the crenulation peaks. For the case shown in Figures 5 - 7, the values of stress on the imaginary crenulated interface at these locations correspond to those on the imaginary circular interface. This is also true at the locations which lie halfway between the dia-

mond symbols. These locations correspond to the minimum fiber radius locations. This should be expected because at the maxima and minima of the crenulated radius the tangent to the crenulated locus is parallel to the tangent to the circular locus. For the actual crenulated fiber in a matrix this equality of stresses will not necessarily occur due to the mechanics of interaction between the fiber and the matrix.

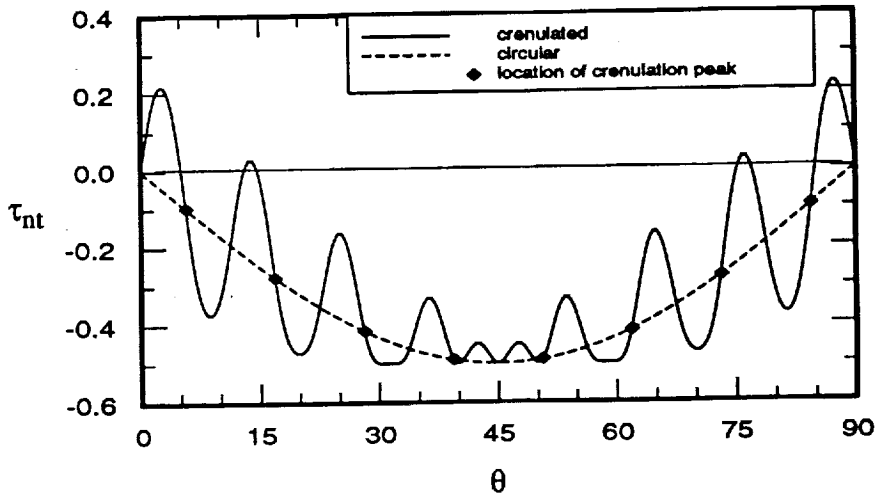

Figure 6. Shear Stresses on Imaginary Interface

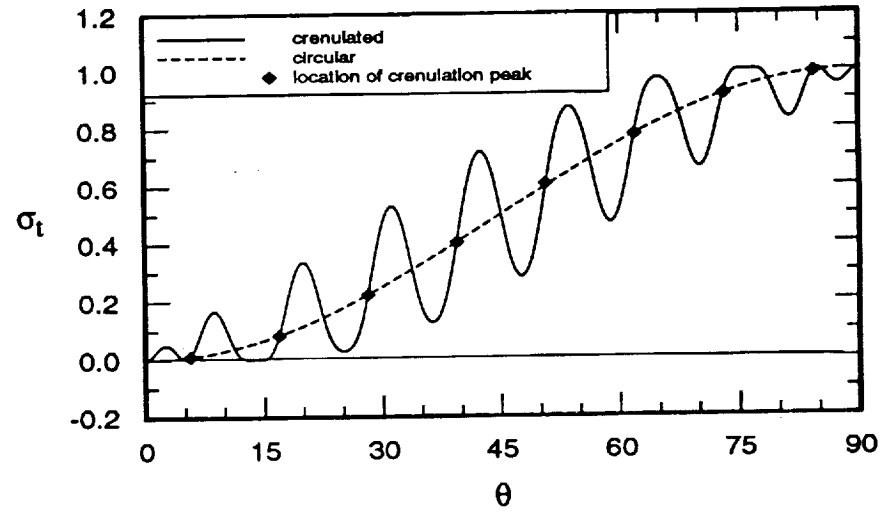

Figure 7. Tangential Stresses on Imaginary Interface

2.3 Finite Element Modeling Considerations

The commercially available finite element code ABAQUS is used for the analysis while the program PATRAN is used for pre- and postprocessing of the input and output data. Linear elastic response and a condition of generalized plane strain are assumed for both the thermal and mechanical loading. Since the analysis is linear elastic, the actual size of the unit cell is not important. Rather, it is important to represent the volume fraction and material properties of each constituent correctly. For this analysis, the dimensions of the unit cell, shown in Figure 2, are assumed to be 1.0 by 1.0. The total area of the unit cell in the x-y plane is therefore 1.0. The dimensions of the quarter model region are then 0.5 by 0.5.

A typical finite element mesh is shown in Figure 8. The arrows indicate the position of the fiber/matrix interface. The mesh shown is for a fiber volume fraction of 60% and a crenulation amplitude of 0.02. Models of the perfectly bonded composite contain a total of 2040 triangular and quadrilateral elements with 6105 total nodes, while models of the disbonded cases contain an extra 128 special interface elements and a total of 6364 nodes.

The elements used for modeling the fiber and matrix are 8-node quadratic triangular and 10-node biquadratic quadrilateral generalized plane strain elements. Under conditions of generalized plane strain it is assumed that there is no gradient in any strain component in one material direction. In this case, the unique direction corresponds to the fiber axis or z direction, which is the out of the plane direction in past figures. The elements are of unit thickness (thickness defined to be in the z direction) and lie between two parallel bounding planes which are initially perpendicular to the z axis and which can move relative to each

other while remaining planar. With the scheme in ABAQUS, each generalized plane strain element is then defined by 6 or 8 conventional nodes for the triangular and quadratic elements, respectively, plus a set of two additional nodes which act to describe the motion of these two bounding planes. The first extra node has only one degree of freedom. This degree of freedom corresponds to the z direction strain of the element. The second additional node has two degrees of freedom. These degrees of freedom correspond to the components of rotation of one bounding plane with respect to the other. For this analysis these two degrees of freedom were set to zero so that axial strain in all elements is the same and the bounding planes remain parallel after loading. In general, the same two extra nodes may be used for all elements in the mesh. For the disbonded case, however, to prevent interaction of the fiber and the matrix in the axial direction, one set of additional nodes is prescribed to the elements in the fiber and a separate set of additional nodes is prescribed to the elements in the matrix.

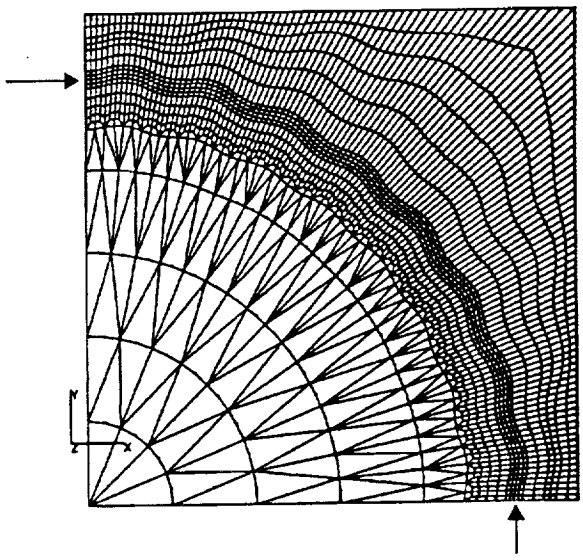

Figure 8. Typical Finite Element Mesh

To model the disbond between the fiber and the matrix special three-node interface elements available in ABAQUS were used. These elements are able to model interactions between elastically deforming bodies which may contact each other at any number of points along their boundaries. The nodes on these interface elements correspond to the nodes along the surface of the fiber at the interface. The interface elements are then associated with a node set containing all the nodes along the surface of the matrix at the interface. The node set for the matrix at the interface is defined as a "slide line" in ABAQUS. The interface elements may contact the slide line at any point but may not cross it. Stresses and strains in these elements are computed in a local system which is normal and tangential to the slide line at every point. For this analysis a frictionless slide line, or contact surface, is assumed. Two disbond gaps are investigated in this work, one being $1x10^{-5}$ times the mean fiber diameter $d_o(= 2r_o)$ and the other, smaller at $1x10^{-6}\ d_o$.

Representative pitch-based carbon fiber and carbon matrix properties are assumed in the analyses. These properties are based on values found in the following sources: Adams (1975), Amoco Performance Products, Inc. (1989), Bowles (1990), Chamis (1984), Dean and Turner (1973), Dieffendorf and Tokarsky (1975), Edie and Stoner (1992), Kriz and Ledbetter (1985), Kriz and Stinchcomb (1979), Maahs (1990), Perry and Adams (1974), Rozploch and Marciniak (1986), Schmidt (1972), and Smith (1972). The matrix is considered fully isotropic with the following properties

$$\begin{aligned} E &= 6.0 \text{ Msi} \\ \nu &= 0.3 \\ G &= 2.31 \text{ Msi} \\ CTE &= 1.67x10^{-6} / {}^{o}F, \end{aligned} \tag{13}$$

where E is Young's modulus, ν is Poisson's ratio, G is the shear modulus, and CTE is the coefficient of thermal expansion. The properties used for the fiber, which is assumed to be

transversely isotropic, are

$$\begin{aligned} E_L &= 50.0 \text{ Msi} & E_T &= 2.0 \text{ Msi} \\ \nu_{TT} &= 0.49 & \nu_{TL} &= 0.0132 \\ G_{TT} &= 0.67 \text{ Msi} & G_{LT} &= 0.6 \text{ Msi} \\ CTE_L &= 0.0 / {}^{o}F & CTE_T &= 5.0 \times 10^{-6} / {}^{o}F, \end{aligned} \tag{14}$$

where L represents the fiber direction and T represents the transverse direction.

For the case of thermal loading, a uniform temperature change $\Delta T = -1.0\ {}^{o}F$ is applied to all elements in the model. As implied by the material properties, linear thermal expansion is assumed. Due to the quarter symmetry of the model, as shown in Figure 2, constraints must be enforced on the displacements of the nodes along the lines $x = 0$ and $y = 0$, and on the origin which corresponds to the fiber center. All nodes along the line $x = 0$ are constrained to have zero displacement in the y direction, while all nodes along the line $y = 0$ are constrained to have no x direction displacement. Multipoint constraints are also placed on the lines $x = 0.5$ and $y = 0.5$, which correspond to the right edge and top edge of the finite element mesh, respectively. These constraints require that the nodes along these two lines have equal displacements in the x and y directions respectively, i.e., each line remains straight and parallel to its original position.

In the case of transverse loading, an average x direction strain $\bar{\varepsilon}_x$ equal to 1000 μin/in is applied by uniformly displacing all nodes along the line $x = 0.5$ in the x direction. The same constraints due to symmetry are placed on the nodes along $x = 0$ and $y = 0$ as in the thermal loading case, and a similar multipoint constraint is applied to the nodes along $y = 0.5$. As stated, the rotation about any axis of the parallel planes that bound the model is prevented in both loading cases.

Stresses induced by the temperature change are normalized by the Young's modulus of the matrix times its coefficient of thermal expansion times the magnitude of the temperature change applied, $E_m CTE_m |\Delta T|$, the product being equal to 10.02 psi. Stresses due to the transverse tensile loading are normalized by the modulus of the matrix times the applied average tensile strain, $E_m \bar{\varepsilon}_x$, this product being equal to 6000 psi. Since the analyses of the fully bonded and no-fiber cases are linearly elastic, stress states due to a larger temperature change or different applied transverse tensile strain could be easily determined by scaling the results for the load cases presented here. Analysis of the fully disbonded case is non-linear and, therefore, can not be scaled in this manner.

Certain average composite properties are calculated from the finite element data for each loading condition considered. For the case of a temperature change, the coefficients of thermal expansion of the composite in the x, y, and z directions (α_x, α_y and α_z, respectively) are determined from strain and displacement data. For the case of applied transverse strain, an average effective transverse modulus of the composite, $\bar{E}_x$, is calculated from stress data and the Poisson's ratios, ν_{xy} and ν_{xz}, are determined from strain and displacement results.

The next chapter begins the discussion of the various analyses conducted using the modelling factors just presented. Specifically, the next chapter considers the response of the composite to a unit temperature decrease.

3.0 Response Due to a Temperature Change

As carbon-carbon materials are cooled from the high temperatures at which they are processed to lower temperatures at which they will be used, stresses are induced in the fiber and matrix due to the difference in their coefficients of thermal expansion. These thermal stresses exist in the composite prior to any mechanical loading that will be seen in use and, therefore, can affect the composite's performance in use. In this chapter stresses at the interface of perfectly bonded circular and crenulated fibers induced by a temperature change $\Delta T = -1.0\ ^{o}F$ are presented and compared. The effects on these stresses of increasing fiber crenulation amplitude and fiber volume fraction are also discussed.

With the generalized plane deformation model being used here, cooling results in a uniform contraction in the x-y plane because both the fiber and the matrix are isotropic in this plane and boundary conditions are symmetric. As a result, all interface normal and tangential stress states are symmetric about $\theta = 45^{o}$, while all interface shear stress states are antisymmetric about $\theta = 45^{o}$. Note, the stresses as presented are normalized by a factor which contains the absolute value of the temperature change and that linear thermal expansion is assumed. The signs of the normalized stresses are thus associated with a temperature decrease. Also, stresses induced by a larger decrease in temperature would appear

identical to those shown here.

3.1 Fully Bonded Circular Fiber, $v_f = 40\%$

To provide a basis for comparison, the stress state in a unidirectional composite containing fully bonded circular fibers at 40% fiber volume fraction is first considered. The interface stresses σ_n, τ_{nt}, and σ_t are shown in Figures 9, 10, and 11, respectively. It should be noted that these figures have been scaled for ease of comparison with the noncircular cases to be studied later.

Examination of Figure 9 reveals that with a temperature decrease, the interface normal stress is tensile at all circumferential locations. This results from the difference between the coefficients of thermal expansion of the fiber and of the matrix. The coefficient of thermal expansion of the fiber in the x-y plane is greater than that of the matrix (5.0×10^{-6} / °F vs. 1.67×10^{-6} / °F). The fiber therefore tends to contract more upon cooling and pull away from the matrix. When fully bonded, the matrix resists the contraction of the fiber, causing tensile normal stresses to arise at the interface. The maximum normal stresses for this circular fiber case occur at $\theta = 0^o$ and $\theta = 90^o$, locations where the least amount of matrix material exists in the model. This small amount of matrix material must resist the contraction of the fiber at these circumferential locations as much as the matrix material at other circumferential locations does so that the edges of the model satisfy the boundary conditions, i.e., they remain straight and parallel to their original positions. Therefore, higher stresses arise in these regions. The lowest normal interface stress is seen at $\theta = 45^o$, the location where the most matrix material is present to resist the contraction of the fiber.

The interface shear stress for this circular fiber case is shown in Figure 10. As stated, the shear component is antisymmetric about $\theta = 45^o$. In this case, negative shear stresses occur at the interface in the region $\theta < 45^o$, while positive stresses occur at the interface in the region $\theta > 45^o$. The shear stress vanishes at $\theta = 45^o$, $\theta = 0^o$, and $\theta = 90^o$, as required by boundary conditions and the symmetry of the problem. By comparing Figures 9 and 10, it is seen that the magnitude of the interface shear stress is small compared to the magnitude of the interface normal stress.

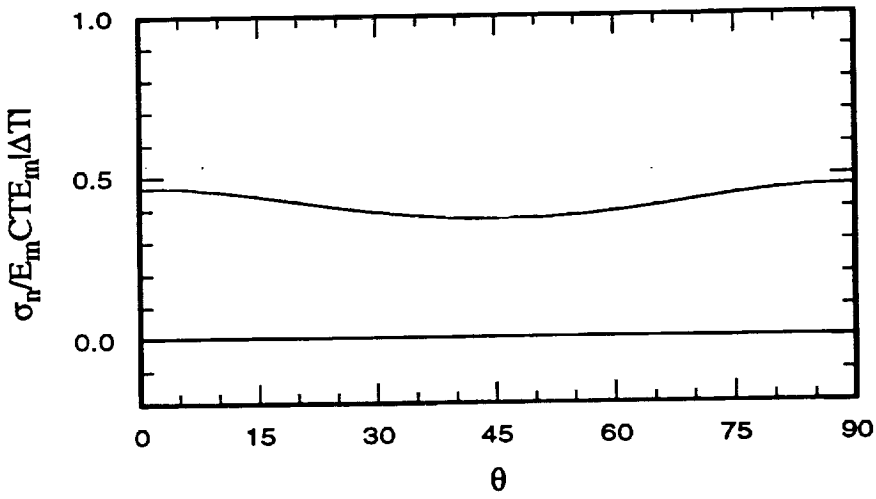

Figure 9. Interface Normal Stress Due to Temperature Change for Fully Bonded Circular Fiber, $v_f = 40\%$

The tangential component of stress at the interface in both the fiber and the matrix is shown in Figure 11. The matrix is in compression in the tangential direction while the fiber is in tension. This is again a result of the tendency of the fiber to pull away from the matrix due to the greater coefficient of thermal expansion in the fiber. Note, the maximum compressive tangential stress in the matrix occurs at $\theta = 0^o$ and $\theta = 90^o$, while the maximum tension in the fiber occurs at $\theta = 45^o$. It can be seen that the magnitude of the tangen-

tial stress in the matrix is considerably larger than the magnitude of the tangential stress in the fiber, and the magnitude of all the other stress components.

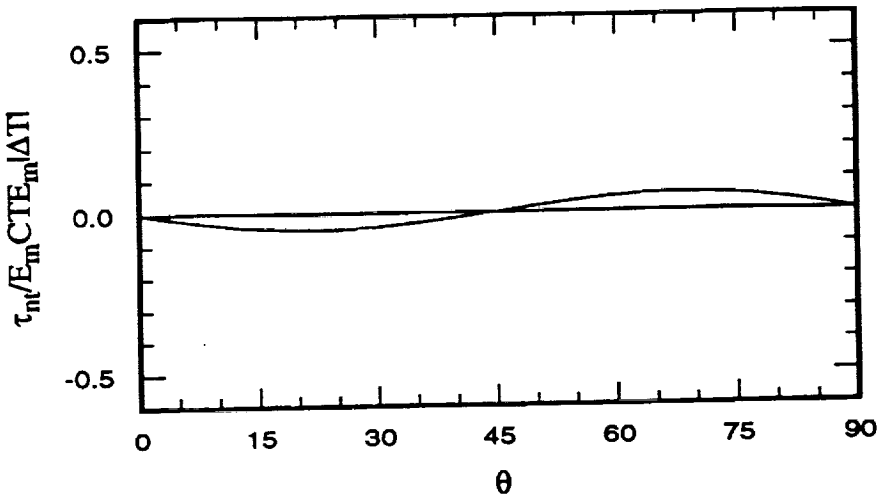

Figure 10. Interface Shear Stress Due to Temperature Change for Fully Bonded Circular Fiber, $v_f = 40\%$

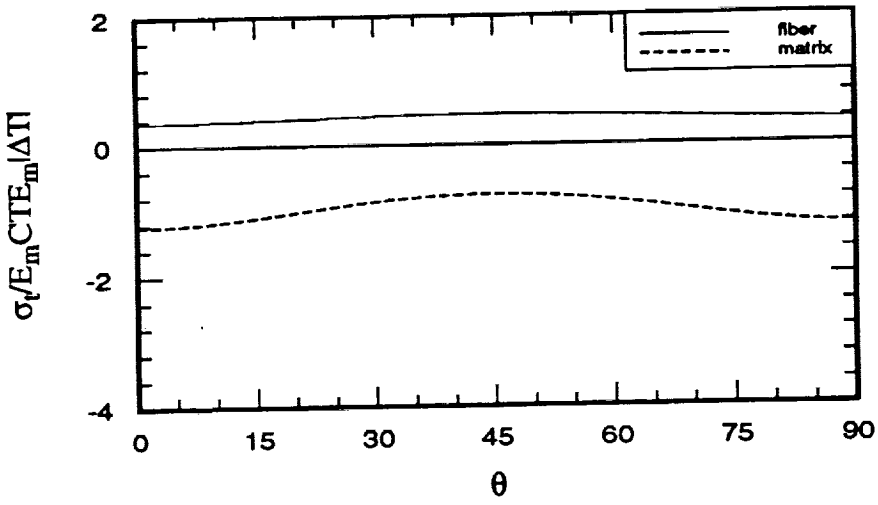

Figure 11. Interface Tangential Stress Due to Temperature Change for Fully Bonded Circular Fiber, $v_f = 40\%$

3.2 Fully Bonded Crenulated Fiber, $\alpha = 0.02$, $v_f = 40\%$

Next, the cooling of a composite containing a slightly crenulated fiber is considered. Interface stresses about a fiber with a crenulation amplitude of $\alpha = 0.02$ and a fiber volume fraction of 40% are shown in Figures 12, 13, and 14. The circular fiber stress states just presented are also shown on each figure to facilitate comparison. Examination of Figure 12, the interface normal stress, shows that the introduction of the fiber crenulation causes stress to vary above and below the stress level seen in the circular fiber case. Note the maximum normal stress for this mildly crenulated case is greater than in the circular case and no longer occurs at $\theta = 0^o$ and $\theta = 90^o$, but occurs slightly away from the $\theta = 0^o$ and $\theta = 90^o$ locations. As discussed previously, the diamond markers on the figure indicate the θ locations at which the fiber radius is at its maximum, i.e., the positions of the peaks in the fiber crenulation. In this case, the local maxima in the variations of the normal stress correspond to the positions of these crenulation peaks.

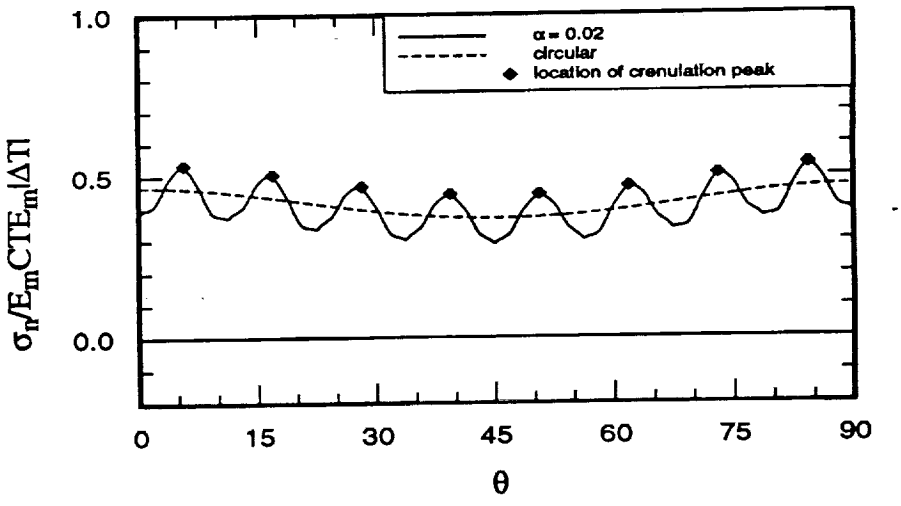

Figure 12. Interface Normal Stress Due to Temperature Change for Fully Bonded Crenulated Fiber, $\alpha = 0.02$, $v_f = 40\%$

The interface shear stress component about the mildly crenulated fiber is shown in Figure 13. This stress component also follows the general trend of the shear stress in the circular fiber case, but again varies locally above and below the stress level for the circular fiber. The stress state remains antisymmetric about $\theta = 45^{o}$ and still goes to zero at $\theta = 0^{o}$, 45^{o}, and 90^{o}, as in the circular case. As with the normal stress component, however, the maximum shear stress value is higher and the minimum shear stress value is lower in the crenulated case. Also, these maximum and minimum stresses do not occur at the same θ locations as in the circular case. Here, referring to the diamond symbols, the position of the peaks in stress variation do not coincide with the positions of the fiber crenulation peaks. Values of shear stress at the θ locations that correspond to the peaks in crenulation are halfway between the local maxima and minima of the stress variations.

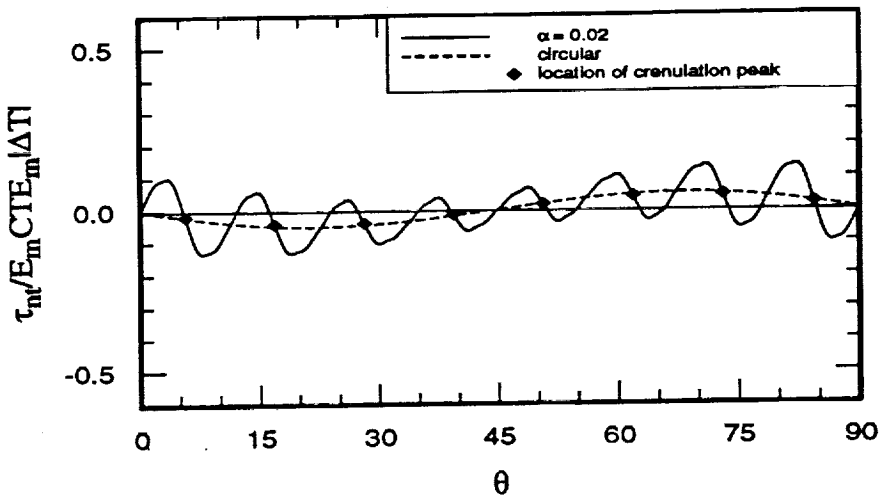

Figure 13. Interface Shear Stress Due to Temperature Change for Fully Bonded Crenulated Fiber, $\alpha = 0.02$, $v_f = 40\%$

Tangential stresses at the interface in both the fiber and matrix are shown in Figure 14. The variation of stress levels about the level for the circular cases is seen here, too. Note, the

local variations in the matrix tangential component are greater than those in the fiber tangential component. In both constituents, the maximum stresses are higher about the crenulated fiber than about the circular fiber, and the minimum stresses are lower. Here, the maximum magnitude tangential stress no longer occurs at $\theta = 0^o$ and $\theta = 90^o$, as in the circular case, but is shifted slightly from these locations. Also, the positions of the crenulation peaks correspond to the locations of the local minima in the variations of the tangential stresses. Recall from Figures 12 and 13 that the local maximums in normal stress variations corresponded to locations of peaks in the fiber radius, whereas with the local shear stress variations, the peaks in the fiber radius were approximately midway between the local maxima and local minima in stress variation.

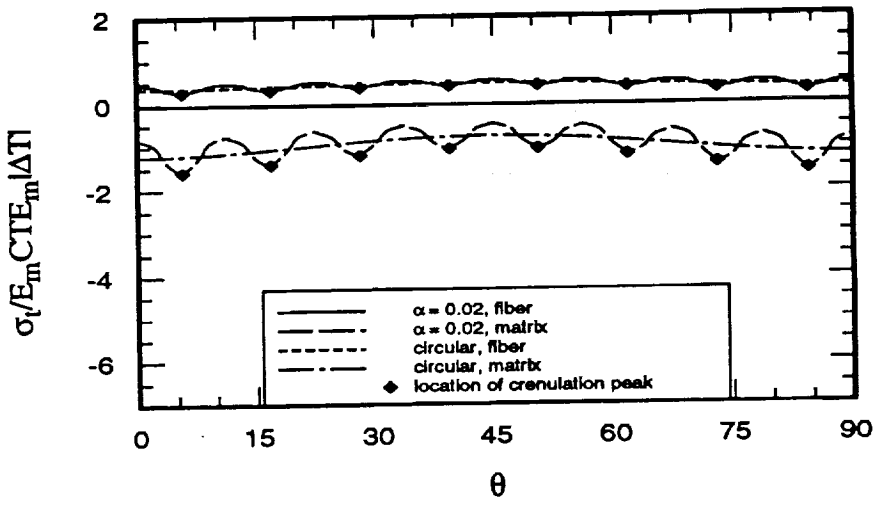

Figure 14. Interface Tangential Stress Due to Temperature Change for Fully Bonded Crenulated Fiber, $\alpha = 0.02$, $v_f = 40\%$

3.3 Fully Bonded Crenulated Fiber, $\alpha = 0.05$, $v_f = 40\%$

The geometric difference between the two crenulation amplitudes considered in this analysis can be seen in Figure 15, which shows the finite element meshes at a fiber volume fraction of 40% for crenulation amplitudes of 0.02 and 0.05. The effect of increasing crenulation amplitude from $\alpha = 0.02$ to $\alpha = 0.05$ on the three interface stress components induced by cooling the composite is shown in Figures 16, 17, and 18.

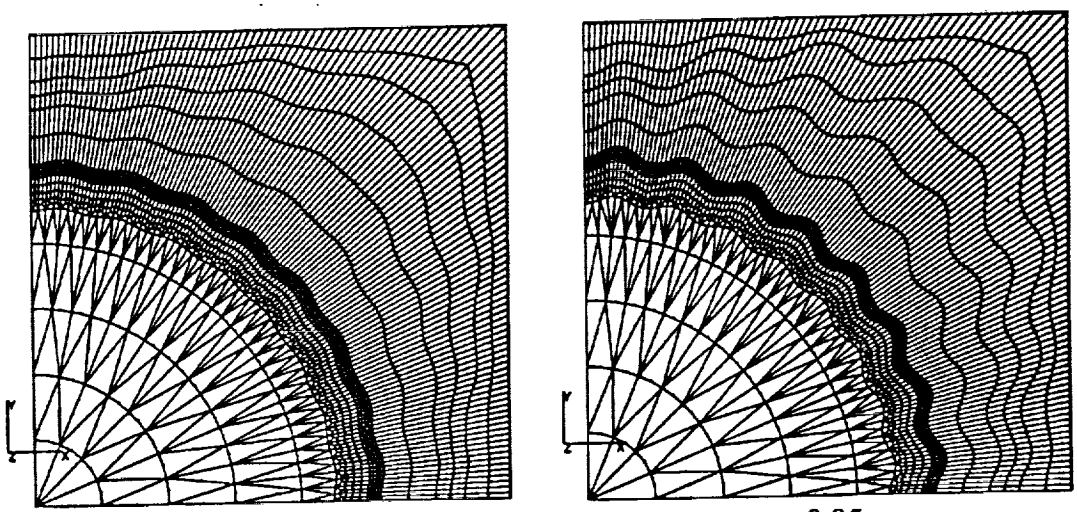

Figure 15. Comparison of Fiber Crenulation Amplitudes

Figure 16 shows the interface normal stress component about the circular fiber, a fiber with a crenulation amplitude $\alpha = 0.02$, and one with a crenulation amplitude $\alpha = 0.05$. Clearly, increasing fiber crenulation amplitude increases the variation of the stress state about that found in the circular fiber case. The maxima in the stress variations continue to occur at the θ locations corresponding to the fiber crenulation peaks.

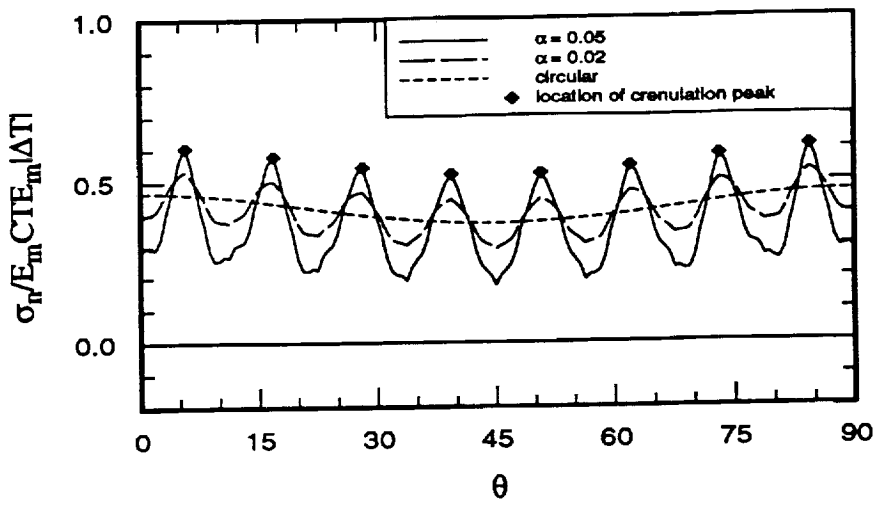

Figure 16. Interface Normal Stress Due to Temperature Change for Fully Bonded Crenulated Fiber, $\alpha = 0.05$, $v_f = 40\%$

Figure 17 shows similar results for the shear stress component. Much larger stress variations are seen in the case of the larger crenulation amplitude. Note, particularly large shear stresses now occur near $\theta = 0^o$ and $\theta = 90^o$ and that the sign of the shear stress changes rapidly with θ. Relative to the $\alpha = 0.02$ case, the magnitude of the interface shear stresses have more than doubled, whereas compared to the circular case, the magnitude of the interface stress is approximately a factor of five greater. Again, the value of the shear stress at the crenulation peaks is between the maxima and minima of the local stress variations.

The tangential stress component in the fiber and the matrix is shown in Figure 18. Here, the increase in fiber crenulation amplitude also causes an increase in the stress variation about the circular level. As before, variations in the matrix tangential component appear to be greater than those in the fiber tangential component. On a percentage basis, however, near $\theta = 0^o$ and $\theta = 90^o$ the variations in the fiber tangential stress are greater than in the

matrix. Local extremum values in the tangential stresses in both the fiber and the matrix again occur at the positions of the fiber crenulation peaks.

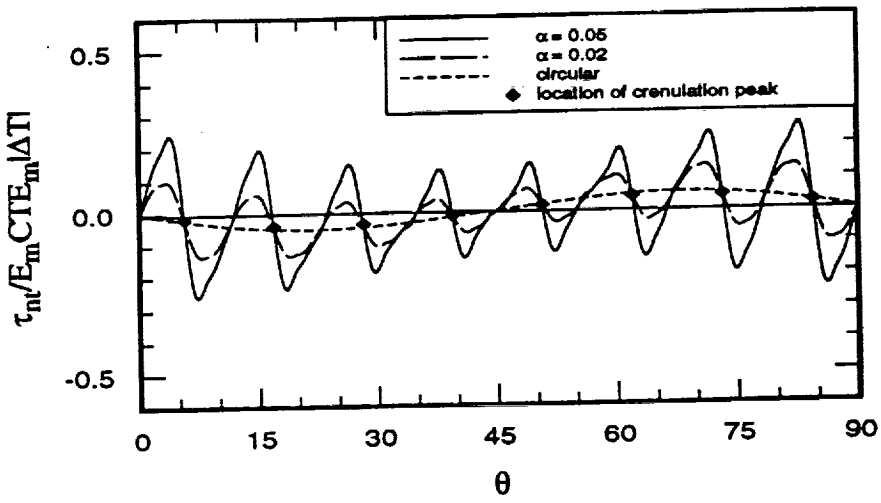

Figure 17. Interface Shear Stress Due to Temperature Change for Fully Bonded Crenulated Fiber, $\alpha = 0.05$, $v_f = 40\%$

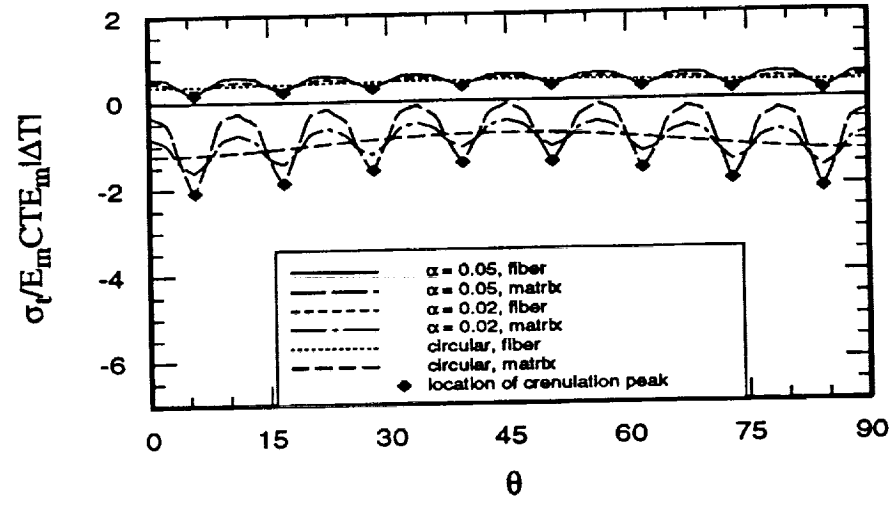

Figure 18. Interface Tangential Stress Due to Temperature Change for Fully Bonded Crenulated Fiber, $\alpha = 0.05$, $v_f = 40\%$

3.4 Effect of Increasing Fiber Volume Fraction on Stresses Due to Temperature Change: Fully Bonded Case

The effect of increasing the fiber volume fraction is shown in Figures 19, 20 and 21. These figures show the three interface stress components about circular fibers, and fibers with crenulation amplitudes of $\alpha = 0.02$ and $\alpha = 0.05$, all at a fiber volume fraction of 60%. Note that to facilitate comparison, these figures are shown on the same scale as the figures for 40% fiber volume fraction.

Comparison of Figures 16 and 19 shows that the increase in fiber volume fraction causes normal interface stresses to be reduced slightly. This is true for both the circular and crenulated cases. At this larger volume fraction the normal stresses around the crenulated fibers still follow the general trend of the normal stress around the circular fiber, but the local variations in stress at both crenulation amplitudes appear to be greater than those that occur at the lower volume fraction. Note that with 60% fiber volume fraction and the higher crenulation amplitude, the larger stress variations cause compressive normal stresses to arise at certain circumferential locations, specifically at radius minima in the range $20^o \leq \theta \leq 70^o$. The relation between the local maxima in the interface normal stress variation and the positions of the crenulation peaks remains the same at this higher volume fraction as at the lower volume fraction.

By examining Figures 17 and 20, it is seen that increasing the fiber volume fraction has a significant effect on the interface shear stress. The increase in fiber volume fraction causes increased interface shear stresses. The shear stress again changes sign rapidly with θ and quite large stresses occur near $\theta = 0^o$ and $\theta = 90^o$. The positions of the peaks in the fiber

crenulation still occur between the local maxima and minima of the stress variations. Note, however, additional variations in the stress that were not seen at the lower fiber volume fraction arise at this higher volume fraction with the crenulation amplitude $\alpha = 0.05$. That is, where as the variation with θ of the stresses for the case of $\alpha = 0.02$ tend to follow the variations with θ of the crenulation amplitude, for $\alpha = 0.05$, the variations with θ of the stresses seem to include perturbations, or "higher harmonics".

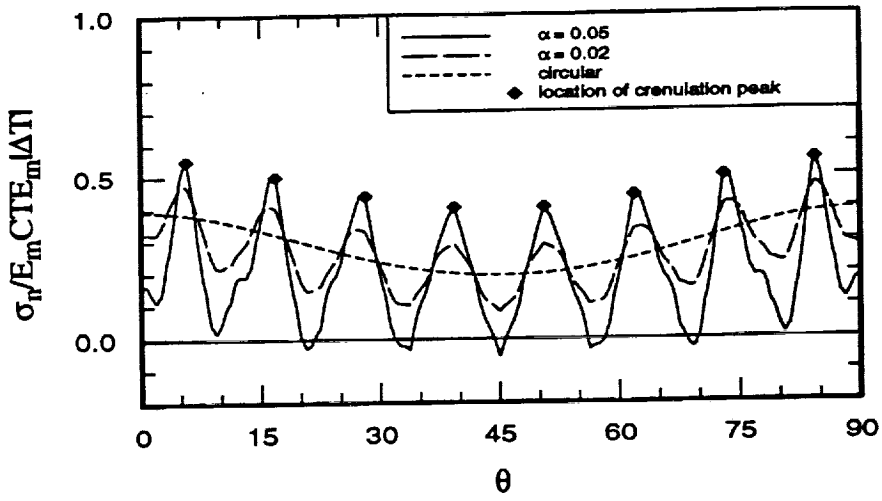

Figure 19. Interface Normal Stress Due to Temperature Change for Fully Bonded Crenulated Fiber, $\alpha = 0.02$ and $\alpha = 0.05$, $v_f = 60\%$

Figure 21 shows both the fiber and matrix tangential stresses for the circular fiber and the crenulated fiber with $\alpha = 0.02$ and 0.05 for a fiber volume fraction of 60%. Comparing this figure to Figure 18 shows that the increase in fiber volume fraction causes both the fiber and the matrix stress levels to shift slightly in the negative direction. The variations in stress due to increase in crenulation amplitude again appear to be increased by the increase in fiber volume fraction. Also, compressive stresses arise at certain θ locations on the fiber side of the interface at the higher crenulation amplitude, whereas fiber tangential stresses

are completely positive at the lower fiber volume fraction. As before, the local extremes in stress variation correspond to the positions of the peaks in fiber crenulation.

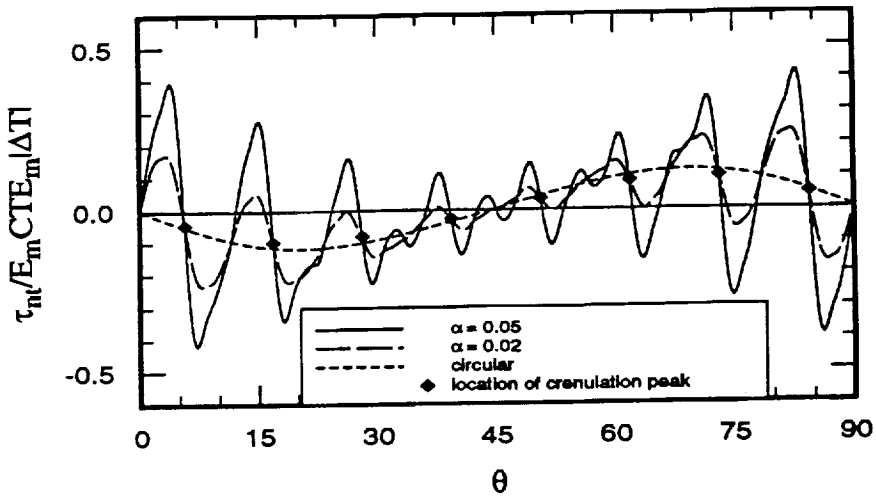

Figure 20. Interface Shear Stress Due to Temperature Change for Fully Bonded Crenulated Fiber, $\alpha = 0.02$ and $\alpha = 0.05$, $v_f = 60\%$

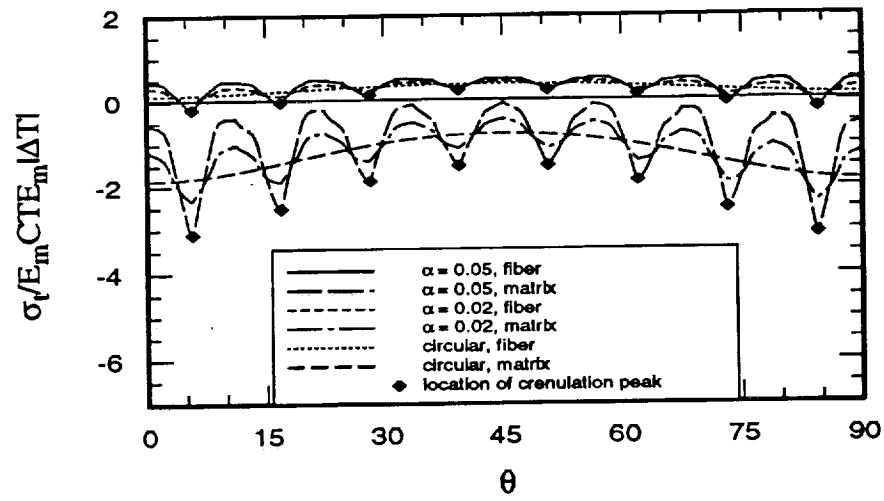

Figure 21. Interface Tangential Stress Due to Temperature Change for Fully Bonded Crenulated Fiber, $\alpha = 0.02$ and $\alpha = 0.05$, $v_f = 60\%$

3.5 Response Due to Temperature Change of Fully Disbonded Fiber

As noted previously, the coefficient of thermal expansion of the fiber in the x-y plane is greater than that of the matrix. This difference causes the fiber material to tend to pull away from the matrix material when the composite is cooled. Analysis of a model containing fully disbonded fibers subjected to a temperature change of $\Delta T = -1.0\ ^{o}F$ is therefore trivial. The fiber shrinks away from the matrix and no interaction between the two occurs. Both fiber and matrix experience free thermal contraction. Therefore, no stresses are induced in either material. Similarly, no stresses arise in a model of just the matrix alone containing a fiber-shaped hole. This model will also undergo free thermal contraction upon cooling and generate no stresses.

3.6 Discussion of Variations in Stress Due to Temperature Change

In the previous figures, the crenulated case and the circular case have been compared. In particular, comments have been made regarding the variations in the stresses for the crenulated case relative to the circular case. If the variation in the normal stress component relative to the circular case is defined as

$$\Delta\sigma_n = (\sigma_n)_{\text{crenulated}} - (\sigma_n)_{\text{circular}}, \tag{15}$$

then for a particular volume fraction and crenulation amplitude $\Delta\sigma_n$ can be computed as a function of circumferential location. At some circumferential location, the variation in $\Delta\sigma_n$ attains a maximum value. Figure 22 shows the values of the maximum variation in

each stress component as a function of fiber volume fraction and crenulation amplitude. The figure shows that for this thermal loading case the variations in all interface stress components increase as both crenulation amplitude and fiber volume fraction are increased. The increase in the variations in the tangential stress component in the matrix, however, are much larger than those in the shear stress component, normal stress component, or tangential stress component in the fiber.

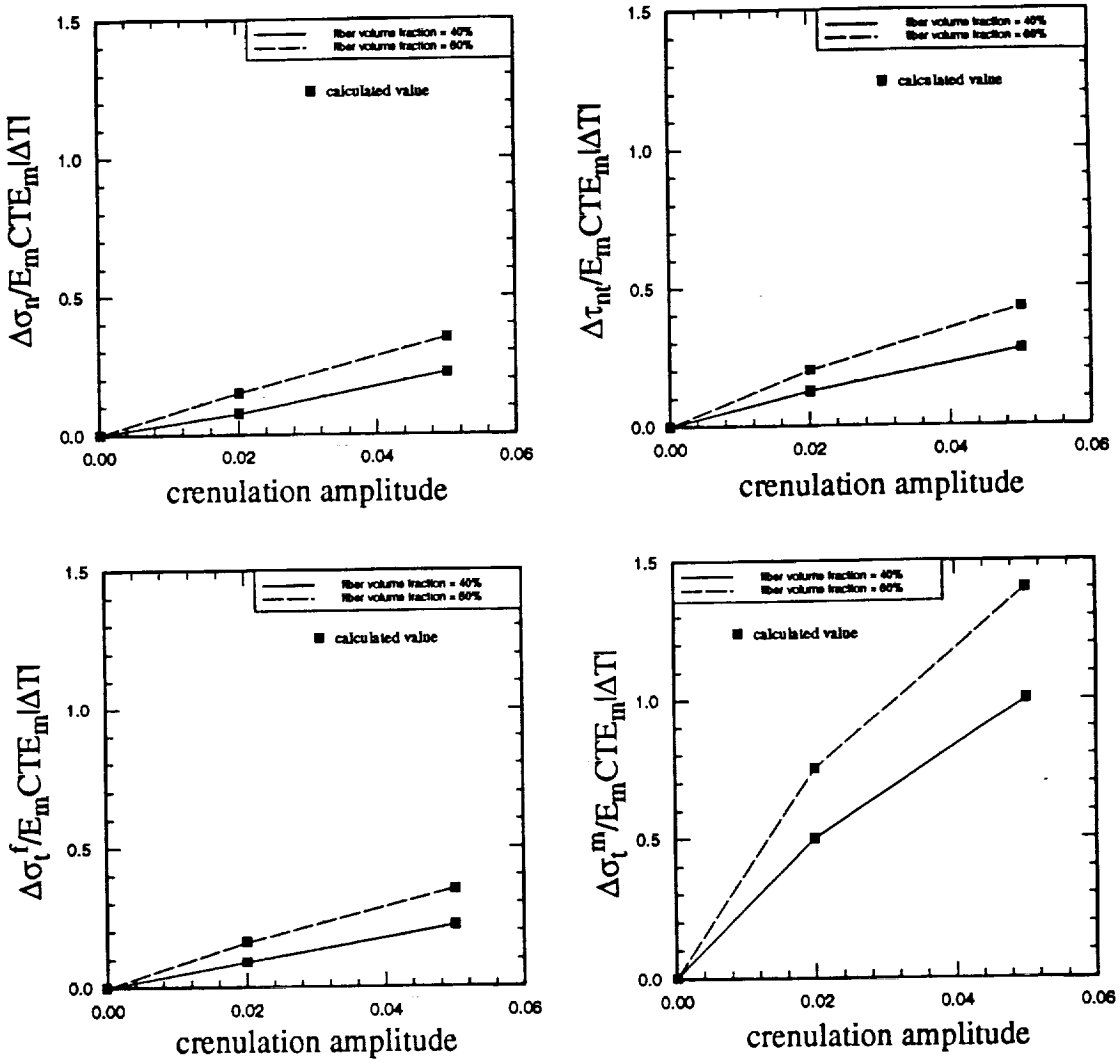

Figure 22. Comparison of Maximum Stress Variations Due to Temperature Change for Fully bonded Fiber

3.7 Composite Properties: Coefficients of Thermal Expansion

The computed composite coefficients of thermal expansion for the fully bonded case are shown in Table 1. For the temperature change considered, $\Delta T = -1.0\ ^{o}F$, and a unit cell of dimensions 1.0 by 1.0, these values are computed as follows: The total x direction strain in the unit cell is taken to be equal to twice the x direction displacement, Δx, of the nodes along the right edge ($x = 0.5$) of the quarter model, divided by the original x direction length of the unit cell, l_x, which is equal to 1.0. The coefficient of thermal expansion α_x is then equal to this strain divided by the temperature change of $-1.0\ ^{o}F$. That is,

$$\alpha_x = -\frac{\Delta x}{l_x} \ . \tag{16}$$

Similarly,

$$\alpha_y = -\frac{\Delta y}{l_y} \ . \tag{17}$$

Because both the fiber and the matrix are isotropic in the x-y plane, α_x and α_y are equal. The coefficient of thermal expansion in the fiber direction α_z is equal to the strain of the model in the z direction, ε_z, which is given by the displacement of the first additional node divided by the temperature change, i.e.,

$$\alpha_z = -\varepsilon_z \ . \tag{18}$$

For comparison, The coefficients of thermal expansion of the fiber and the matrix are given in Table 1. As shown, the computed composite properties for the fully bonded case lie between those of the constituent materials. Changes in crenulation amplitude appear to have little effect on the magnitude of the coefficients at each fiber volume fraction. Note, expansion in the fiber direction is decreased as fiber volume fraction is increased from 40% to 60%. Expansion in the x-y plane increases, however, with increasing fiber volume

fraction. In the fully disbonded and no-fiber cases discussed in the previous section, the x and y direction coefficients of thermal expansion of the composite are equal to that of the matrix alone. The z direction coefficient of thermal expansion of the composite is, of course, also equal to that of the matrix in the no-fiber case. For the fully disbonded fiber case α_z is undefined, as fiber and matrix do not experience equal out-of-plane strain.

Table 1: Composite Thermal Expansion Coefficients

			$\alpha_x = \alpha_y$ ($\times 10^{-6}$ / °F)	α_z ($\times 10^{-6}$ / °F)
fiber			5.0	0.0
matrix			1.67	1.67
Fully Bonded	$v_f = 40\%$	circular	2.95	0.259
		$\alpha = 0.02$	2.95	0.259
		$\alpha = 0.05$	2.95	0.259
	$v_f = 60\%$	circular	3.54	0.127
		$\alpha = 0.02$	3.50	0.128
		$\alpha = 0.05$	3.55	0.127

In the next chapter similar variations in interface stresses due to increasing crenulation amplitude and fiber volume fraction will be presented and compared for the case of transverse tensile loading of a composite containing fully bonded circular and crenulated fibers. The stress variations for the transverse loading case will be seen to be similar to those shown in this chapter for the thermal loading case.

4.0 Response Due to Transverse Tensile Strain: Fully Bonded Case

A major motivation for studying noncircular fibers, as noted previously, is the desire to increase the transverse tensile strength of carbon-carbon composites. This strength is, in general, low due to the lack of fiber/matrix adhesion. The influence of noncircular fibers on the interface stress states induced in carbon-carbon by the application of a transverse tensile load will now be considered. One extreme, stresses in a composite containing fully bonded fibers, is presented in this chapter. Another extreme, the case of fully disbonded fiber and matrix, will be discussed in the two chapters that follow. As stated, the actual degree of bonding in carbon-carbon is thought to lie between these two extremes. Results analogous to those seen in the previous chapter will be presented for this transverse loading case in this chapter. An average transverse tensile strain of 1000 μin/in in the x direction (refer to Figure 2), denoted by $\bar{\varepsilon}_x$ = 1000 μin/in, is applied to a composite containing fully bonded circular and fully bonded crenulated fibers. Effects on interface stress states of increasing fiber volume fraction and crenulation amplitude are again considered.

4.1 Fully Bonded Circular Fiber, $v_f = 40\%$

As in the preceding chapter, interface stresses around a perfectly bonded circular fiber with a 40% fiber volume fraction are considered initially. The normal, shear, and tangential interface stresses induced in this model by the application of $\bar{\varepsilon}_x$ = 1000 μin/in are shown in Figures 23, 24, and 25, respectively. Here, interface stresses are normalized by the Young's modulus of the matrix times the average tensile strain in the x direction, i.e., $E_m\bar{\varepsilon}_x$ (6000 psi).

The interface normal stress is shown in Figure 23. As expected, normal stress at the interface is greatest at $\theta = 0^o$, where the loading direction is directly normal to the interface. The stresses then decrease to a minimum at $\theta = 90^o$, where the loading direction is parallel to the interface. In this transverse tension case the matrix is pulling away from the fiber due to both the applied strain and to the Poisson's contraction of the materials. Therefore, the normal stress is completely tensile in this circular fiber case. Note that in the transverse loading case, the loading and boundary conditions are not identical in the x and y directions as they were in the thermal loading case. The normal stress state is therefore no longer symmetric about $\theta = 45^o$.

Similarly, the shear stress component, shown in Figure 24, is no longer antisymmetric about $\theta = 45^o$. It reaches a minimum value at a θ value slightly greater than 45^o and again goes to zero at $\theta = 0^o$and $\theta = 90^o$. The zero values at $\theta = 0^o$and $\theta = 90^o$ might be expected due to the symmetry of the model. The shear stress is negative at all circumferential locations for this circular fiber case.

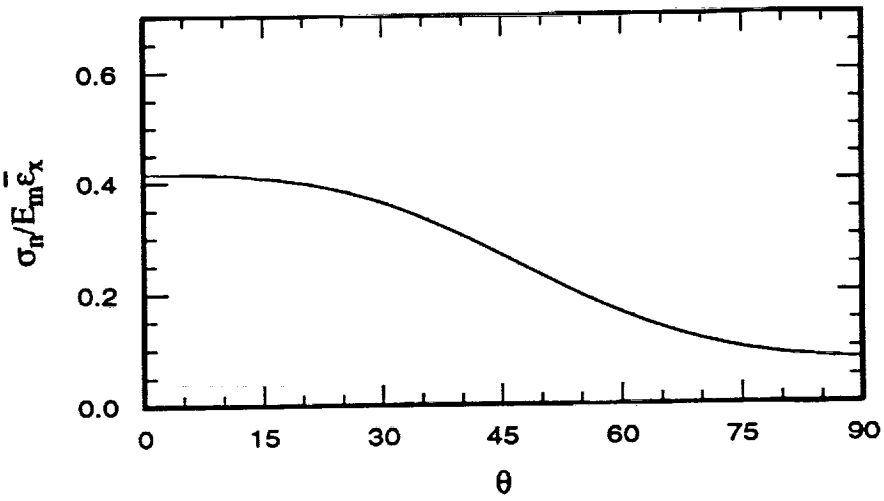

Figure 23. Interface Normal Stress Due to Transverse Strain for Fully Bonded Circular Fiber, $v_f = 40\%$

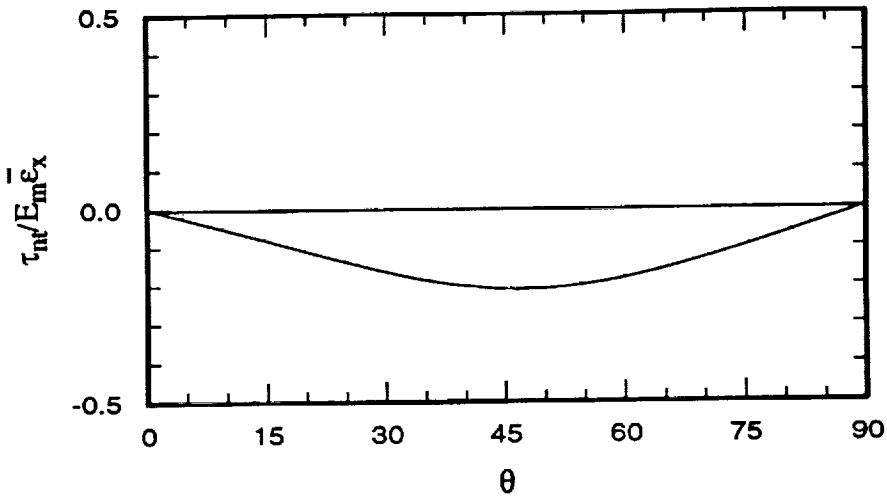

Figure 24. Interface Shear Stress Due to Transverse Strain for Fully Bonded Circular Fiber, $v_f = 40\%$

The tangential stresses at the interface in the fiber and the matrix, shown in Figure 25, are highest at $\theta = 90^o$, where the loading direction is parallel to the interface, and lowest at $\theta = 0^o$, where loading is directly normal to the interface. Note, the fiber tangential stress is

completely tensile and increases in magnitude from $\theta = 0^o$ to $\theta = 90^o$. The tangential stress in the matrix is actually negative near $\theta = 0^o$and rises to a maximum tensile value at $\theta = 90^o$ that is three times the maximum value reached in the fiber. This occurs because the Young's modulus of the matrix in the x-y plane is higher than that of the fiber.

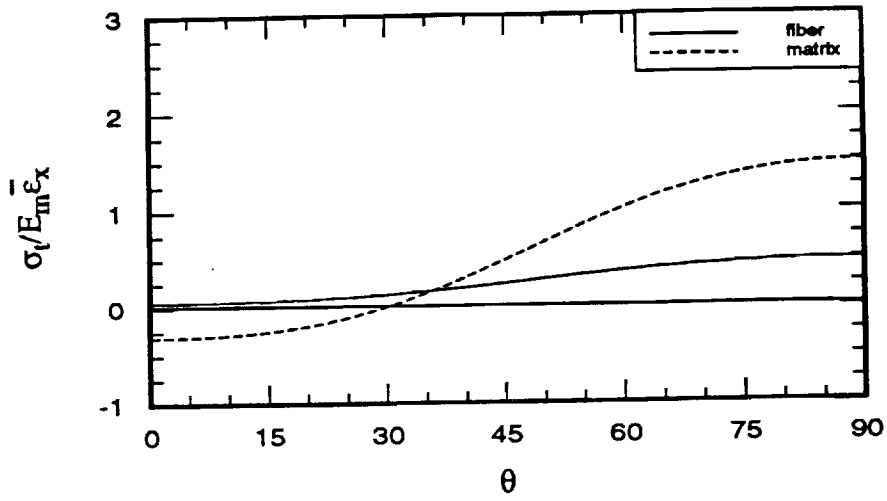

Figure 25. Interface Tangential Stress Due to Transverse Strain for Fully Bonded Circular Fiber, $v_f = 40\%$

4.2 Fully Bonded Crenulated Fiber, $\alpha = 0.02$, $v_f = 40\%$

Next, the transverse loading of a composite containing fibers with crenulation amplitude $\alpha = 0.02$ is presented and compared to the circular fiber stress states just discussed. The three interface stress components for this case are shown in Figures 26, 27, and 28. The circular data are included in each figure. As before, the diamond shaped markers which indicate the θ locations of the peaks in the fiber crenulation are also included.

Examination of Figure 26, the normal stress component, shows that the existence of crenu-

lation results in variations in the stress state about the circular stress level. At this crenulation amplitude, however, the stresses appear to follow the general trend of the circular fiber stresses. Note, the maximum normal stress about the crenulated fiber is greater than that about the circular fiber and occurs near $\theta = 25^{o}$, not at $\theta = 0^{o}$, as in the circular case. Also, the minimum normal stress is lower than that in the circular case, although the entire stress state remains tensile. Here, the local maxima in the stress state do not correspond to the location of the crenulation peaks as in the thermal loading case. The θ locations of the crenulation peaks lie between the local maxima and minima of the stress variations and appear to shift toward the minima locations as θ values approach 90^{o}.

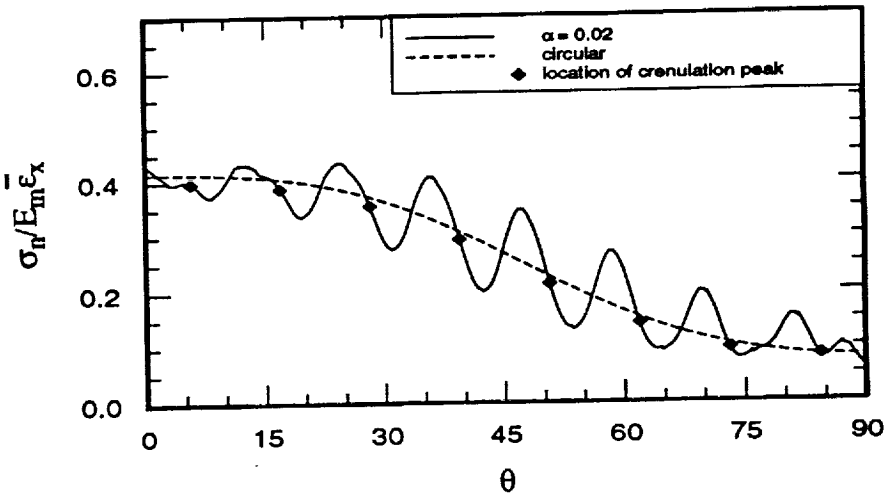

Figure 26. Interface Normal Stress Due to Transverse Strain for Fully Bonded Crenulated Fiber, $\alpha = 0.02$, $v_f = 40\%$

The variations in stress introduced by the fiber crenulation are again seen in Figure 27, which shows the interface shear stress. Here, the maximum negative shear stress occurs at a greater θ location than in the circular case and is greater in magnitude. Also, both positive and negative shear stresses are seen, with the largest positive shear stresses occurring

near $\theta = 0^o$ and $\theta = 90^o$. The location of the peaks in fiber crenulation fall between the local maximum and minimum of the stress variations. Except near $\theta = 0^o$ and $\theta = 90^o$, these locations are no longer at the points where the crenulated and circular stress data coincide. Recall that in the thermal loading case, Figure 13, the points where the stress data for the crenulated and circular fiber coincide did correspond to the peaks in the crenulation amplitudes.

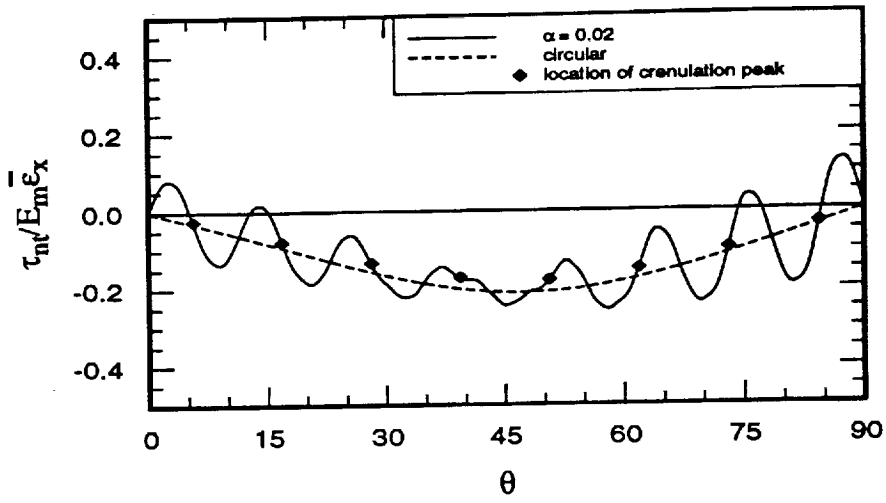

Figure 27. Interface Shear Stress Due to Transverse Strain for fully Bonded Crenulated Fiber, $\alpha = 0.02$, $v_f = 40\%$

The tangential stresses at the interface in both the fiber and the matrix are shown in Figure 28. The variations in the stresses due to the fiber crenulation appear to be greater in the matrix than in the fiber but, on a percentage basis, are about the same. In both materials the maximum tangential stresses about the crenulated fiber are greater than those about the circular fiber, and they occur at a θ location slightly less than 90^o. Here, the locations of the crenulation peaks appear to correspond to the local minima in stress in both the fiber and the matrix near $\theta = 0^o$. This relationship then changes, however, so that near $\theta = 90^o$

the locations of crenulation peaks correspond to the local maxima in the tangential stresses.

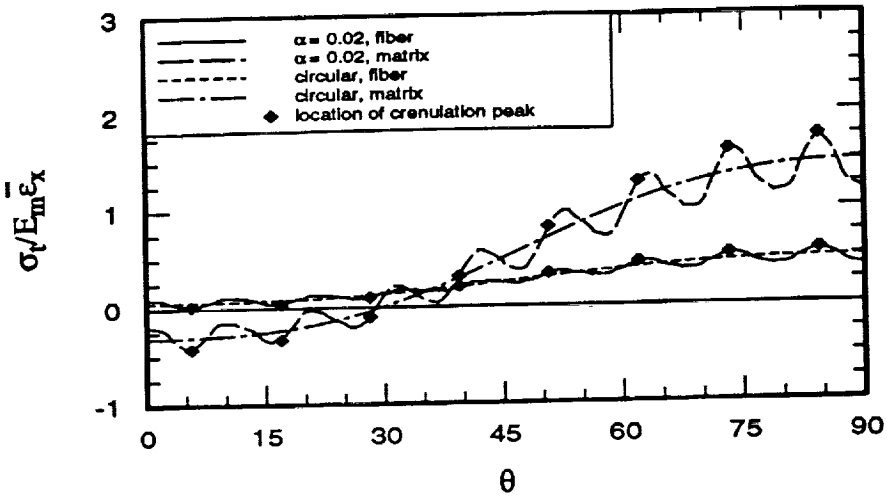

Figure 28. Interface Tangential Stress Due to Transverse strain for Fully Bonded Crenulated Fiber, $\alpha = 0.02$, $v_f = 40\%$

4.3 Fully Bonded Crenulated Fiber, $\alpha = 0.05$, $v_f = 40\%$

The effect on the interface stresses of increasing the crenulation amplitude from $\alpha = 0.02$ to $\alpha = 0.05$, while the fiber volume fraction is kept constant at 40%, is now considered. The three interface stress components in a composite containing these more deeply crenulated fibers under transverse tensile loading are shown in Figures 29, 30, and 31. The circular fiber data and the data previously presented for a fiber with a crenulation amplitude of $\alpha = 0.02$ are also shown on each figure.

Examination of Figure 29 shows that the variations in the interface normal stress are much greater at the higher crenulation amplitude. The stresses about the fiber with crenulation

amplitude $\alpha = 0.05$ no longer follow the general trend of the stresses about the circular fiber. The stress state instead appears to have its own mean variation with θ. The maximum normal stress, which occurred at $\theta = 0^o$ in the circular case, and near $\theta = 25^o$ in the mildly crenulated case, now occurs near $\theta = 35^o$ with this higher crenulation amplitude. All normal interface stresses remain tensile, however. The locations of the crenulation peaks again occur between local maxima and minima in the normal stress state and shift toward the minima near $\theta = 90^o$. Note that the higher crenulation amplitude leads to "higher harmonics" or additional variations in the normal stress.

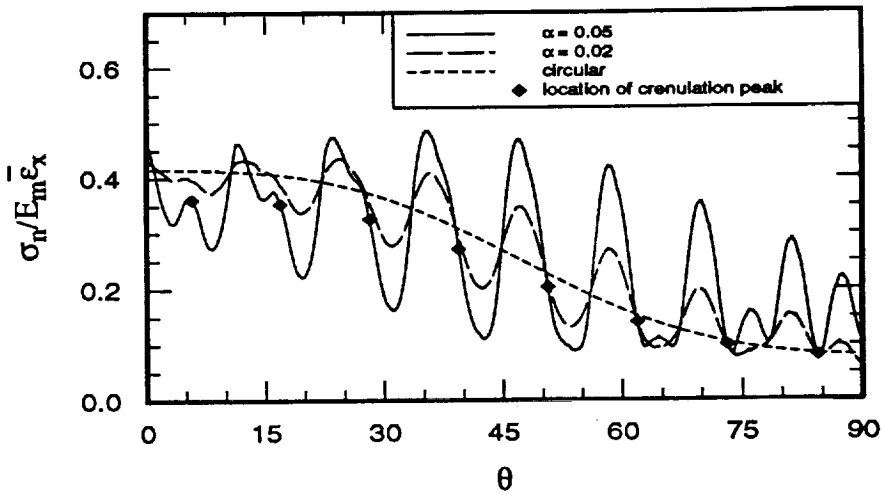

Figure 29. Interface Normal Stress Due to Transverse Strain for Fully Bonded Crenulated Fiber, α=0.05, $v_f = 40\%$

Similar results are seen in Figure 30, which shows the shear stress component for the circular fiber case and for crenulation amplitudes $\alpha = 0.02$ and $\alpha = 0.05$. The variations in stress about the circular level are much greater at the higher crenulation amplitude. The positive shear stresses which arise near $\theta = 0^o$ and $\theta = 90^o$ in the crenulated case increase in magnitude as crenulation amplitude is increased. As before, the θ locations of the

crenulation peaks correspond to values which are between local maxima and minima in the stress data but, once again, they coincide with the circular stress data only near $\theta = 0^o$ and $\theta = 90^o$. At the higher crenulation amplitude additional stress variations, i.e., "higher harmonics", are also seen near $\theta = 45^o$.

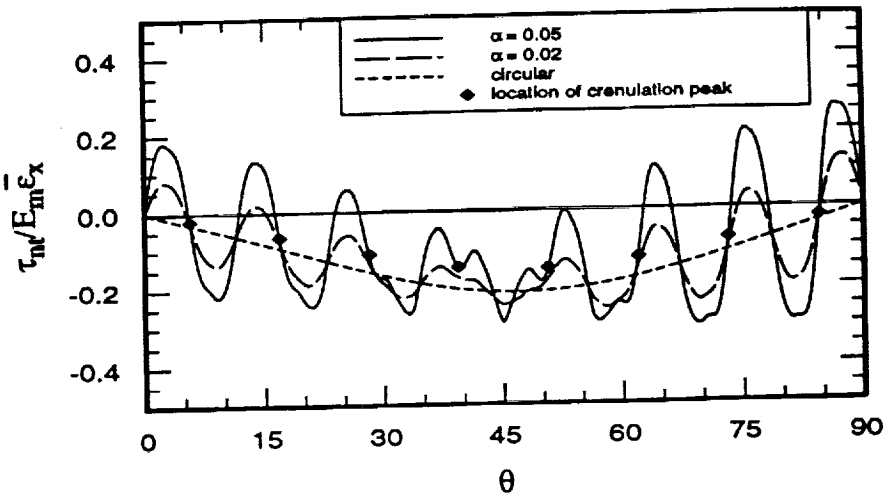

Figure 30. Interface Shear Stress Due to Transverse Strain for Fully Bonded Crenulated Fiber, $\alpha = 0.05$, $v_f = 40\%$

The fiber and matrix tangential stresses are shown in Figure 31. Increasing fiber crenulation amplitude again increases the stress variation about the circular stress level. Here, on a percentage basis, near $\theta = 90^o$, variations in the fiber are larger than those in the matrix. The relationship of the stress variation to the locations of the fiber crenulation peaks is the same as noted at the lower crenulation amplitude, with the peaks corresponding to local minima near $\theta = 0^o$ and to local maxima near $\theta = 90^o$. Note, particularly high stress concentrations occur near $\theta = 90^o$ in the matrix.

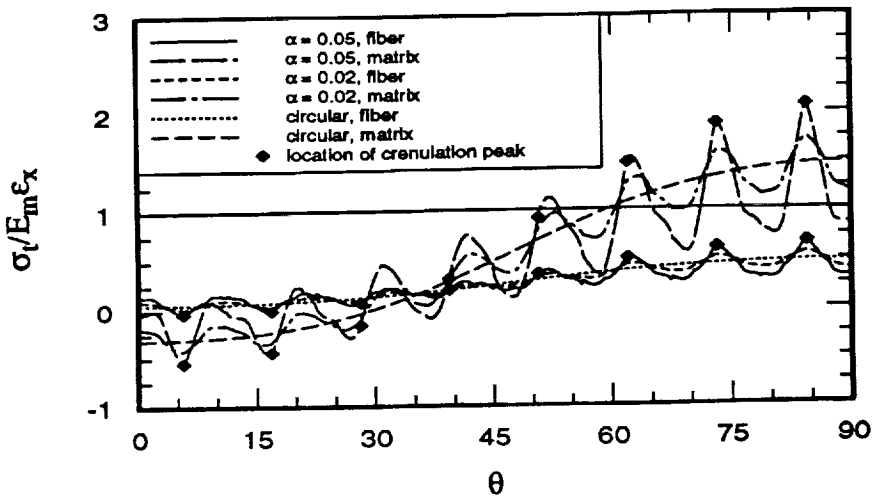

Figure 31. Interface Tangential Stress Due to Transverse Strain for Fully Bonded Crenulated Fiber, $\alpha = 0.05$, $v_f = 40\%$

4.4 Effect of Increasing Fiber Volume Fraction on Stresses Due to Transverse Strain: Fully Bonded Case

As in the previous chapter, the effect on the interface stress state of increasing the fiber volume fraction from 40% to 60% will now be considered. The three interface stress components about circular fibers and fibers with crenulation amplitudes of $\alpha = 0.02$ and $\alpha = 0.05$ at 60% fiber volume fraction are shown in Figures 32, 33, and 34. These figures are graphed on the same scale as Figures 29, 30, and 31 to facilitate comparison.

Comparison of Figures 29 and 32 shows that increasing fiber volume fraction causes a slight overall downward trend in the normal stress level. However, relative to the circular case, the variations in the stresses due to the fiber crenulation appear to be slightly larger at the higher fiber volume fraction. The minimum interface normal stress appears to be

slightly lower, and a greater maximum normal stress is reached at 60% fiber volume fraction. The relationship between the locations of the crenulation peaks and the variations in the stress states are the same at this higher fiber volume fraction and all normal stresses remain tensile. The perturbations in stress ("higher harmonics") which were seen previously near $\theta = 90^{o}$ for the deeper crenulation amplitude at 40% fiber volume fraction are also present at a fiber volume fraction of 60%.

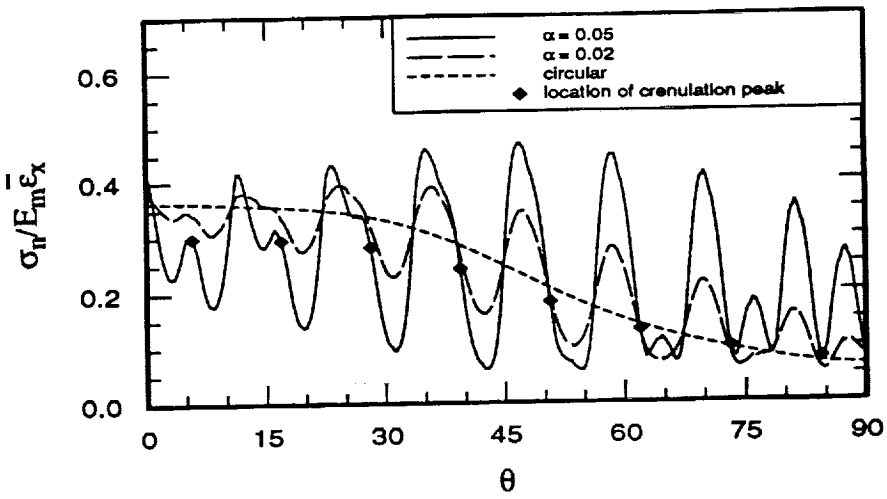

Figure 32. Interface Normal Stress Due to Transverse Strain for Fully Bonded Crenulated Fibers, $\alpha = 0.02$ and $\alpha = 0.05$, $v_f = 60\%$

Comparison of Figures 30 and 33, the interface shear stresses, shows that increasing fiber volume fraction has little effect on the variations in the interface shear stresses about the crenulated fibers, except to change their amplitudes slightly. As a result, a greater maximum shear stress is seen at this higher fiber volume fraction. The location of the crenulation peaks fall between the local maxima and minima of the stress variations at both fiber volume fractions and the additional variations in stress that arise at the higher crenulation amplitude are seen at both fiber volume fractions.

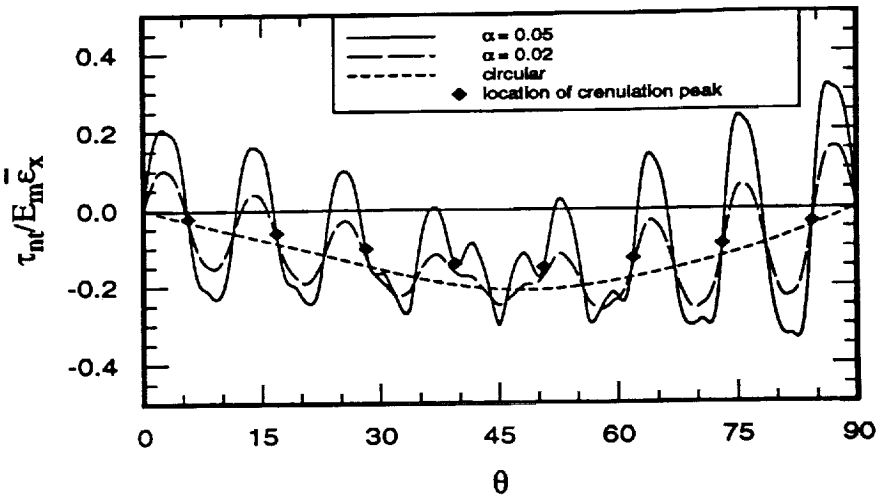

Figure 33. Interface Shear Stress Due to Transverse Strain for Fully Bonded Crenulated Fibers, $\alpha = 0.02$ and $\alpha = 0.05$, $v_f = 60\%$

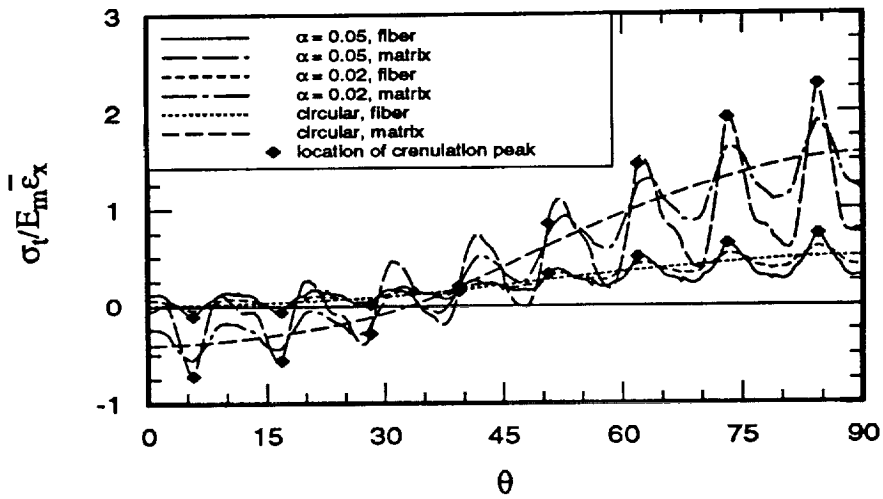

Figure 34. Interface Tangential Stress Due to Transverse Strain for Fully Bonded Crenulated Fibers, $\alpha = 0.02$ and $\alpha = 0.05$, $v_f = 60\%$

A comparison of the tangential stress components, which are shown in Figures 31 and 34, shows stress variations are increased at the higher fiber volume fraction. Greater stress

variations are seen in both the fiber and the matrix, with particularly high stress concentrations seen near $\theta = 90^{o}$ in the matrix. The relationship between the location of the crenulation peaks and the local maxima and minima of the stress states is again similar to that seen at the lower fiber volume fraction.

4.5 Discussion of Variations in Stress Due to Transverse Strain: Fully Bonded Case

Again, it is of interest to quantify the level of variation in the stress components relative to the circular case. The values of the maximum variation in each stress component relative to the circular stress level, as defined in equation 15, are shown in Figure 35. From each figure it is obvious that variations in stress increase with increases in crenulation amplitude and with increases in fiber volume fraction. However, the effect of these increases is much greater in the tangential stress component in the matrix than in any of the other stress components. Recall from Figure 22, particularly high stress concentrations were seen in the tangential stress component in the matrix material as crenulation amplitude and fiber volume were increased for the fully bonded fiber case and a temperature change.

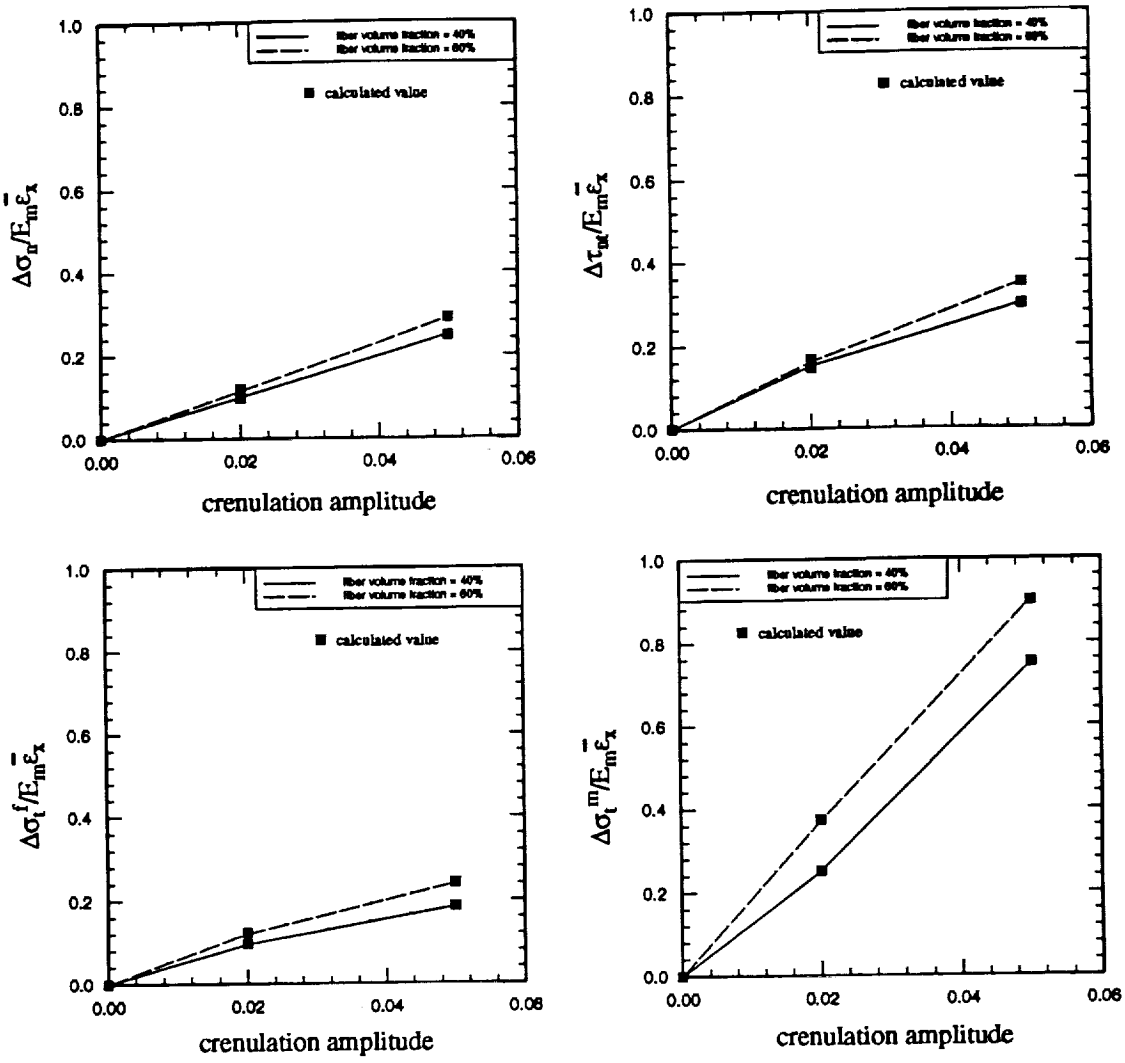

Figure 35. Comparison of Maximum Stress Variations Due to Transverse Strain for Fully Bonded Fibers

4.6 Composite Properties: Transverse Modulus and Poisson's Ratio

The composite properties for the case of transverse straining of the fully bonded case, as

well as those for the disbonded cases to be discussed in the following two chapters, are shown in Table 2. Recall, the constituent material properties were given by equations 13 and 14. Here the average transverse modulus of the composite, $\bar{E}_x$, is taken as the average stress $\bar{\sigma}_x$ along the right edge (x = 0.5) of the quarter model divided by the applied average tensile strain of 1000 μin/in. That is,

$$\bar{E}_x = \frac{\bar{\sigma}_x}{\bar{\varepsilon}_x} \tag{19}$$

The Poisson's ratio, ν_{xy}, is taken as the total strain in the y direction of the unit cell (twice the displacement of the nodes along y = 0.5 in the quarter model, divided by l_y = 1.0), divided by the applied average tensile strain, i.e.,

$$\upsilon_{xy} = -\frac{\varepsilon_y}{\bar{\varepsilon}_x} \tag{20}$$

where

$$\varepsilon_y = \frac{\Delta y}{l_y} \tag{21}$$

Then ν_{xz} is equal to the z direction strain of the model given by the displacement of the first extra node in the ABAQUS model, divided by $\bar{\varepsilon}_x$ or,

$$\upsilon_{xz} = -\frac{\varepsilon_z}{\bar{\varepsilon}_x} \tag{22}$$

The computed composite properties once again are seen to lie between the corresponding properties of the fiber and the matrix which were given in Chapter 2. Note, $\bar{E}_x$ decreases as fiber volume is increased, as does ν_{xz}. The Poisson's ratio ν_{xy} increases with increasing fiber volume fraction. Also, increases in crenulation amplitude appear to have little effect

on the composite properties at each fiber volume fraction for this fully bonded case.

In the next two chapters variations in interface stresses induced by the same transverse tensile strain and due to increasing crenulation amplitude and fiber volume fraction will be presented. These interface stresses will be for a composite containing completely disbonded circular and crenulated fibers, however.

Table 2: Composite Transverse Elastic Properties

			E_x (Msi)	ν_{xy}	ν_{xz}
Fully Bonded	$v_f = 40\%$	circular	4.082	0.396	0.055
		$\alpha = 0.02$	4.083	0.396	0.055
		$\alpha = 0.05$	4.075	0.396	0.055
	$v_f = 60\%$	circular	3.319	0.412	0.033
		$\alpha = 0.02$	3.316	0.412	0.033
		$\alpha = 0.05$	3.303	0.413	0.033
No-Fiber	$v_f = 40\%$	circular	2.401	0.166	0.203
		$\alpha = 0.02$	2.393	0.166	0.202
		$\alpha = 0.05$	2.365	0.164	0.200
	$v_f = 60\%$	circular	1.329	0.081	0.170
		$\alpha = 0.02$	1.315	0.080	0.168
		$\alpha = 0.05$	1.259	0.077	0.161
Fully Disbonded $\Delta = 10^{-5}$	$v_f = 40\%$	circular	2.401	0.158	*NA
		$\alpha = 0.02$	2.395	0.153	*NA
		$\alpha = 0.05$	2.374	0.136	*NA
	$v_f = 60\%$	circular	1.328	0.081	*NA
		$\alpha = 0.02$	1.316	0.076	*NA
		$\alpha = 0.05$	1.271	0.031	*NA
Fully Disbonded $\Delta = 10^{-6}$	$v_f = 40\%$	circular	2.402	0.155	*NA
		$\alpha = 0.02$	2.396	0.150	*NA
		$\alpha = 0.05$	2.376	0.133	*NA
	$v_f = 60\%$	circular	1.328	0.079	*NA
		$\alpha = 0.02$	1.317	0.071	*NA
		$\alpha = 0.05$	1.269	0.026	*NA

*Fiber and matrix are not acting together, therefore this property is undefined.

5.0 Response Due to Transverse Tensile Strain: No-Fiber Case

The first case of complete fiber/matrix disbond, that in which the gap between the fiber and the matrix is large enough that the two materials do not interact for the cases considered, even under loading, is investigated in this chapter. As stated previously, this extreme of disbond is modeled by considering the matrix alone, containing a fiber-shaped hole. As in the previous chapters, a composite containing circular fibers, or in this case, circular-shaped holes, with a volume fraction of 40% is examined initially as a basis for comparison. The stresses in the matrix at the edge of the fiber-shaped hole are presented here as "interface" stresses. The effect on these stresses of increasing volume fraction and amplitude of crenulation will be considered in this chapter. Note, for this no-fiber case the interface corresponds to a free surface of the matrix. All normal and shear stresses on this surface must therefore be zero. Thus, only the tangential component of stress in the matrix along the surface of the hole is of interest and will be presented here.

5.1 Circular Shaped Hole, $v_f = 40\%$

The tangential stress in the matrix at the edge of a circular-shaped hole of 40% volume

fraction is shown in Figure 36. As an aid in interpreting the data, the interface tangential stress in the matrix for the fully bonded fiber case, which was presented in the previous chapter, is included in the figure. Note, the lack of interaction between the fiber and the matrix in the no-fiber case results in higher tangential stresses in the matrix, except in the range $30^o < \theta < 45^o$, where stresses for the fully bonded case and the no-fiber case are nearly identical. In both cases tangential stresses are compressive over the range $0^o < \theta < 30^o$ and rise to maxima at $\theta = 90^o$. An effective stress concentration of 1.75 is seen in the no-fiber case at $\theta = 90^o$ where, for the fully bonded case, an effective stress concentration of 1.5 is seen. That the no-fiber case results in higher tangential stresses is important. With a fiber filling the hole in the matrix, some of the transverse load passes from the matrix to the fiber through the interface in the form of normal and shear stresses. Thus, the matrix, particularly near $\theta = 90^o$, does not have to transmit as much of the transverse load as it must when no fiber is present.

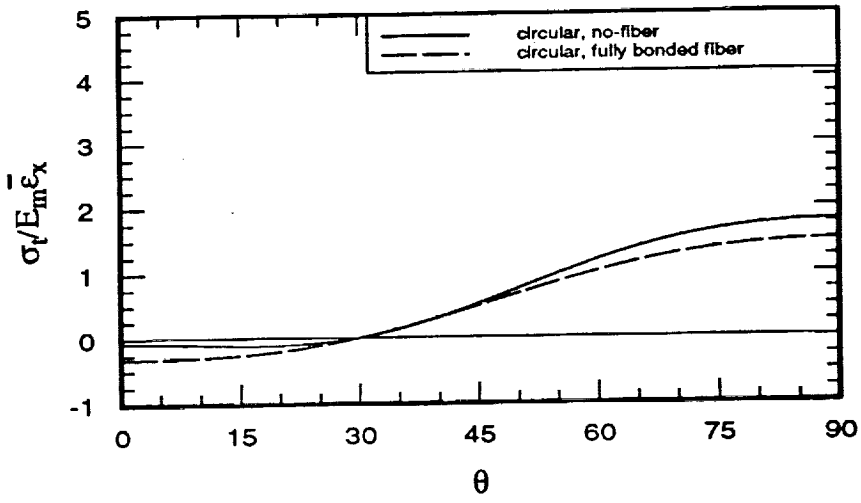

Figure 36. Tangential Stress Due to Transverse Strain at Circular-Shaped Hole, $v_f = 40\%$

5.2 Crenulated Shaped Hole, $\alpha = 0.02$, $v_f = 40\%$

The effect of introducing a mild crenulation, $\alpha = 0.02$, in the fiber-shaped hole on the stresses in the matrix is shown in Figure 37. The interface tangential stress in the matrix for the fully bonded fiber with $\alpha = 0.02$ and $v_f = 40\%$ is also included in the figure. As in previous chapters, the diamond shaped markers indicate the θ locations of the peaks in crenulation. For both the no-fiber and the fully bonded cases, these peaks appear to correspond to the locations of the local minima in the stress variation near $\theta = 0^o$. The data then shifts, however, so that the peaks in crenulation correspond to the locations of the local maxima in the stress variations near $\theta = 90^o$. As was seen in Figure 36, lack of interaction between the fiber and the matrix causes an increase in the stresses in the matrix. The greatest increases occur near $\theta = 90^o$. Note, however, that the local variations in the tangential stress for $\theta \leq 55^o$ are smaller in the no-fiber case than in the fully bonded case. Also, at certain θ locations in the range $20^o \leq \theta \leq 55^o$ the stresses seen in the fully bonded case are greater than those seen in the no-fiber case.

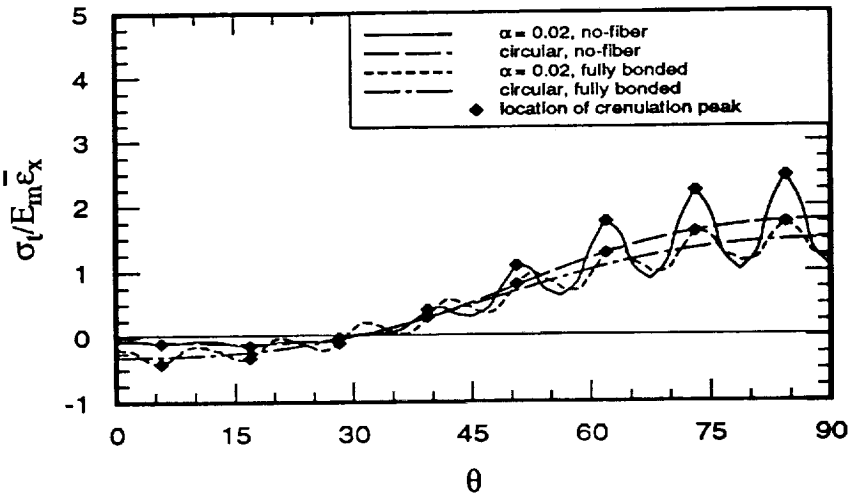

Figure 37. Tangential Stress Due to Transverse Strain at Crenulated-Shaped Hole, $\alpha = 0.02$, $v_f = 40\%$

5.3 Crenulated Shaped Hole, $\alpha = 0.05$, $v_f = 40\%$

The effect of increasing the amplitude of crenulation to $\alpha = 0.05$ on the tangential stresses in the matrix is shown in Figure 38. As seen in Chapters 3 and 4, increasing crenulation amplitude causes an increase in the local stress variations. Here, stress variations appear to increase by a factor of two relative to the circular case. The relationship between the local maxima and minima in the stress data and the locations of the crenulation peaks, as indicated by the diamond-shaped markers, is similar to that seen at the lower crenulation amplitude. A maximum effective stress concentration of 3.25 is seen at the higher crenulation amplitude, whereas the maximum stress concentrations are 2.5 and 1.75 for $\alpha = 0.02$ and the circular cases, respectively. Although the data for the perfectly bonded case is not shown on this figure, as in the two previous figures, comparison to Figure 31 shows stresses are again increased considerably due to lack of fiber/matrix interaction.

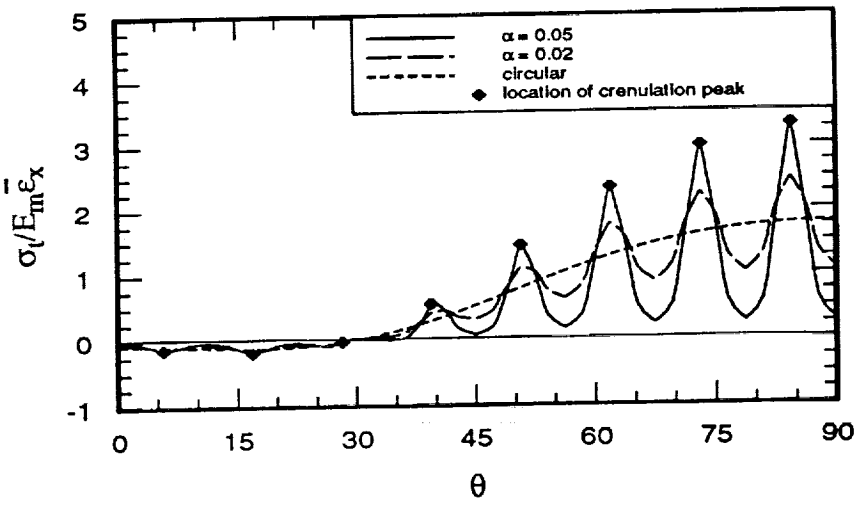

Figure 38. Tangential Stress Due to Transverse Strain at Crenulated-Shaped Hole, $\alpha = 0.05$, $v_f = 40\%$

5.4 Effect of Increasing Fiber Volume Fraction on Stresses Due to Transverse Strain: No-Fiber Case

The effect of increasing fiber volume fraction to 60% on the tangential stresses at the edge of the fiber-shaped hole is shown in Figure 39. This figure is the analog to Figure 38, but for a higher volume fraction. Recall, for the perfectly bonded case presented in the previous chapter, increasing fiber volume fraction caused the variations in the interface stresses to increase for both fiber crenulation amplitudes at all circumferential locations. For this no-fiber case, however, local maxima in the stresses at 60% fiber volume fraction are actually lower than those at $v_f = 40\%$ over the interval $25^o < \theta < 75^o$ at both crenulation amplitudes. Near $\theta = 90^o$, however, the tangential stresses for the no-fiber case are severe. The maximum stress concentration reached is 4.0 at $v_f = 60\%$, whereas that at $v_f = 40\%$, as just mentioned, is 3.25. The relationship between the location of the peaks in crenulation and the local variations in stress is the same at both volume fractions shown.

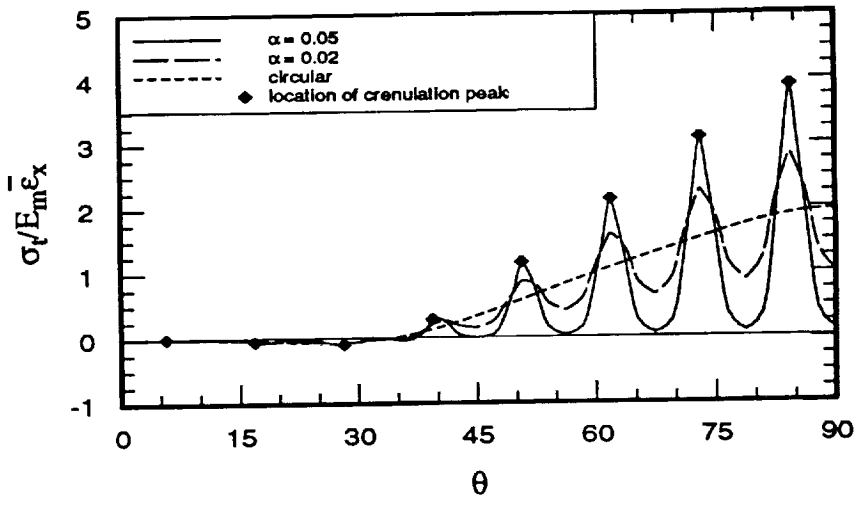

Figure 39. Tangential Stresses Due to Transverse Strain at Crenulated-Shaped Hole, $\alpha = 0.02$ and $\alpha = 0.05$, $v_f = 60\%$

5.5 Discussion of Variations in Interface Stress and Composite Properties: No-Fiber Case

The value of the maximum variations in the tangential stress in the matrix at the edge of the fiber-shaped hole relative to the circular hole stress level are shown in Figure 40. Equation 15 is a basis for this figure. As was seen in the fully bonded case, stress variations increase with both increasing volume fraction and increasing crenulation amplitude. The maximum stress variation for this no-fiber case, however, is double that seen for the fully bonded case which was shown in Figure 35.

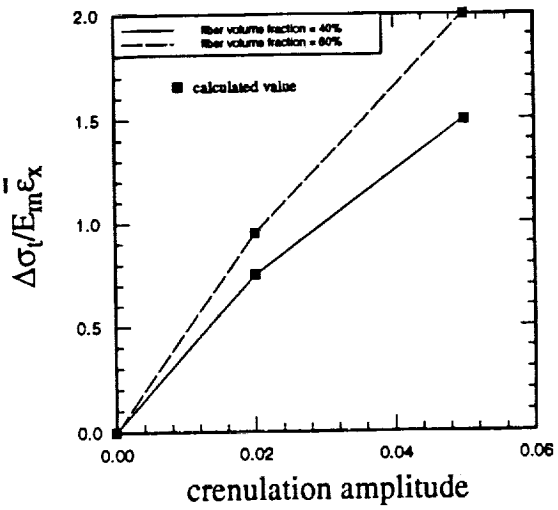

Figure 40. Comparison of Maximum Stress Variations Due to Transverse Strain for No-fiber Case

The composite properties, $\bar{E}_x$, ν_{xy}, and ν_{xz}, for this no-fiber case are given in Table 2 on page 58. Note in the table that for this no-fiber case the average transverse modulus of the composite is lower than either that of the fully bonded fiber and matrix, or the matrix

material alone. The value of $\overline{E}_x$ also decreases as the volume fraction of the fiber shaped hole is increased. The Poisson's ratio ν_{xy} is also lower in the no-fiber case than in the fully bonded case but, ν_{xz} is greater. Both Poisson's ratios decrease with increasing fiber volume fraction. Values of each composite property are still relatively constant with increasing crenulation amplitude at each fiber volume fraction but do vary more than in the fully bonded case. This is particularly apparent at $v_f = 60\%$, where each composite property appears to decrease slightly as crenulation amplitude is increased.

In the next chapter, the fully disbonded case will be considered from a different perspective. A composite which contains small gaps between the fiber and the matrix will be considered. The gap sizes chosen are small enough that fiber and matrix interact under loading. Contact will therefore occur between the fiber and the matrix at certain points along the interface as transverse tensile strain is applied. At these contact points interface normal stresses arise, in addition to the interface tangential stresses which were seen in the no-fiber case. As noted in Chapter 2, the contact surface is considered frictionless. Shear stresses can therefore not develop at the interface, even at points where the fiber and matrix contact. The influence of fiber crenulation amplitude and fiber volume fraction on the interface normal and tangential stresses will be examined in the next chapter for this representation of full fiber/matrix disbond.

6.0 Response Due to Transverse Tensile Strain: Fully Disbonded Case

As in the previous chapter, interface stresses about fully disbonded circular and crenulated fibers at two fiber volume fractions and due to a transverse tensile strain of 1000 μin/in are presented and discussed here. In the previous chapter the distance between the fiber and the matrix was assumed to be so large that no interaction occurred between the two when the composite was loaded. Here, a much smaller disbond gap is assumed so that the fiber and the matrix contact at certain points along the interface when the composite is subjected to transverse tensile strain. The stresses which arise at these points of fiber/matrix contact, as well as the interface normal and tangential stresses caused by the application of the transverse strain, are discussed in this chapter.

6.1 Geometry of the Fiber/Matrix Disbond

Before the interface stresses are presented, the geometry of the disbond must be more clearly defined. The actual disbond gap size, δ, is defined as the radial distance from the fiber to the matrix at any point along the interface. This distance is indicated by the arrows in Figure 41, which shows an enlargement of a portion of the finite element mesh along

the fiber/matrix interface. This actual distance is normalized in the analysis by the mean fiber diameter, d_o, to give the normalized disbond gap size, Δ. That is

$$\Delta = \frac{\delta}{d_o} . \tag{23}$$

Stresses in composites for each of two values of Δ are investigated here, The values of Δ considered are $\Delta = 10^{-5}$ and $\Delta = 10^{-6}$. For each of these normalized gap sizes, interface normal and tangential stresses for the values of fiber volume fraction and crenulation amplitude considered previously are discussed. As stated, the fiber/matrix interface is considered to be frictionless in this analysis. Therefore, all interface shear stresses are zero.

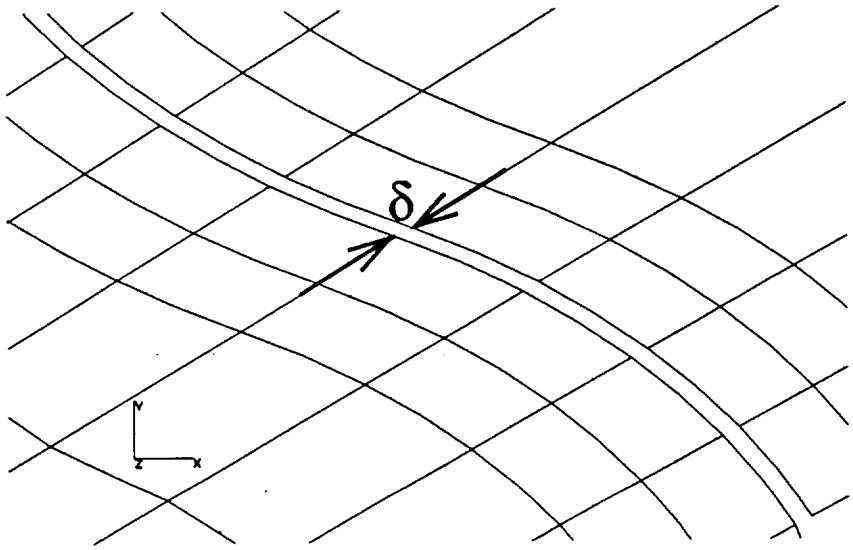

Figure 41. Geometry of the Fiber/Matrix Disbond

Maximum contact stresses are also presented in this chapter for each of the cases considered. The contact stress is defined in the finite element code ABAQUS to be the "pressure" between a node of an interface element and the slide line with which it interacts. Recall, the interface elements and slide line were defined in Chapter 2. The contact stresses between the two act in a direction which is normal to the slide line at the point of contact.

Maximum contact stresses are presented in Table 3 and will be discussed for each case shortly.

Table 3: Maximum Contact Stresses

			Contact Stress (psi)		
			Region 1	Region 2	Region 3
$\Delta = 10^{-5}$	$v_f = 40\%$	circular	303.3	no contact	no contact
		$\alpha = 0.02$	782.5	3504	no contact
		$\alpha = 0.05$	495.5	6783	8948
	$v_f = 60\%$	circular	no contact	no contact	no contact
		$\alpha = 0.02$	83.41	1373	no contact
		$\alpha = 0.05$	no contact	6888	7746
$\Delta = 10^{-6}$	$v_f = 40\%$	circular	366.2	no contact	no contact
		$\alpha = 0.02$	846.2	3606	no contact
		$\alpha = 0.05$	584.1	6774	9552
	$v_f = 60\%$	circular	82.65	no contact	no contact
		$\alpha = 0.02$	290.8	2145	no contact
		$\alpha = 0.05$	no contact	7108	8334

6.2 Fully Disbonded Circular Fiber, $\Delta = 10^{-5}$, $v_f = 40\%$

As a basis for comparison, the circular fiber case at 40% fiber volume fraction will again be presented. Here, the larger of the two gap sizes, $\Delta = 10^{-5}$ is considered first. The deformed mesh for this case is shown in Figure 42. It should be noted that actual displacements are used to create the portion of the figure which depicts the entire mesh, while dis-

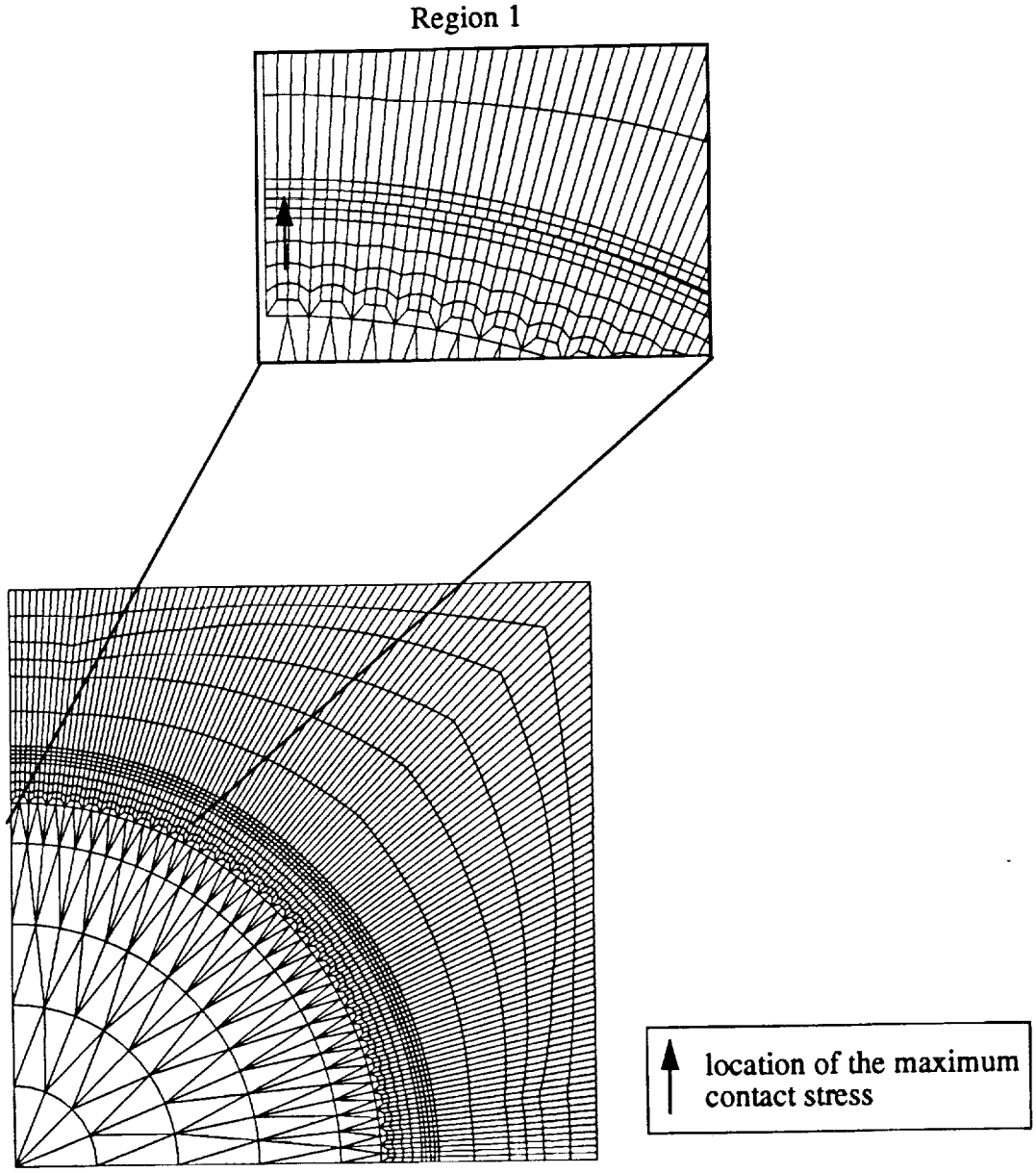

Figure 42. Deformed Mesh for Fully Disbonded Circular Fiber Case, $\Delta = 10^{-5}$, $v_f = 40\%$, Displacements in Contact Region Scaled by Factor of 10

placements in the portion of the mesh which is enlarged are scaled by a factor of 10 for viewing clarity. In this case, a region of contact between the fiber and the matrix forms near $\theta = 90^{o}$ as shown. This region is labeled Region 1 in Table 3. As the table shows, the maximum contact stress within this region for the circular fiber case is 303.3 psi. The location of this maximum is indicated in the figure by the arrow. As can be seen at the right end of the enlarged portion of the mesh, away from the contact region there is a gap between the fiber and the matrix. Also, as the radial lines of the finite element mesh in the matrix and in the fiber are not aligned, slippage of the matrix relative to the fiber is evident.

Figure 43 shows the interface normal stress in the matrix for this initial case. This and the interface stress figures which follow are scaled to facilitate comparison. Obviously the contact stresses are interpreted as compressive normal stresses in the region over which contact between the fiber and the matrix occurs. Over the remaining range of θ, normal stresses must be zero as the interface remains a free surface.

The tangential stress at the interface in the matrix for this case is shown in Figure 44. For comparison, the corresponding data for the no-fiber case, which was presented in the previous chapter, is also included in the figure. Note, the data for these two cases are nearly identical. Very small differences in the data appear over the range of θ where contact between the fiber and the matrix occurs. The stress in the disbonded case appears to be only slightly lower than that in the no-fiber case in this region. Also, for $\theta \leq 30^{o}$, the stresses in the no-fiber case are slightly more negative than those in the fully bonded case.

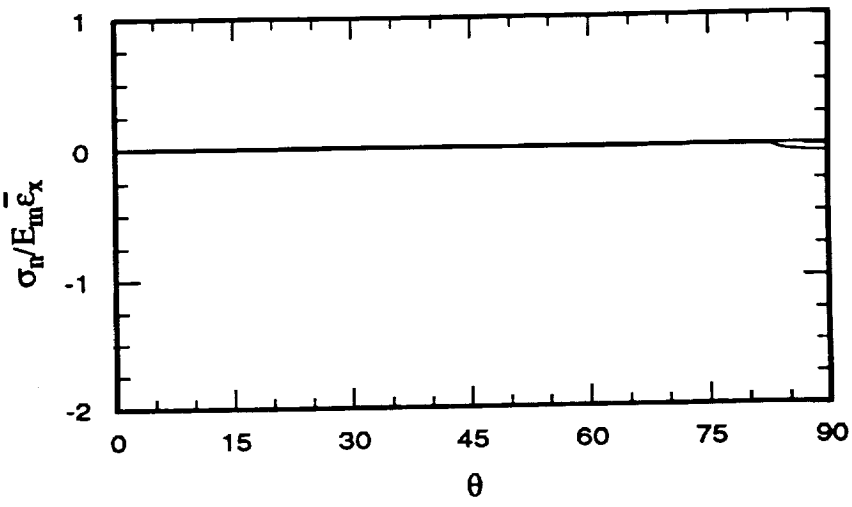

Figure 43. Interface Normal Stress Due to Transverse Strain for Fully Disbonded Circular Fiber, $\Delta = 10^{-5}$, $v_f = 40\%$

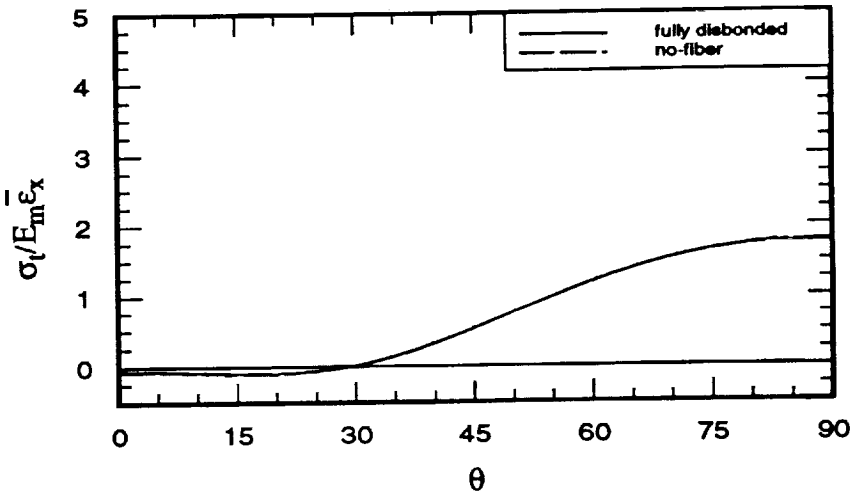

Figure 44. Interface Tangential Stress Due to Transverse Strain for Fully Disbonded Circular Fiber, $\Delta = 10^{-5}$, $v_f = 40\%$

6.3 Fully Disbonded Crenulated Fiber, $\alpha = 0.02$, $\Delta = 10^{-5}$, $v_f = 40\%$

The deformed mesh for the mildly crenulated fiber at 40% fiber volume fraction with a disbond gap $\Delta = 10^{-5}$ is shown in Figure 45. Note, the presence of fiber crenulation causes two regions of contact between the fiber and the matrix to develop. The first of these regions, that near $\theta = 90^{o}$, appears to be slightly smaller than the contact region seen in the circular fiber case. The maximum contact stress in each region is given in Table 3. The locations of these maxima are again indicated by the arrows in the figure. Here, the absolute maximum contact stress, 3504 psi, occurs in Region 2 near $\theta = 75^{o}$ and is an order of magnitude greater than that seen in the circular fiber case. Also, the maximum compressive normal stress in Region 1 is about twice that seen in the circular case. Because contact between the fiber and matrix occurs at a location other than on the peak or valley of the crenulation, it is clear that some form of interlocking is taking place between the fiber and the matrix.

The interface normal stress in the matrix for this case is shown in Figure 46. Because of the nature of the contact, the distribution of interface normal stresses degenerates to discrete peaks. The circular case data, which was just discussed, is also included in the figure. As before, the diamond shaped markers indicate the locations of the peaks in fiber crenulation. Note, the points of fiber/matrix contact where the compressive stresses arise occur at θ locations slightly greater than the locations of the two crenulation peaks which are closest to $\theta = 90^{o}$.

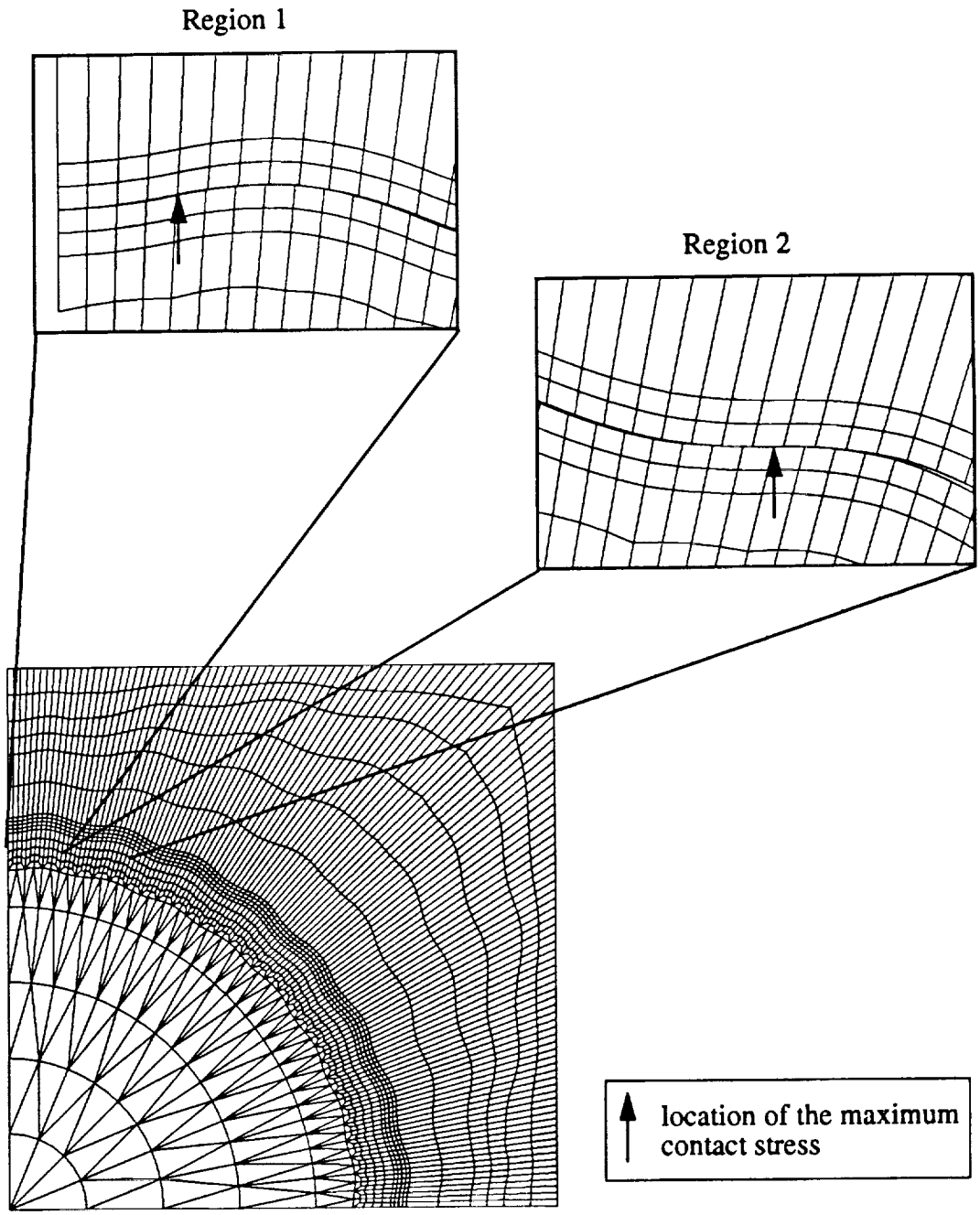

Figure 45. Deformed Mesh for Fully Disbonded Crenulated Fiber Case, $\alpha = 0.02$, $\Delta = 10^{-5}$, $v_f = 40\%$, Displacements in Contact Region Scaled by Factor of 10

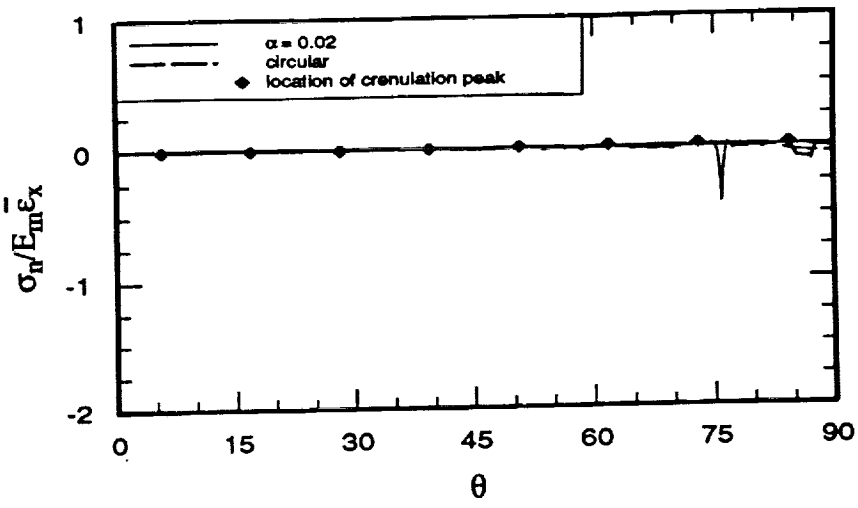

Figure 46. Interface Normal Stress Due to Transverse Strain for Fully Disbonded Crenulated Fiber, $\alpha = 0.02$, $\Delta = 10^{-5}$, $v_f = 40\%$

The tangential stress at the interface in the matrix for this mildly crenulated case is shown in Figure 47. As expected, the introduction of fiber crenulation causes stress variations above and below the circular stress level. Comparison of this figure and the corresponding figure for the no-fiber case (Figure 37) shows these two stress states are nearly identical. Only slight variations are seen in the fully disbonded case near the θ locations at which fiber/matrix contacts occur. As in the no-fiber case, the locations of the peaks in fiber crenulation correspond to local minima in the tangential stress near $\theta = 0^o$ and to local maxima near $\theta = 90^o$.

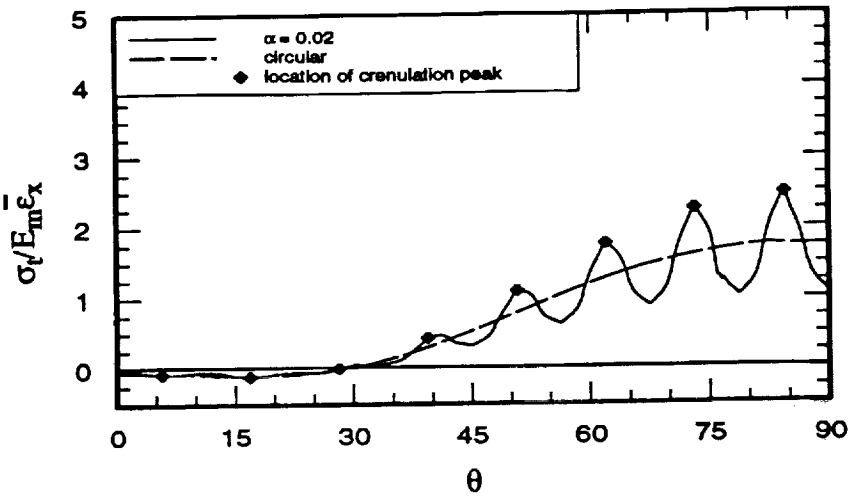

Figure 47. Interface Tangential Stress Due to Transverse Strain for Fully Disbonded Crenulated Fiber, $\alpha = 0.02$, $\Delta = 10^{-5}$, $v_f = 40\%$

6.4 Fully Disbonded Crenulated Fiber, $\alpha = 0.05$, $\Delta = 10^{-5}$, $v_f = 40\%$

The effect on interface stresses of increasing crenulation amplitude to $\alpha = 0.05$ while fiber volume fraction and gap size are kept constant is shown in Figure 48. Here, the deformed mesh shows three regions of contact between the fiber and the matrix. Note, the first and second of these regions are slightly smaller than those which occur with $\alpha = 0.02$. As shown in Table 3, the maximum contact stress occurs in Region 3 near $\theta = 65^{o}$, that contact stress being 8948 psi. Also, the maximum stress in Region 2 in this case is nearly twice that seen with the lower crenulation amplitude, but the contact stress in Region 1 is much lower than that with $\alpha = 0.02$. Note that increasing the crenulation amplitude moves the region of most severe contact away from $\theta = 90^{o}$.

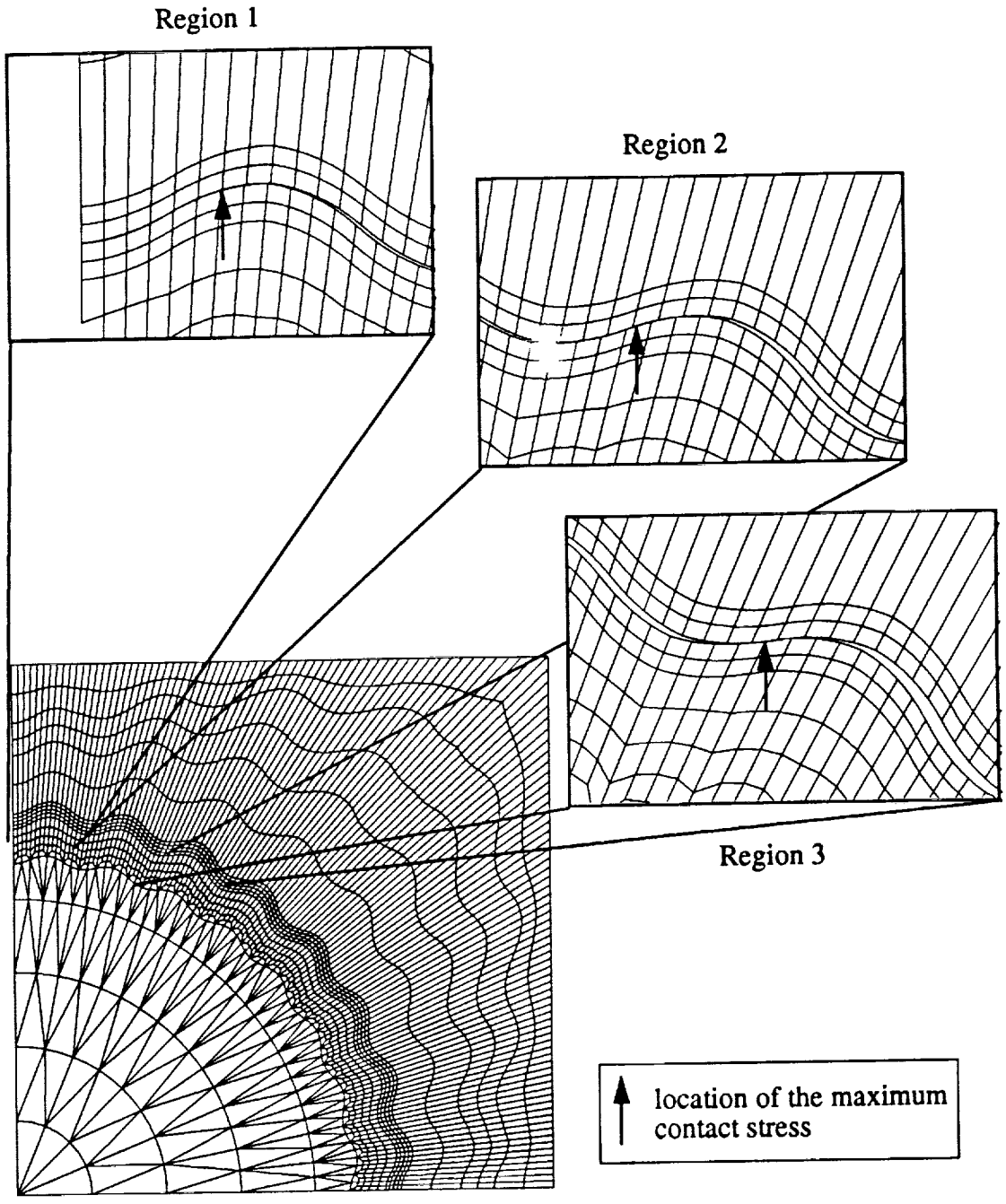

Figure 48. Deformed Mesh for Fully Disbonded Crenulated Fiber Case, $\alpha = 0.05$, $\Delta = 10^{-5}$, $v_f = 40\%$, Displacements in Contact Region Scaled by Factor of 10

The interface normal stress for this higher crenulation amplitude is shown in Figure 49, the distribution reducing to discrete peaks. As just discussed, the maximum compressive normal stress occurs in Region 3 near $\theta = 65^o$, and high compressive stresses also occur in Region 2, but stresses near $\theta = 90^o$ appear to be much smaller, on the order of those in the circular case. These high compressive normal stresses again occur at θ locations that are slightly greater than the locations of the peaks in fiber crenulation. Slight tensile interface normal stresses also appear at the locations which correspond to the peaks in fiber crenulation for $\theta > 45^o$. These anomalous tensile stresses are a result of the numerical scheme used in modeling the contact region.

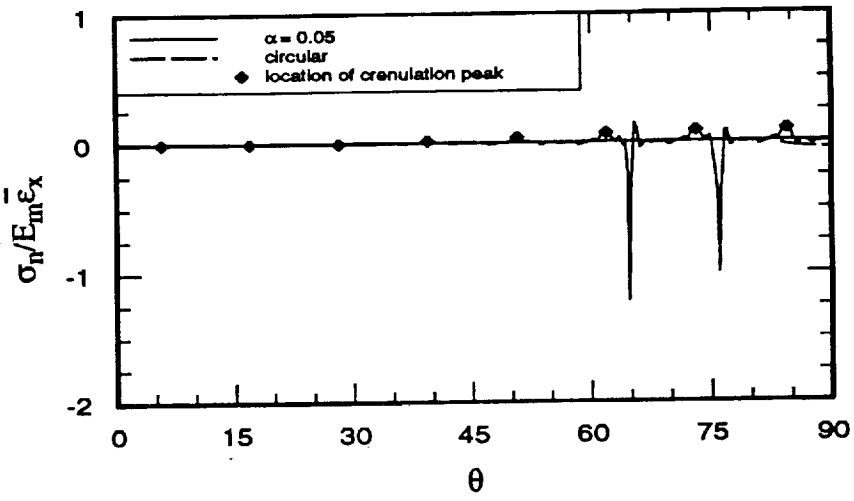

Figure 49. Interface Normal Stress Due to Transverse Strain for Fully Disbonded Crenulated Fiber, $\alpha = 0.05$, $\Delta = 10^{-5}$, $v_f = 40\%$

The interface tangential stress for this more deeply crenulated case is shown in Figure 50. As expected, increasing crenulation amplitude increases the variations in the tangential stress about the circular case stress level. The crenulation peaks again correspond to local minima near $\theta = 0^o$ and local maxima near $\theta = 90^o$. Comparison of this figure to Figure

38, which shows the corresponding no-fiber case, again shows little difference exists between the two cases except at the locations of contact between the fiber and the matrix. In these locations slight additional variations in the tangential stress arise in the fully disbonded case.

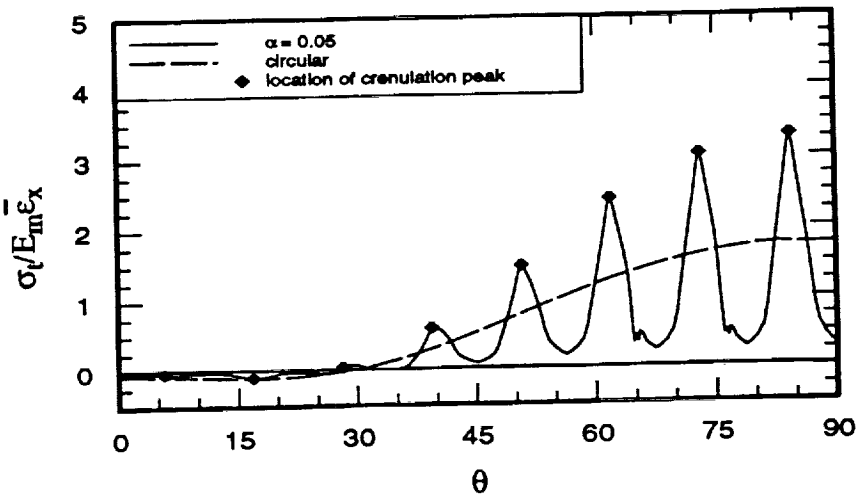

Figure 50. Interface Tangential Stress Due to Transverse Strain for Fully Disbonded Crenulated Fiber, $\alpha = 0.05$, $\Delta = 10^{-5}$, $v_f = 40\%$

6.5 Effect of Increasing Fiber Volume Fraction on Stresses Due to Transverse Strain: Fully Disbonded Case, $\Delta = 10^{-5}$

As shown in Table 3, no contact occurs between the fiber and the matrix for the circular fiber case with 60% fiber volume fraction and with a disbond gap size $\Delta = 10^{-5}$. This occurs in this case because the Poisson's contraction of the matrix near $\theta = 90^{o}$ causes the gap between the fiber and the matrix to open. Interface normal stresses must therefore be zero at all circumferential locations. Interface tangential stresses would be identical to those shown in the corresponding no-fiber case.

The deformed mesh for the mildly crenulated case at 60% fiber volume fraction with a disbond gap of $\Delta = 10^{-5}$ is shown in Figure 51. As was true at 40% fiber volume fraction, two regions of contact are seen. Comparison with Figure 45 shows that these regions are slightly smaller than those which arise at 40% fiber volume fraction. The maximum contact stresses still occurs in Region 2, the value being 1373 psi. However, the maximum stresses in both regions of contact are lower than those seen at 40% fiber volume fraction.

The interface normal stress in the matrix for this case is shown in Figure 52. The two regions of compressive normal stresses are seen here. The relationship between the location of the crenulation peaks and the locations of the fiber/matrix contact remains the same at this higher fiber volume fraction. The tangential interface stress in the matrix would again appear nearly identical to that shown previously for the no-fiber case and is therefore not presented here.

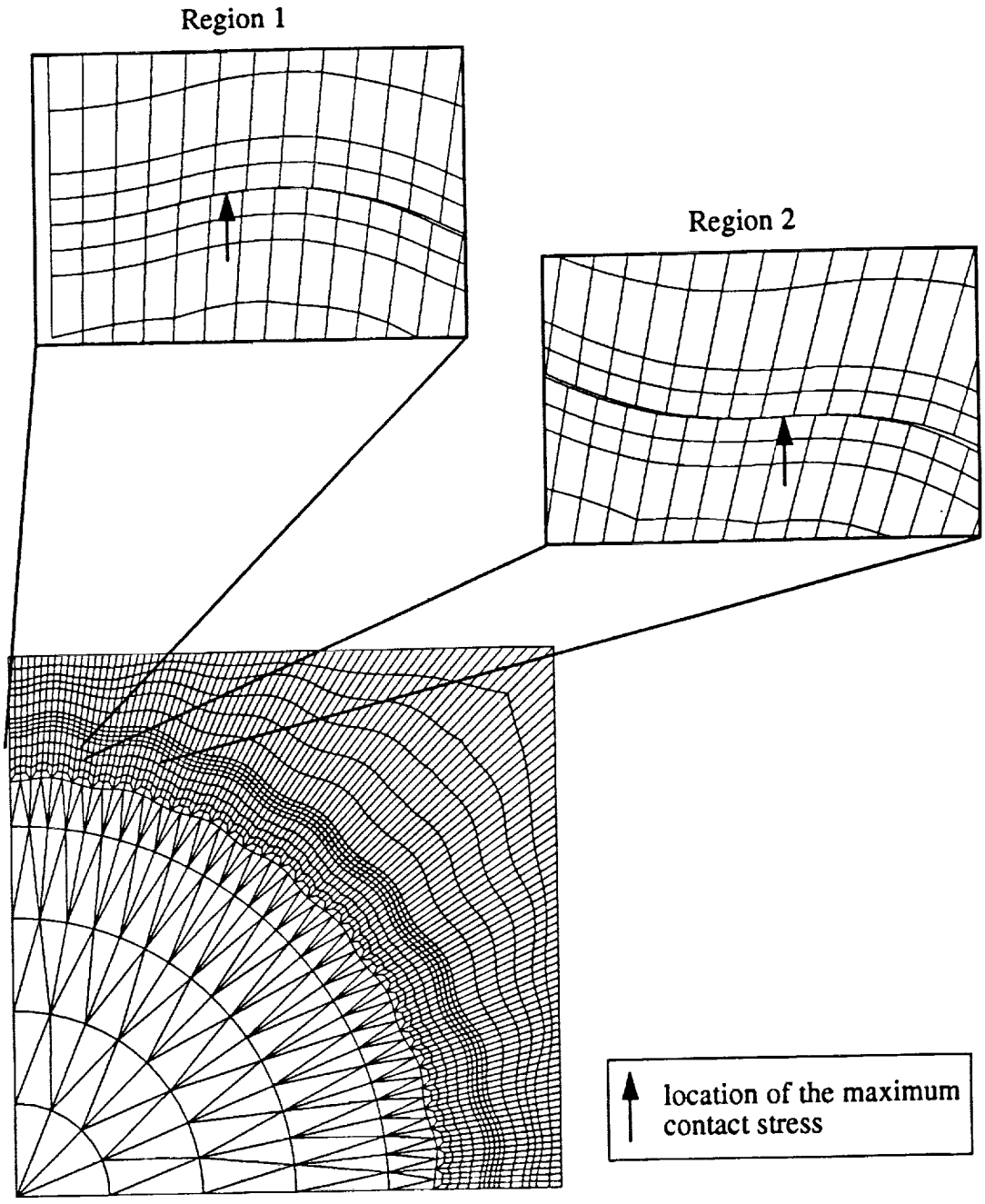

Figure 51. Deformed Mesh for Fully Disbonded Crenulated Fiber Case, $\alpha = 0.02$, $\Delta = 10^{-5}$, $v_f = 60\%$, Displacements in Contact Region Scaled by Factor of 10

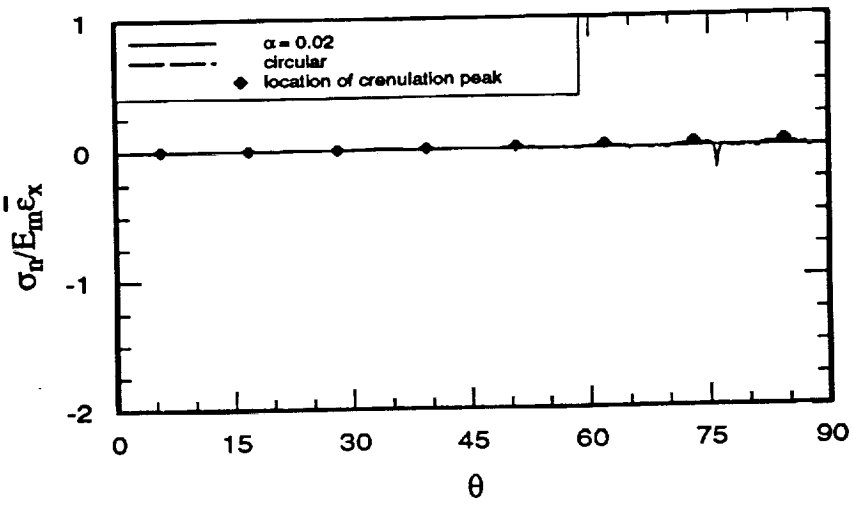

Figure 52. Interface Normal Stress Due to Transverse Strain for Fully Disbonded Crenulated Fiber, $\alpha = 0.02$, $\Delta = 10^{-5}$, $v_f = 60\%$

The deformed mesh for a crenulation amplitude $\alpha = 0.05$ with disbond gap $\Delta = 10^{-5}$ at 60% fiber volume fraction is shown in Figure 53. Here again only two regions of contact are seen, as Poisson's contraction of the matrix again causes the fiber and matrix to move apart in Region 1. The maximum contact stress in each region is shown in Table 3. Note the maximum stress is slightly higher in Region 2 for this case but is lower in Region 3 when compared with the 40% fiber volume fraction case.

The interface normal stress is shown in Figure 54. The relative magnitude of the peaks and the magnitude of the peaks relative to Figure 49, which shows the interface normal stresses at 40% fiber volume fraction, reflect the data of Table 3. Slight anomalous tensile normal stresses again appear in the locations of the crenulation peaks for $\theta > 45^{o}$.

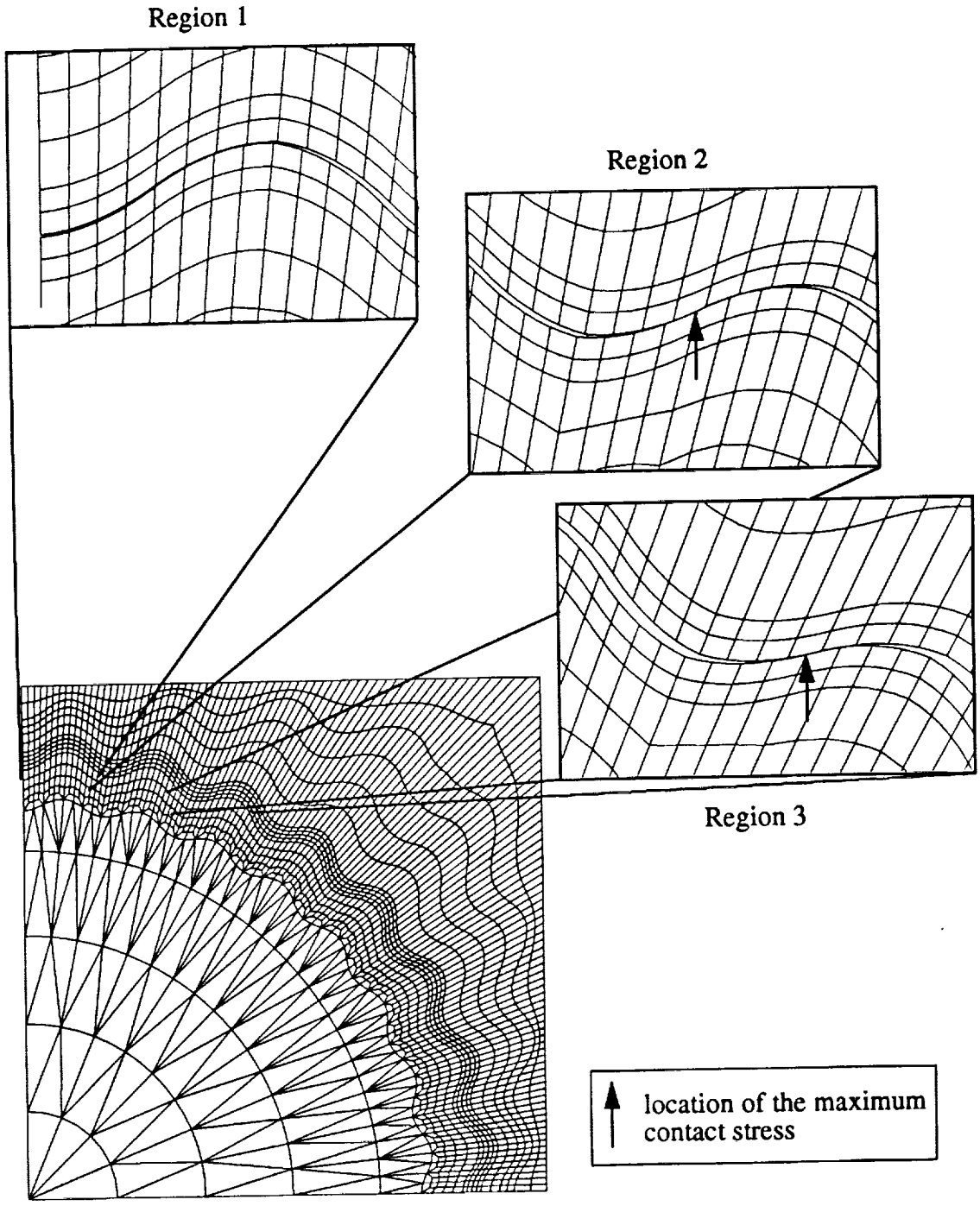

Figure 53. Deformed Mesh for Fully Disbonded Crenulated Fiber Case, $\alpha = 0.05$, $\Delta = 10^{-5}$, $v_f = 60\%$, Displacements in Contact Region scaled by Factor of 10

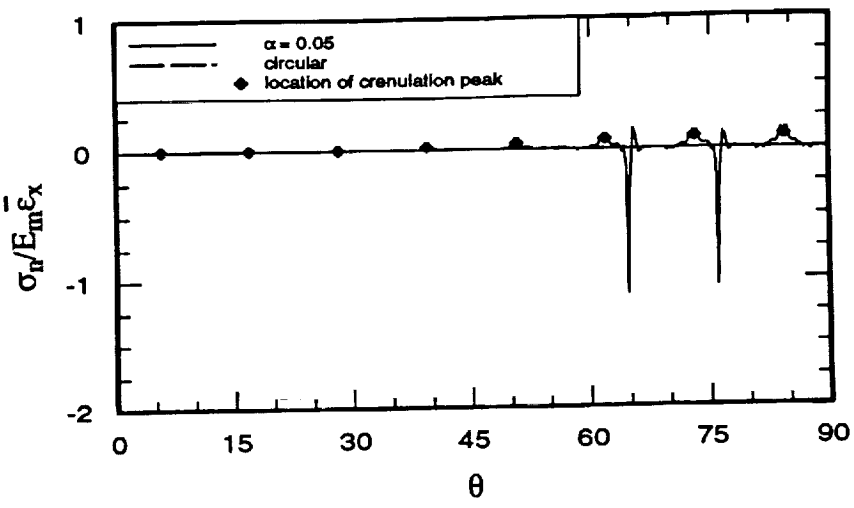

Figure 54. Interface Normal Stress Due to Transverse Strain for Fully Disbonded Crenulated Fiber, $\alpha = 0.05$, $\Delta = 10^{-5}$, $v_f = 60\%$

6.6 Effect of Decreasing Disbond Gap Size

The effect of decreasing the normalized gap size by an order of magnitude to $\Delta = 10^{-6}$ will now be discussed. As before, the circular fiber case at 40% fiber volume fraction is presented as a basis for comparison. All figures showing interface normal stresses are on the same scale as those presented for the larger disbond gap size so that the two may be readily compared. Interface tangential stresses will not be presented in the following cases as they are again identical to those for the no-fiber cases, except for slight variations which arise near points of fiber/matrix contact.

The deformed mesh for the circular fiber case at 40% fiber volume fraction with a disbond gap size $\Delta = 10^{-6}$ is shown in Figure 55. This figure is nearly identical to that for the larger disbond gap size shown in Figure 42. Contact between the fiber and the matrix occurs over

C-2

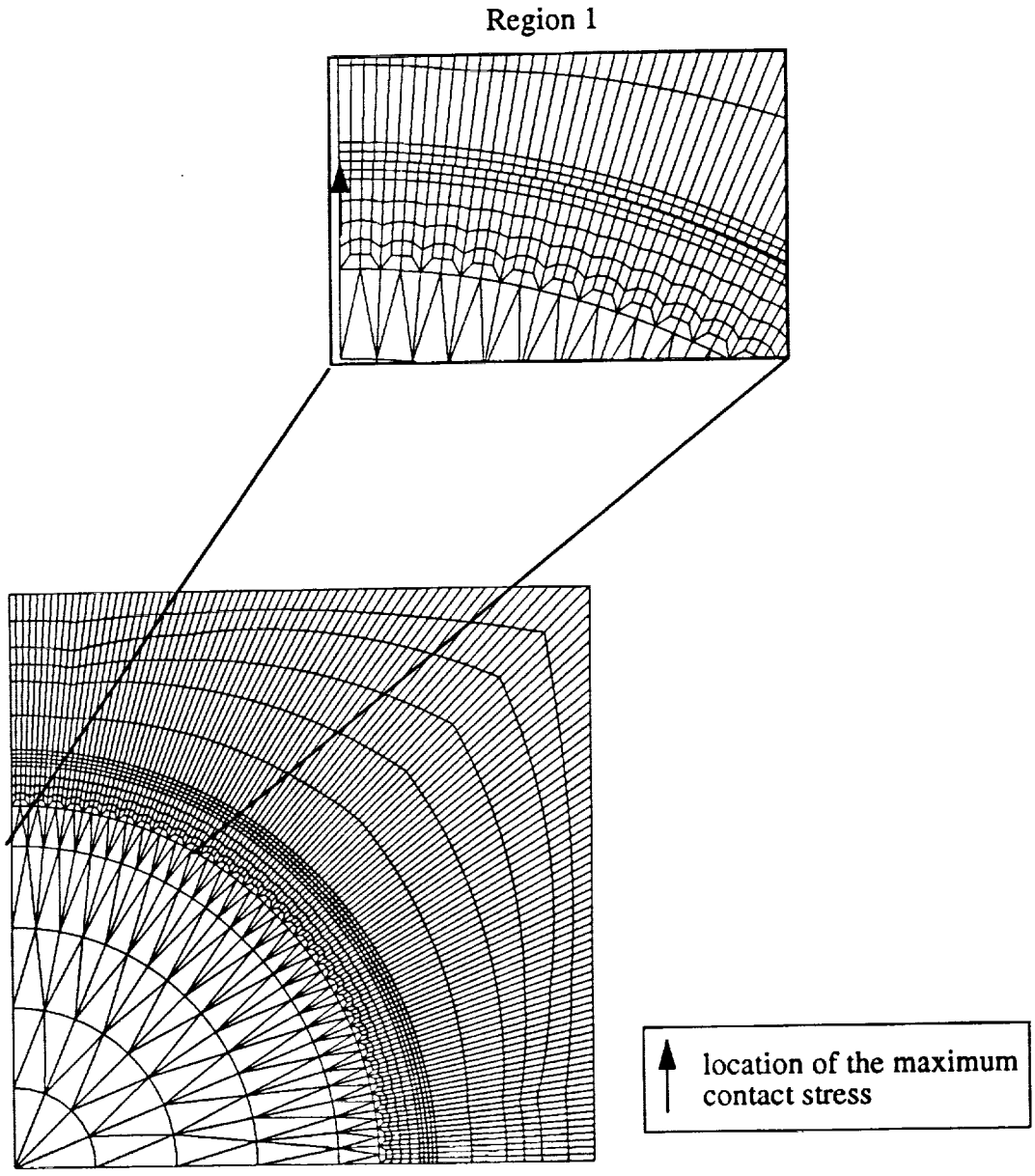

Figure 55. Deformed Mesh for Fully Disbonded Circular Fiber Case, $\Delta = 10^{-6}$, $v_f = 40\%$, Displacements in Contact Region Scaled by Factor of 10

nearly the same region. As shown in Table 3 the maximum contact stress over this region for the smaller disbond gap size is slightly larger than that in the previous case, as might be expected.

The interface normal stress for this case is shown in Figure 56. Careful comparison to Figure 43, which shows the interface normal stresses for the circular case with the larger disbond gap, reveals that compressive normal stresses for the case of the smaller gap size occur over a slightly larger range of θ and are slightly greater in magnitude.

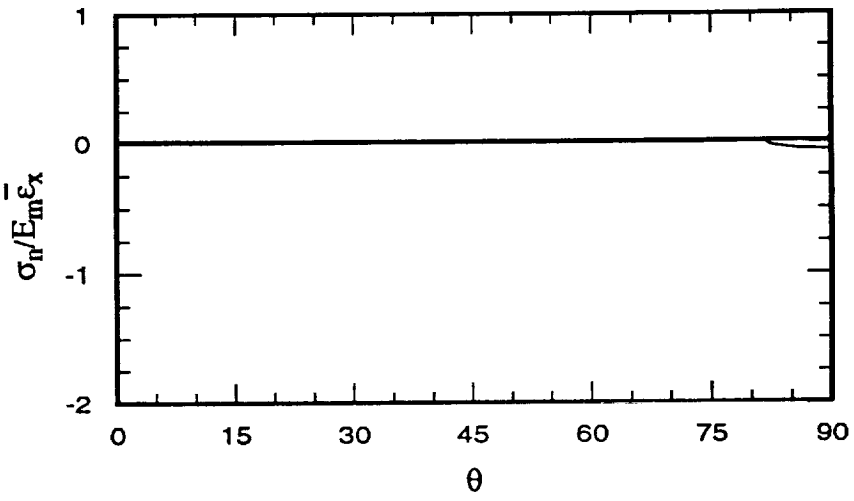

Figure 56. Interface Normal Stress Due to Transverse Strain for Fully Disbonded Circular Fiber, $\Delta = 10^{-6}$, $v_f = 40\%$

The effect of introducing fiber crenulation with an amplitude $\alpha = 0.02$ is shown in the deformed mesh in Figure 57. Two regions of fiber/matrix contact arise in this case, as was true at the larger disbond gap size. These regions are slightly larger in this case, however. The contact stresses shown in Table 3 which occur in these regions are larger than those that occur with the larger disbond gap size, as might be expected. The contact stress which

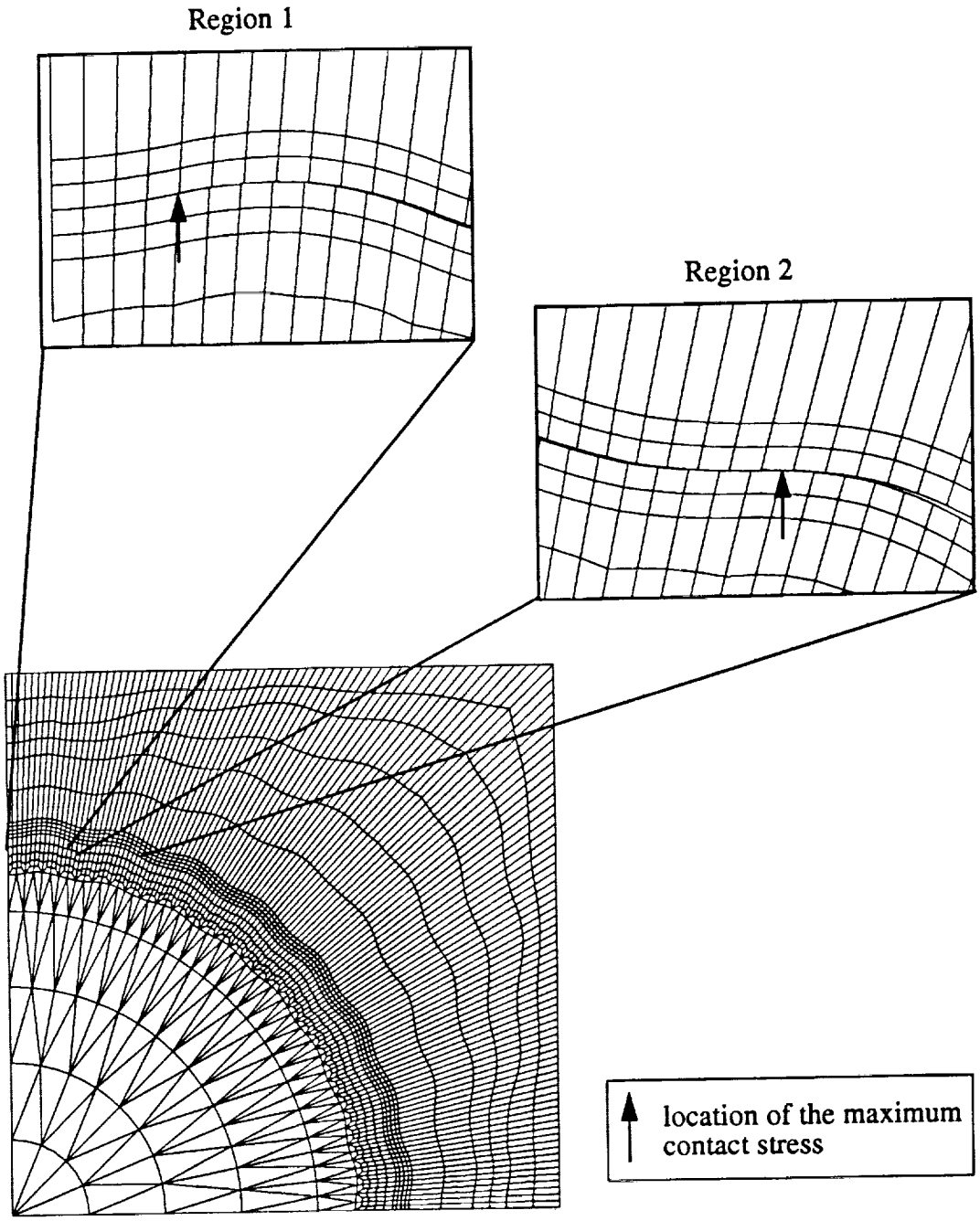

Figure 57. Deformed Mesh for Fully Disbonded Crenulated Fiber Case, $\alpha = 0.02$, $\Delta = 10^{-6}$, $v_f = 40\%$, Displacements in Contact Region Scaled by Factor of 10

occurs in Region 1 for this case, 846.2 psi, is more than twice that seen in the circular case with $\Delta = 10^{-6}$, and the overall maximum contact stress, 3606 psi, is an order of magnitude greater than that which occurs in the circular case. This occurs because, as in the past cases, the nature of contact with the crenulated fiber is one of interlocking where the matrix is trying to move past the fiber in the x direction. The nature of the contact with the circular fiber, however, consists of the matrix trying to move into the fiber in the y direction. Since the applied load is in the x direction, the former interference results in a higher contact stress. The interface normal stress about this mildly crenulated fiber for the disbond gap $\Delta = 10^{-6}$ is shown in Figure 58. The peaks in fiber crenulation again occur at θ locations that are lightly lower than the locations of fiber/matrix contact.

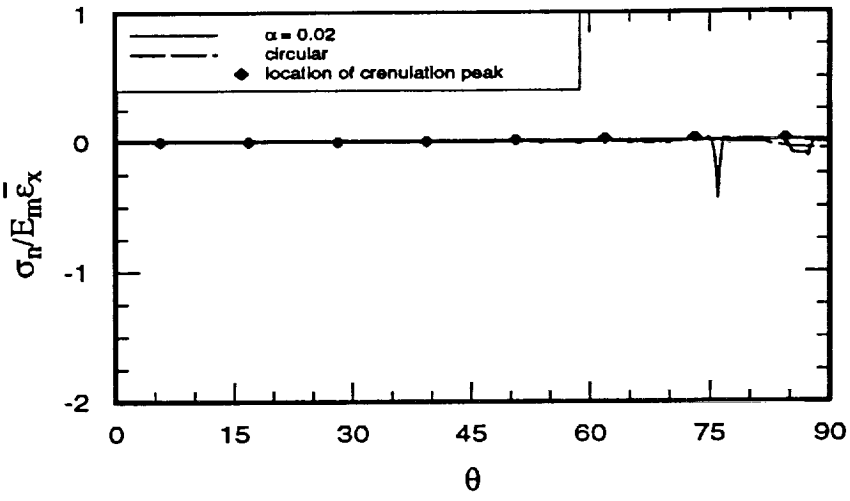

Figure 58. Interface Normal Stress Due to Transverse Strain for Fully Disbonded Crenulated Fiber, $\alpha = 0.02$, $\Delta = 10^{-6}$, $v_f = 40\%$

The deformed mesh for the case of the more deeply crenulated fiber at 40% fiber volume fraction with a disbond gap of $\Delta = 10^{-6}$ is shown in Figure 59. Three contact regions are again evident. These regions are slightly larger than those which occur with the larger dis-

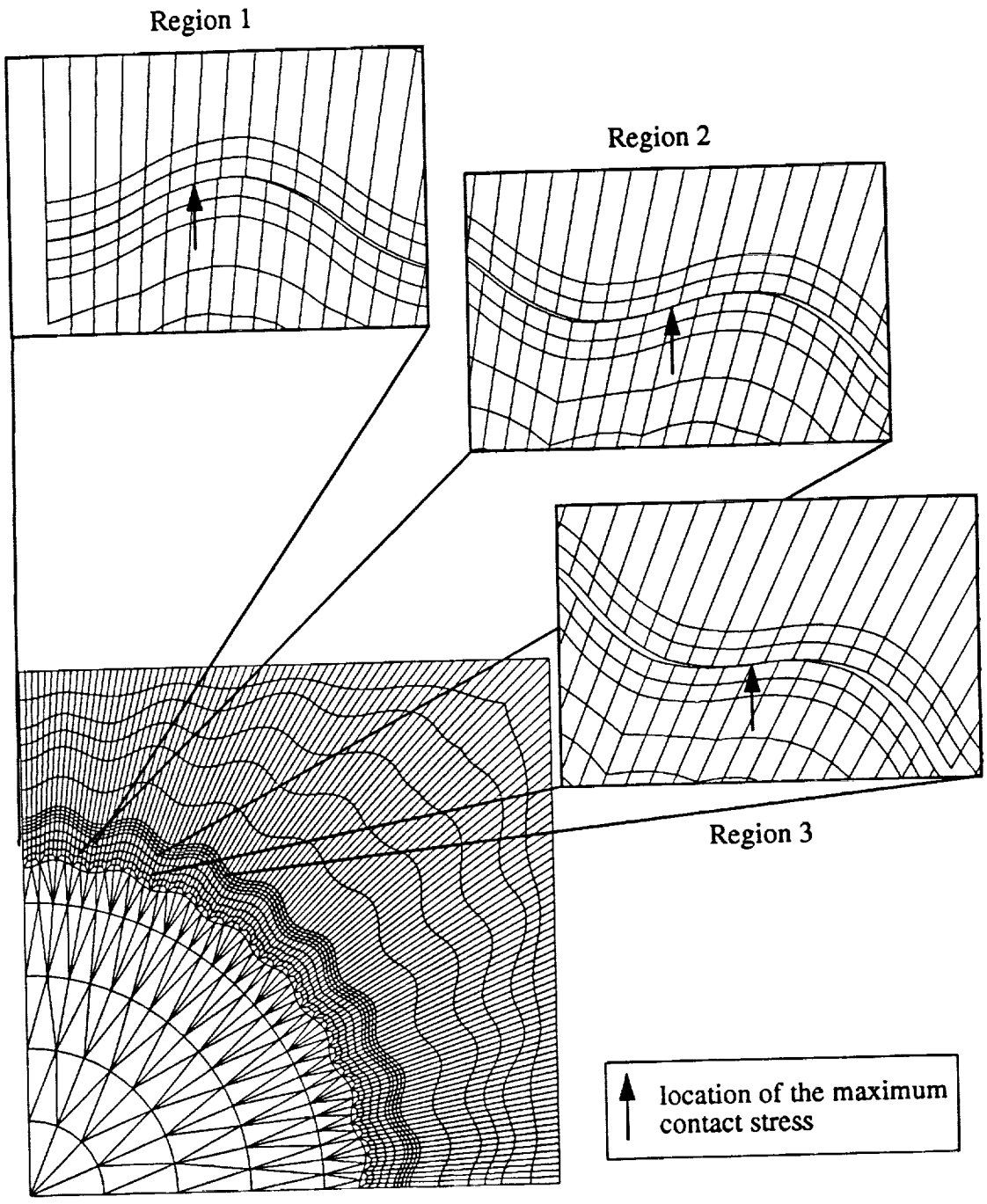

Figure 59. Deformed Mesh for Fully Disbonded Crenulated Fiber Case, $\alpha = 0.05$, $\Delta = 10^{-6}$, $v_f = 40\%$, Displacements in Contact Region Scaled by Factor of 10

bond gap size, Figure 48. Also, the contact stresses which occur in Regions 1 and 3, 584.1 and 9552 psi, respectively, are greater than those which occur in the corresponding regions with the larger disbond gap size. The contact stress which occurs in Region 2, 6774 psi, is slightly less, however, than that seen with the larger disbond gap size, as shown in Table 3. The interface normal stresses for this case are shown in Figure 60. The companion figure for the case of the larger disbond gap size is Figure 49.

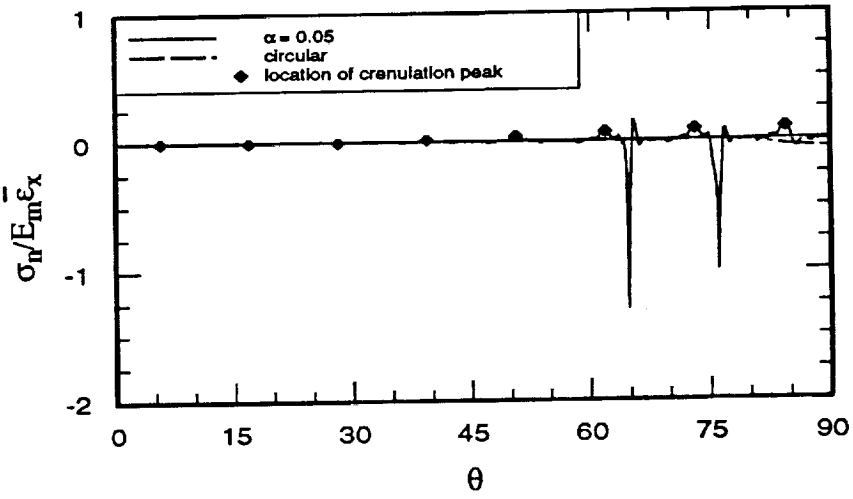

Figure 60. Interface Normal Stress Due to Transverse Strain for Fully Disbonded Crenulated Fiber, $\alpha = 0.05$, $\Delta = 10^{-6}$, $v_f = 40\%$

The deformed mesh for the circular fiber case with 60% fiber volume fraction with a disbond gap size $\Delta = 10^{-6}$ is shown in Figure 61. Once again only one region of contact between the fiber and the matrix is seen. This region is smaller in this case, however, than those seen for the previous circular fiber cases with 40% fiber volume fraction, Figures 42 and 55. Recall that the circular fiber case with 60% fiber volume fraction with $\Delta = 10^{-5}$ showed no fiber/matrix contact. As shown in Table 3, the maximum contact stress which arises in this region is much smaller than that which occurs at the lower fiber volume frac-

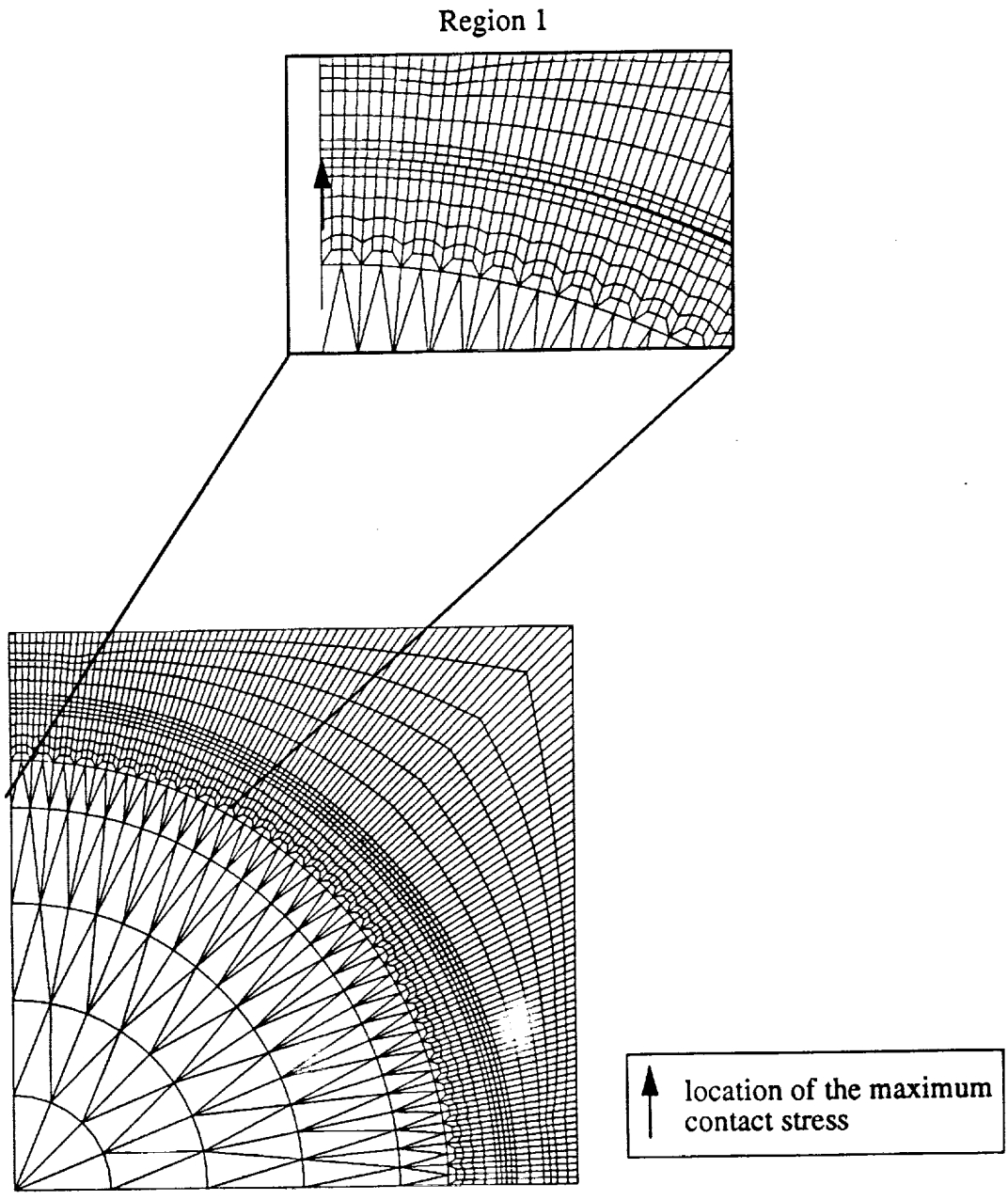

Figure 61. Deformed Mesh for Fully Disbonded Circular Fiber Case, $\Delta = 10^{-6}$, $v_f = 60\%$, Displacements in Contact Region Scaled by Factor of 10

tion with either disbond gap size.

The interface normal stress for this circular fiber case is shown in Figure 62. Compressive stresses which occur over the region of fiber/matrix contact in this case are so small that they are unnoticeable at the scale on which the figure is graphed.

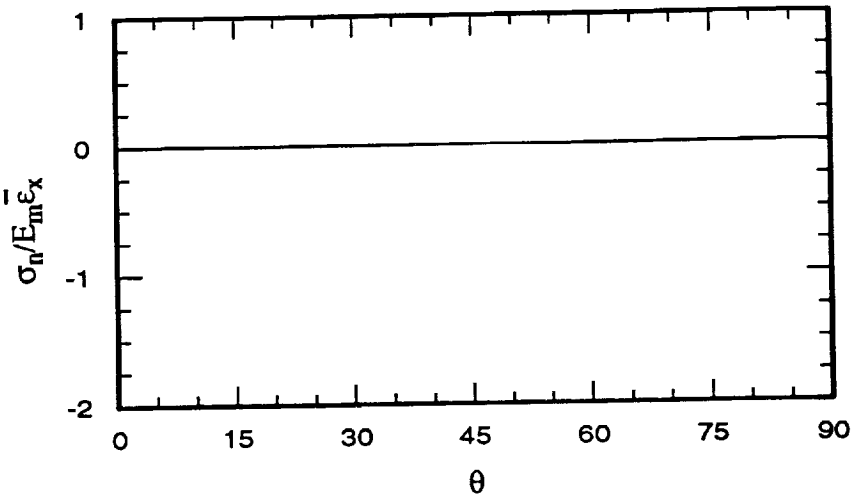

Figure 62. Interface Normal Stress Due to Transverse Strain for Fully Disbonded Circular Fiber, $\Delta = 10^{-6}$, $v_f = 60\%$

The deformed mesh for a fiber crenulation amplitude $\alpha = 0.02$ at 60% fiber volume fraction with $\Delta = 10^{-6}$ is shown in Figure 63. Two regions of fiber matrix contact are again seen. As shown in Table 3, the maximum contact stresses which arise in each region, 290.8 and 2145 psi, are smaller than those seen with this disbond gap size and the lower fiber volume fraction. These stresses are greater, however, than those which occur at 60% fiber volume fraction with the larger disbond gap size.

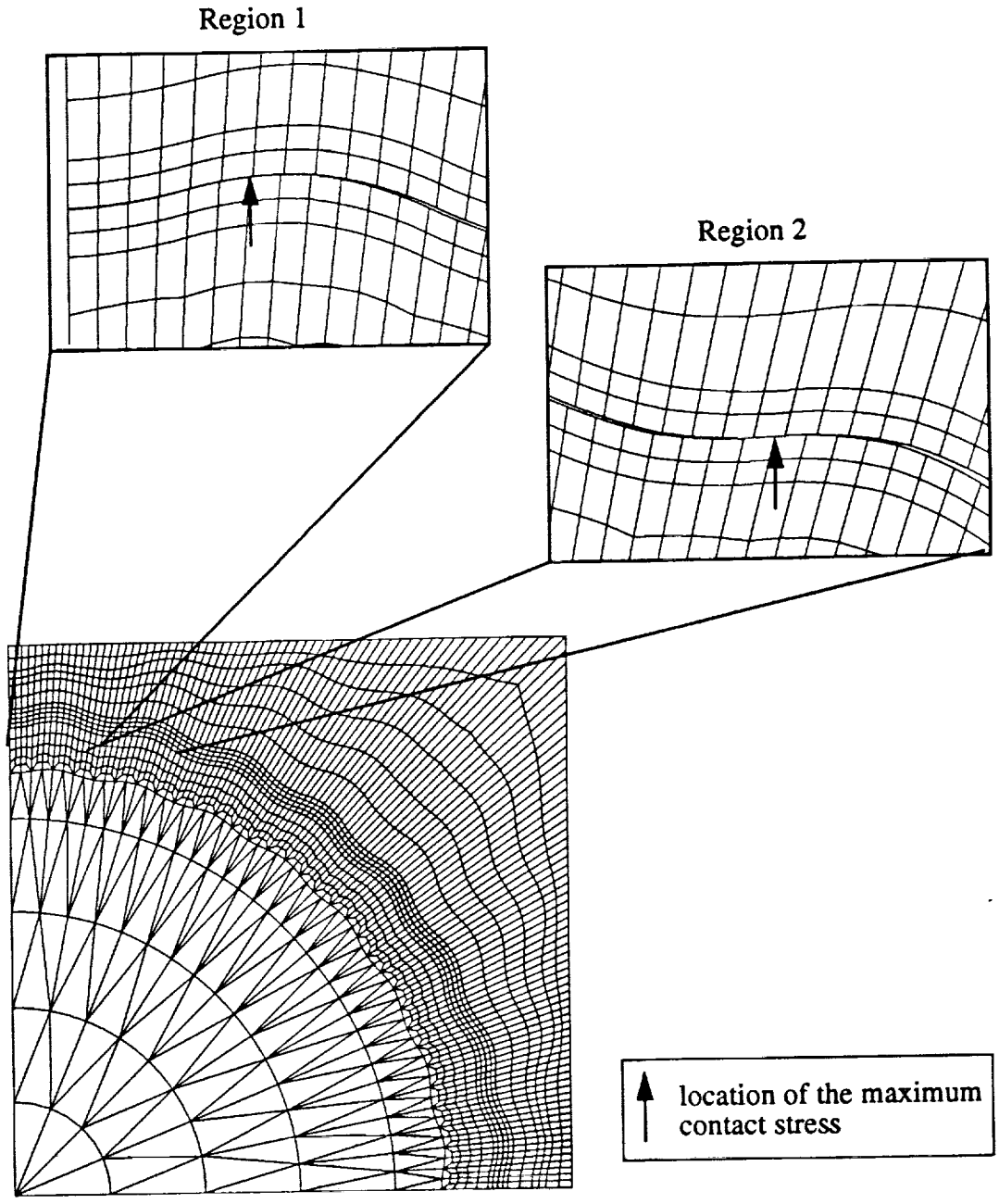

Figure 63. Deformed Mesh for Fully Disbonded Crenulated Fiber Case, $\alpha = 0.02$, $\Delta = 10^{-6}$, $v_f = 60\%$, Displacements in Contact Region Scaled by Factor of 10

The interface normal stress for $\alpha = 0.02$ with 60% fiber volume fraction with the smaller disbond gap size is shown in Figure 64. Compressive normal stresses here are smaller than those seen with 40% fiber volume fraction in Figure 58. These stresses are slightly greater in magnitude, however, than those seen for the corresponding case at 60% fiber volume fraction with the larger disbond gap size which was shown in Figure 52.

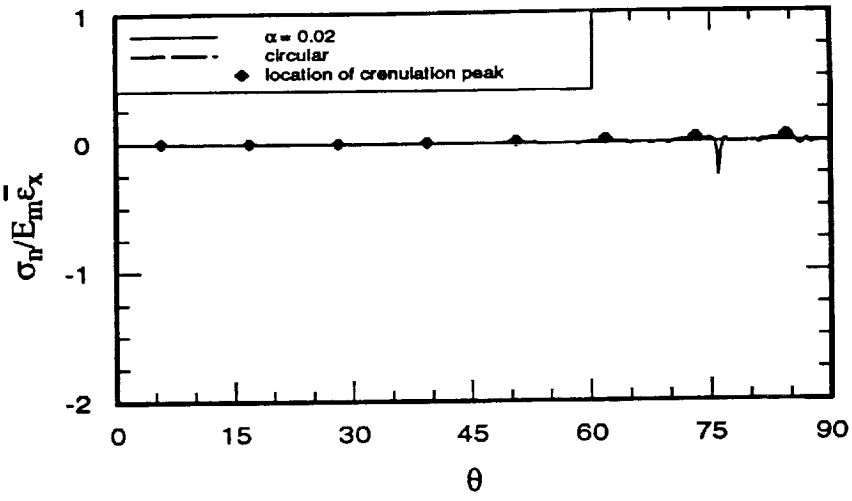

Figure 64. Interface Normal Stress Due to Transverse Strain for Fully Disbonded Crenulated Fiber, $\alpha = 0.02$, $\Delta = 10^{-6}$, $v_f = 60\%$

The deformed mesh for the case of $\alpha = 0.05$ with 60% fiber volume fraction with a disbond gap size $\Delta = 10^{-6}$ is shown in Figure 65. As was true at the higher fiber volume fraction with the larger disbond gap size, Poisson's contraction of the matrix causes the interface to open up near $\theta = 90^0$ and no contact occurs in Region 1. Contact stresses in Region 2 and 3, 7108 and 8334 psi, respectively, are greater than those seen at this fiber volume fraction and the larger disbond. When compared to the contact stresses at 40% fiber volume fraction with the same disbond gap size, the contact stress in Region 2 increases with increasing fiber volume fraction, while that in Region 3 decreases.

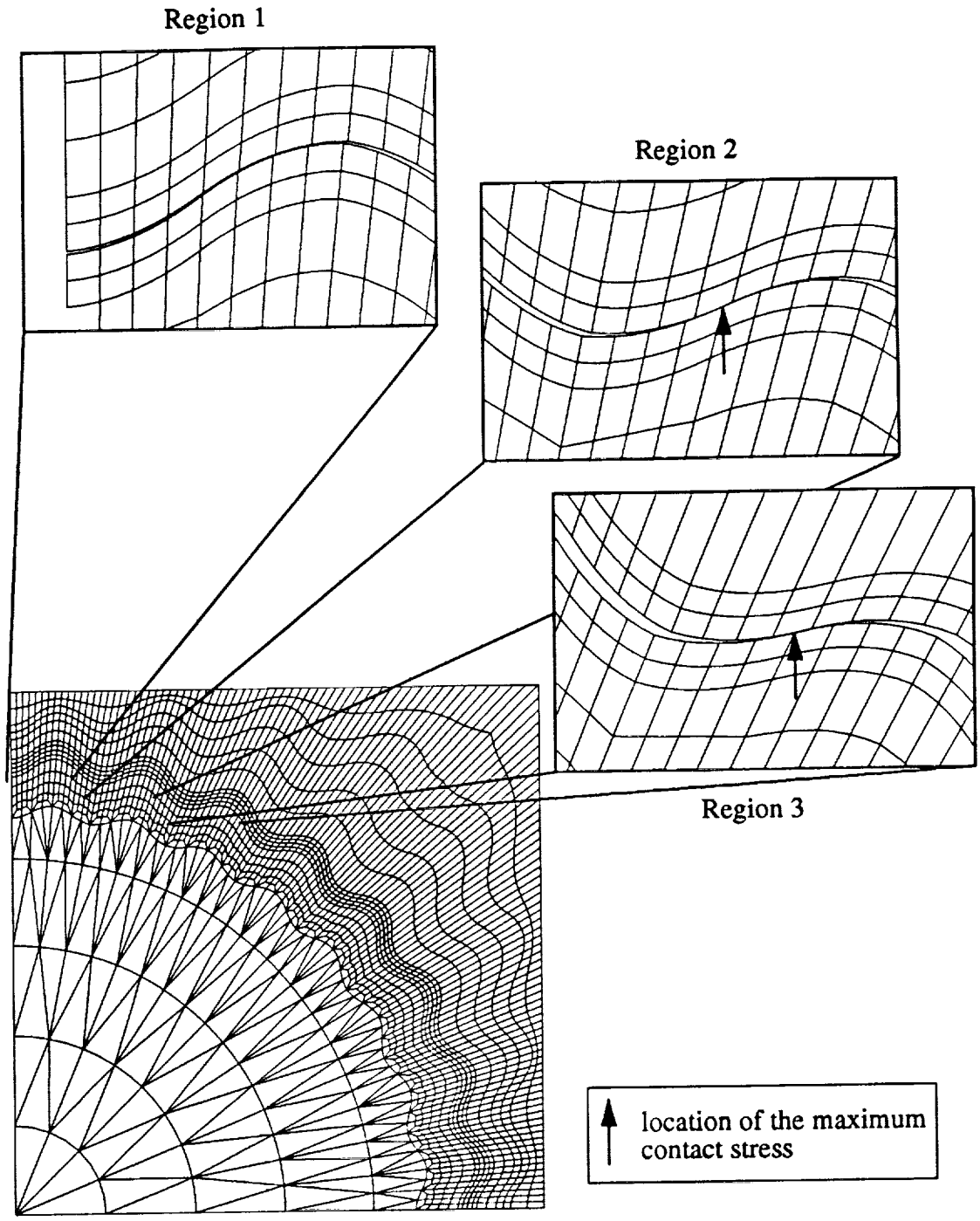

Figure 65. Deformed Mesh for Fully Disbonded Crenulated Fiber Case, $\alpha = 0.05$, $\Delta = 10^{-6}$, $v_f = 60\%$, Displacements in Contact Region Scaled by Factor of 10

The interface normal stress for this case is shown in Figure 66. The compressive stresses which occur near $\theta = 65^o$ in this case are larger than those seen with 40% fiber volume fraction with this same disbond gap size or with 60% fiber volume fraction at the larger disbond gap size. The compressive stress near $\theta = 75^o$ is slightly smaller in this case than at 40% fiber volume fraction and the same disbond gap size. Slight anomalous tensile normal stresses again appear in the locations of the crenulation peaks which occur at θ locations that are slightly smaller than the contact locations.

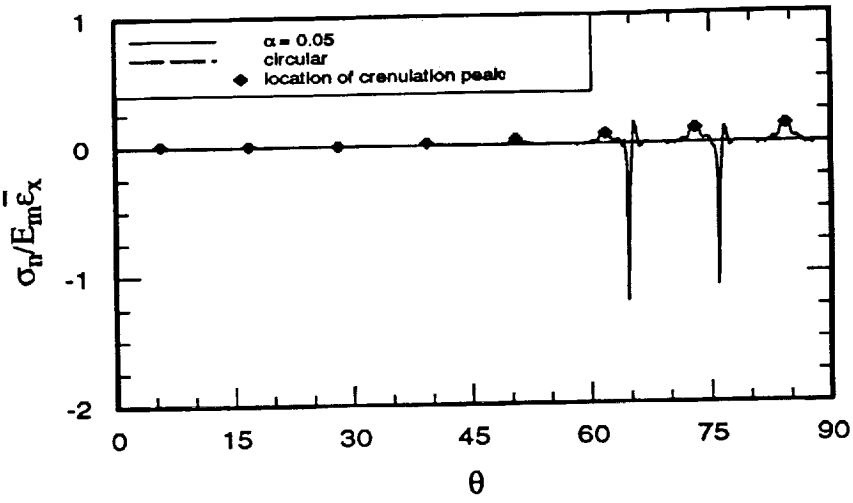

Figure 66. Interface Normal Stress Due to Transverse Strain for Fully Disbonded Crenulated Fiber, $\alpha = 0.05$, $\Delta = 10^{-6}$, $v_f = 60\%$

6.7 Discussion of Maximum Contact Stresses and Composite Properties: Fully Disbonded Case

The magnitudes of the maximum contact stresses for each disbond gap size are shown in Figure 67. Similar figures are not presented for the tangential stress component because they would appear identical to those shown in Figure 40 for the no-fiber case. As with all

previous cases, these figures show that maximum contact stress, σ_n^{max}, increases with increasing crenulation amplitude. For this fully disbonded case, however, stress variations decrease with increasing fiber volume fraction. Note, maximum variations in the normal stress here are much greater than those seen in the normal stress in the fully bonded case shown in Figure 35.

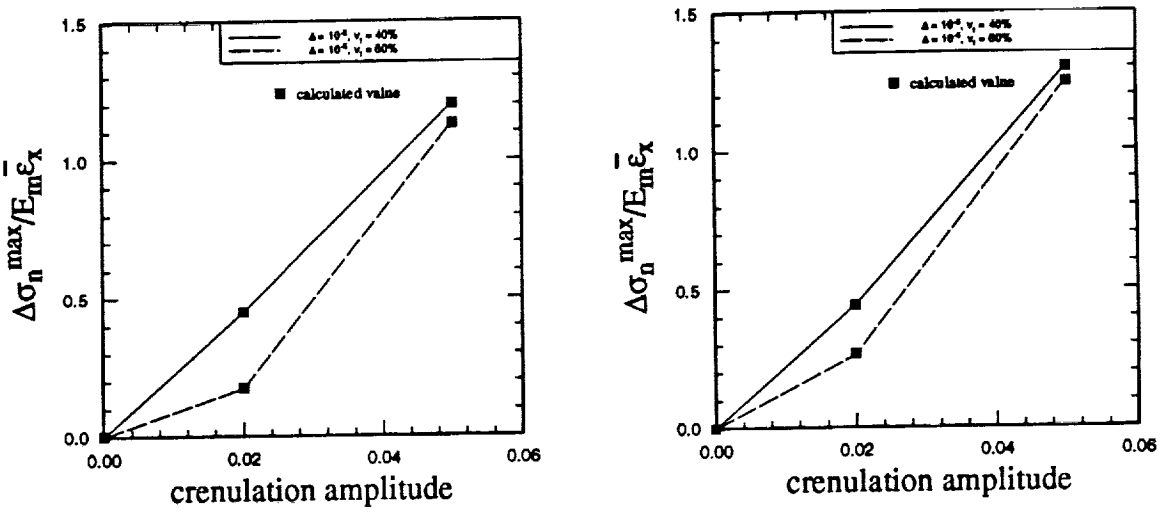

Figure 67. Maximum Contact Stresses Due to Transverse Strain for Fully Disbonded Case

The calculated composite properties for the fully disbonded case are given in Table 2 on page 57. Note, as the fiber and the matrix do not act together, the property ν_{xz} is undefined for the composite containing fully disbonded fibers. The remaining properties $\bar{E}_x$ and ν_{xy} vary only slightly with change in disbond gap size. Both properties also appear to be very close to those calculated for the no-fiber case and follow the same trends with changing fiber volume fraction and crenulation amplitude as in the no-fiber case.

This concludes the study of fiber/matrix interaction for the fully disbonded fiber. A great deal of new and interesting information has been discussed in this and the previous chap-

ters. Of particular value has been the illustrations of the fiber/matrix contact, showing both the degree of contact and the location of the contact around the circumference of the fiber. The following, and concluding, chapter summarizes the important findings of this study, and presents recommendations for future research directions.

7.0 Conclusions and Recommendations for Future Work

As stated in Chapter 1, the major motivation for this study of noncircular fibers was to investigate potential increases in the transverse properties of carbon/carbon composites. These properties are, in general, low due to poor fiber/matrix bonding. In the preceding chapters, much information has been presented concerning the interface stress states in composites containing crenulated fibers subjected to a temperature decrease, and to a transverse strain. Conclusions, which are drawn from this information, regarding the effect these fibers have on the transverse composite properties are presented in this chapter. Additional directions of investigation related to the problem set forth in this study, which could provide further insight into the effect of noncircular fibers on composite behavior, are also suggested in the final section of this work.

7.1 Conclusions

Although two different loading conditions and various degrees of bond and disbond have been discussed, several general conclusions concerning the effects the crenulated fibers have on stress states in the composite can be drawn from all cases. First, all cases considered show that a significant difference exists between the stress state at the circular fiber

interface and the stress state at the crenulated fiber interface. This has been shown to be true regardless of fiber volume fraction, amplitude of crenulation, degree of disbond, etc. Although, as noted previously, some of these differences result from the transformation of the stress at the crenulated interface, their significance must not be overlooked.

All of the cases considered in this work also show that increasing the fiber crenulation amplitude from $\alpha = 0.0$ (circular) to $\alpha = 0.05$ results in an increase in the variation of the interface stresses relative to the circular interface stress level. These variations in several cases become large enough that sign changes occur in the stress components that do not occur at the circular interface. Because of these variations, the introduction of crenulation for each loading case results in larger maximum stresses and lower minimum stresses than those found at the circular interface. In most cases, these maxima and minima also occur at different θ locations than the maxima and minima in the corresponding circular fiber cases. Of particular importance is that the variations, which result from the fiber crenulation, lead to high stress concentrations in the crenulated cases which are not present at the circular fiber interface.

The high stress concentrations are most evident in the tangential stress component in the matrix in each case considered. Recall, Figures 22 and 35 show that the variations in the matrix tangential stress for the fully bonded case due to both temperature change and transverse strain are more than double those seen in the other stress components. For the no-fiber and fully disbonded cases, Figure 40, the variations in the matrix tangential stress are even larger than for the fully bonded cases, as little or no stress is transferred to the fiber in the form of a shear or normal interface stress component. These large positive tangential stresses can result in cracking and tearing of the matrix material at the interface. Thus, they can seriously reduce the strength of the composite as a whole.

Increases in the fiber volume fraction also cause increases in the variations of the interface stresses relative to the circular stress levels in all the fully bonded cases and in the no-fiber case. This is not true, however, for the interface normal stress in the fully disbonded cases. In this instance, increasing the fiber volume fraction causes the normal stress variations to decrease, as shown in Figure 67. This is a result, as explained earlier, of the Poisson's contraction of the matrix material.

Several other factors about the fully disbonded case are of particular interest. Recall, it was stated that, with the noncircular fibers, mechanical interlocking of the fiber and the matrix could serve to increase the transverse composite properties. As seen in the previous chapter, this mechanical interlocking does take place. Examination of the transverse composite modulus $\overline{E}_x$ in Table 2, however, shows that the effect this interlocking has on the composite properties does not result in increased composite stiffness. In fact, $\overline{E}_x$ decreases in all cases as the fiber crenulation amplitude is increased.

Another point of interest concerning the fully disbonded fiber cases is that the maximum variation in the contact stress at the interface in these cases, Figure 67, is nearly as large as that seen in the matrix tangential stress component. Recall that as crenulation amplitude is increased, the location of the most severe contact is moved away from $\theta = 90^o$ and the contact stresses increase greatly. The contact stresses lead to large peaks or "spikes" in the normal stresses in the regions of most severe fiber/matrix contact. Decreasing the disbond gap size, as expected, results in increases in these large contact stresses. Crushing and cracking of the matrix or fiber material at the locations of these severe stresses again could serve to weaken the overall composite.

In summary, the evidence from the cases presented in this work suggests that, although

interlocking between the fiber and the matrix does occur when fiber crenulation is present, serious stress concentrations also result at the noncircular interface. These stress concentrations can result in a weakening of the composite which could far outweigh any possible advantage to the interlocking effect. For the cases considered, a temperature change ΔT = -1.0 ^{o}F and a transverse strain $\bar{\varepsilon}_x$ = 1000 μin/in with both fully bonded and fully disbonded fibers, the use of crenulated fibers therefore, appears to offer no advantage over the use of circular fibers.

As noted previously, the actual bonding in a carbon/carbon composite is somewhere between the fully disbonded and fully bonded cases considered here. Also, many of the assumptions inherent with this analysis can cause the stresses presented here to differ from those that would be seen in an actual composite under the same loading conditions. These assumptions include the transverse isotropy of the fiber, the full isotropy matrix, and the frictionless contact surface at the interface. In order to obtain a truer picture of the behavior of a crenulated carbon fiber in a carbon matrix, additional analyses must be carried out. Suggestions of directions that these analyses might follow are contained in the next, and final, section of this work.

7.2 Suggestions for Future Work

One of the assumptions used in this analysis is that the fiber is considered transversely isotropic in the x-y plane and the matrix is considered fully isotropic. In actuality both of these materials are fully orthotropic. In particular, it has been shown that the graphitic layers which form in the matrix material which lies closest to the fiber tend to align with the fiber. In the case of a crenulated fiber, these graphitic layers would bend and kink along the

crenulation, causing the matrix material properties closest to the interface to vary greatly from those in the bulk matrix material, where the graphitic sheets have a more random orientation. Also, graphitic layers within carbon fibers have been shown to form various ordered orientations. Depending on processing conditions, these graphitic layers may be arranged radially or circumferentially or with some degree of mixing of these two orientations. The orientation of the layers, of course, affects the fiber material properties in the x-y plane. To more accurately model the carbon fiber and matrix, the properties of each material must be considered to be location dependent.

The actual degree of disbond in a carbon/carbon composite has been assumed in this study to lie between the fully bonded and fully disbonded cases presented here. In order to represent the actual degree of bonding in the composite, a scheme for modeling partial disbonding must be devised. Complications arise in this case in deciding the degree, geometry, and number of disbonds to be modeled. In order to create a unit cell of workable size, the mathematical models must have some degree of symmetry. Disbonding in true carbon/carbon is by nature completely random, so that some sort of probabilistic modeling procedure would be required for complete understanding of the partially disbonded composite. The accuracy of such schemes must rely in part on the model size chosen, and the amount of computation time allowed, which will be significant even for limited variation of the random variables.

Another limitation of this analysis is that only two fiber volume fractions and two degrees of fiber crenulation were considered. The values chosen for these parameters in this study are considered to best represent composites which are in the range which is readily modeled and manufactured. Additional values of these parameters could, of course, be considered. However, it is felt that the work presented here establishes the trends one might

expect from changes in these two parameters. The effects of changing the parameter m, which controls the frequency of fiber crenulation, was not examined in this analysis and could be of interest. Difficulties would certainly arise in both modeling and manufacturing the fiber, however, if a higher value of this parameter than that chosen for this analysis were of interest. In addition to changes in the above parameters, the material properties used in this analysis could be easily changed if effects of fiber crenulation on a material other than carbon/carbon were of interest.

As stated in Chapter 1, fiber shapes other than the crenulated geometry have been manufactured. These shapes include the C-shaped fiber and the trilobal-shaped fiber. Analyses similar to those presented in this work for either of these fiber shapes could be of interest. The crenulated fiber was chosen, however, due to its high degree of symmetry. A larger unit cell, larger finite element mesh, and therefore, longer computation time would most likely be involved in modeling either of these other two shapes, as they both have a much lower degree of symmetry.

Finally it should be noted that the results presented in this work are purely analytical. The comparison of the findings of this study to experimental data gained from the testing of carbon/carbon composites containing actual crenulated fibers is of course desirable. To date information of this nature is not available. In addition, a microscopic study of the structure of such a composite could be useful in future work in determining the actual degree of disbond which occurs in such materials, and the variation of the material properties in the fiber and matrix near the interface.

References

Aboudi, J., 1987, "Damage in composites - modeling of imperfect bonding", *Composites Science and Technology*, 28 pp. 103-128.

Aboudi, J., 1989, "Micromechanical analysis of composites by the method of cells", *Applied Mechanics Reviews*, 42 (no. 7) pp. 193-221.

Achenbach, J. D. and Zhu, H., 1989, "Effect of interfacial zone on mechanical behavior and failure of fiber-reinforced composites", *Journal of Mechanics and Physics of Solids*, 37 (no. 3) pp. 381-393.

Adams, D. F., 1975, "Transverse tensile and longitudinal shear behavior of unidirectional carbon-carbon", *Materials Science and Engineering*, 17 pp. 139-158.

Adams, D. F., 1987, "A micromechanics analysis of the influence of the interface on the performance of polymer-matrix composites", *Journal of Reinforced Plastics and Composites*, 6 pp. 66-88.

Adams, D. F. and Crane, D. A., 1984, "Finite element micromechanical analysis of a unidirectional composite including longitudinal shear loading", *Computers and Structures*, 18 (no. 6) pp.1153-1165.

Adams, D. F. and Doner, D. R., 1967, "Transverse normal loading of a unidirectional composite", *Journal of Composite Materials*, 1 pp. 152-164.

Amoco Performance Products, Inc., 1989, Thornel Product Information.

Bowles, D. E., 1990, "Micromechanics analysis of space simulated thermal deformations and stresses in continuous fiber reinforced composites", *NASA Technical Memorandum 102633*.

Chamis, C. C., 1984, "Simplified composite micromechanics equations for hygral, thermal, and mechanical properties", *SAMPE Quarterly*, 15 (no. 3) pp. 14-23.

Chamis, C. C., 1987, "Simplified composite micromechanics for predicting microstresses", *Journal of Reinforced Plastics and Composites*, 6 pp. 268-289.

Dean, G. D. and Turner, P., 1973, "The elastic properties of carbon fibres and their composites", *Composites*, 4 (no. 4) pp. 174-180.

Dieffendorf, R. J. and Torkarsky, E., 1975, "High-performance carbon fibers", *Polymer Engineering and Science*, 15 (no. 3) pp. 150-159.

Edie, D. D., Fox, N. K., Barnett, B. C., and Fain, C. C., 1986, "Melt-spun non-circular car-

bon fibers", *Carbon*, 24 (no. 4) pp. 477-482.

Edie, D. D., Hayes, G. J., Rast, H. E., and Fain, C. C., 1990, "Processing of noncircular pitch-based carbon fibers", *High Temperature - High Pressure*, 22 pp.289-298.

Edie, D. D., and Stoner, E. G., 1992, "Effect of microstructure and shape on carbon fiber properties", *NASA Reference Publication 1254*, pp. 41-70.

Harrison, M. G., Fain, C. C., and Edie, D. D., 1986, "*International Conference, Carbon '86*", Bad Honnef, FRG: Deutche Keramische Gesellschaft, pp. 77-81.

Kriz, R. D. and Ledbetter, H. M, 1985, "Elastic representation surfaces of unidirectional graphite/epoxy composites", *ASTM STP 864*, pp. 661-676.

Kriz, R. D. and Stinchcomb, W. W., 1979, "Elastic moduli of transversely isotropic graphite fibers and their composites", *Experimental Mechanics*, 19 (no. 2) pp. 41-49.

Maahs, H. G., 1990, personal notes.

Manocha, L. M., Bahl, O. P., and Singh, Y. K., 1989, "Fiber/matrix interface in carbon/carbon composites - effect of surface morphology of carbon fibers", *Tanso*, 140 pp. 255-260.

Nimmer, R. P., Bankert, R. J., Russell, E. S., Smith, G. A., and Wright, P. K., 1991, "Micromechanical modeling of fiber/matrix interface effects in transversely loaded SiC/Ti-6-4 metal matrix composites", *Journal of Composites Technology and Research*, 13

(no. 1) pp. 3-13.

Perry, J. C. and Adams, D. F., 1974, "An experimental study of carbon-carbon composite materials", *Journal of Materials Science*, 9 pp. 1764-1774.

Rhee, B., 1990, "New developments with pitch-based carbon fibers", *High Temperature - High Pressure*, 22 pp. 267-274.

Rozploch, f. and Marciniak, W., 1986, "Radial thermal expansion of carbon fibers", *High Temperature - High Pressure*, 18 pp. 585-587.

Schmidt, D. L., 1972, "Carbon/carbon materials", *SAMPE Journal*, 8 (no. 3) pp. 9-19.

Smith, R. E., 1972, "Ultrasonic elastic constants of carbon fibers and their composites", *Journal of Applied Physics*, 43 (no. 6) pp. 2555-2561.

Stoner, E. G., Edie, D. D., and Kennedy, J. M., 1990, "Mechanical properties of noncircular pitch-based carbon fibers", *High Temperature - High Pressure*, 22 pp. 299-308.

Sullivan, B. J., Cassin, T. G., and Rosen, B. W., 1990, "Micromechanical analysis of unidirectional composites with unique fiber geometries and fiber/matrix interface conditions", *Proceedings of the American Society for Composites Fifth Technical Conference*, pp. 144-153, Technomic Publishing Co., Inc., Lancaster, PA.

Takahashi, K. and Chou, T., 1988, "Transverse elastic moduli of unidirectional fiber composites with interfacial debonding", *Metallurgical Transactions*, 19A pp. 129-135.

BIBLIOGRAPHIC DATA SHEET	1. Report No. CCMS-93-01, VPI-E-93-01	2.	3. Recipient's Accession No.
4. Title and Subtitle Micromechanics of Crenulated Fibers in Carbon/Carbon Composites			5. Report Date January 1993 6.
7. Author(s) E.E. Carapella, M.W. Hyer, O.H. Griffin, Jr., and H.G. Maahs			8. Performing Organization Rept. No. VPI-E-93-01, CCMS-93-01
9. Performing Organization Name and Address Virginia Polytechnic Institute and State University Department of Engineering Science and Mechanics Blacksburg, VA 24061-0219			10. Project/Task/Work Unit No. 11. Contract/Grant No. NAG-1-343
12. Sponsoring Organization Name and Address Applied Materials Branch National Aeronautics and Space Administration Langley Research Center Hampton, VA 23681-0001			13. Type of Report & Period Covered Interim Report 92 January 1, 1990 - December 31, 1992 14.

15. Supplementary Notes

This report constitutes the Masters thesis in Engineering Mechanics of the first author. The second and third authors are on the faculty of Virginia Polytechnic Institute and State University, while the fourth author is the Branch Head of the Applied Materials Branch of NASA-Langley Research Center.

16. Abstract

The influence of crenulated noncircular fibers on the micromechanical stress states due to a transverse strain and to a temperature change in carbon/carbon composites is examined using the finite element method. Stresses at the interface of both fully bonded and fully disbonded fibers having two crenulation amplitudes and with two fiber volume fractions are presented. In each case, these interface stresses are compared to stresses at the interface of circular fibers which have the same degree of disbond and fiber volume fraction and are under the same loading conditions. For the disbonded cases, deformed meshes showing locations of fiber/matrix contact are also included. In addition to the interface stress states, selected composite properties are also computed and compared for each case examined. Interest in studying noncircular fibers stems from a desire to increase the transverse properties of carbon/carbon by introducing a mechanical interlocking between the fiber and the matrix. Results presented here indicate that this interlocking does in fact occur. Evidence from the interface stress data suggests, however, that any possible advantage of this interlocking may be outweighed by the disadvantage of stress concentrations which arise at the interface due to the crenulated geometry of the fibers.

17. Key Words and Document Analysis. 17a. Descriptors

Carbon/carbon composite materials, micromechanics, noncircular fibers

17b. Identifiers/Open-Ended Terms

17c. COSATI Field/Group

18. Availability Statement	19. Security Class (This Report) UNCLASSIFIED	21. No. of Pages 121
	20. Security Class (This Page) UNCLASSIFIED	22. Price

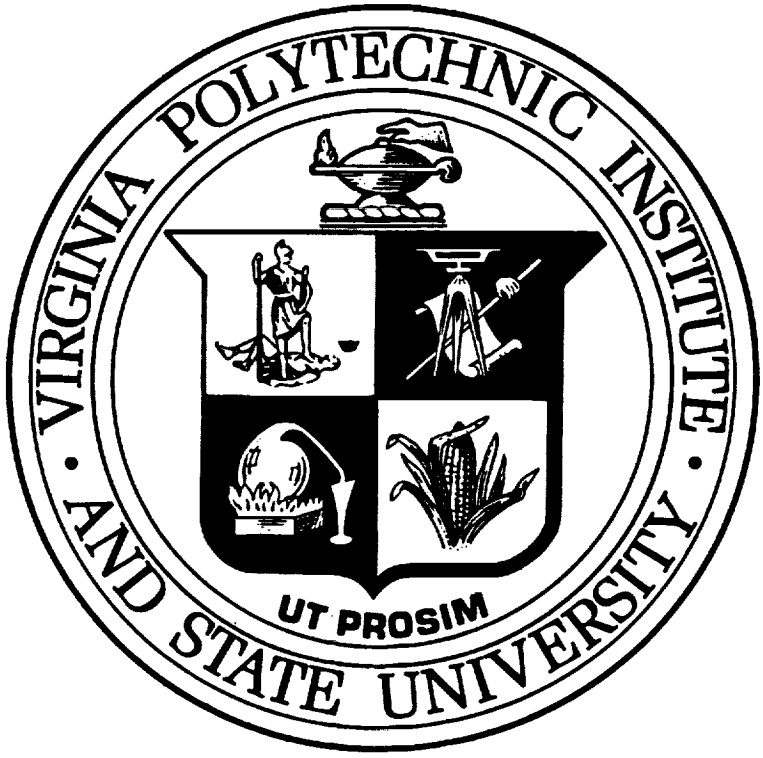

VIRGINIA TECH CENTER FOR COMPOSITE MATERIALS AND STRUCTURES

201 HANCOCK HALL, BLACKSBURG, VA 24061-0257 PHONE: (703) 231-4969 FAX: (703) 231-9452

The Center for Composite Materials and Structures (CCMS) is a supporting and coordinating organization for composite materials research and educational programs at Virginia Tech. The Center is designed to encourage and promote continued advances in the science and technology of composite materials and structures and to enhance the transfer and utilization of these new developments in industries and government organizations in Virginia, the nation, and the world.

The CCMS functions through an annually elected Administrative Board and a Director who is elected for a three-year term. Members of the Center include 46 faculty members in 11 academic departments in the College of Engineering and College of Arts and Sciences; 14 associate members; five technical staff members; approximately 130 graduate students; nine Industrial Affiliates representing a variety of composite materials interests at the national level; and government and industrial Research Sponsors currently supporting more than 55 research grants and contracts exceeding $7 million annually on composite materials and structures.

Specific objectives of the CCMS under this program include:

- providing a formal, interdisciplinary partnership between faculty, technical staff, and students who have active and complementary interests in composite materials and structures;
- providing leadership and coordination to enhance development and promote general success of research and educational activities in composite materials by shared responsibility, cooperative action, interdisciplinary support, and unified service;
- providing a means for the Virginia Tech composite materials and structures program to interact with university, state, national and international agencies, organizations, and industries; and
- promoting continued national and international recognition of the excellence in educational and research programs in composite materials and structures at Virginia Tech.

The CCMS has developed and operates a Composites Fabrication Laboratory to provide composite material fabrication capabilities. This facility is also available for conducting basic and applied research in composite processing and manufacturing. The Laboratory supports the educational and research programs of its membership. It also provides technical assistance to various research programs.

The educational mission of the CCMS is conducted by its members, in concert with the academic departments, at the undergraduate and graduate levels. This mission prepares students for careers in composites research, development, and application. More than 250 graduates of the Virginia Tech composites program have joined industries, government agencies, and universities. These individuals have provided significant advances to the science and technology of composite materials, and have attained positions of national leadership in the field.

The comprehensive research programs of the CCMS members cover the full range of composites science and technology. This includes the development and fabrication of new, improved constituents and material systems to the design and analysis of optimized composite components and structures. The most recent composites research accomplishments are reported in CCMS member's authored refereed papers and technical reports.

In addition to the CCMS Report Series, the CCMS administers:

- a vigorous Seminar Series featuring prominent speakers from leading laboratories and companies around the world, as well as CCMS students and faculty members;
- an Administrative Database to manage general information about the CCMS faculty and students, seminars, reports, alumni, company contacts, and Industrial Affiliates;
- a sesquiannual Technical Review/Workshop with the Center for Adhesive and Sealant Science; and
- the CCMS Bulletin, a bi-monthly newsletter of current events, notices, research opportunity announcements, and technical interest articles.

MEMBERS OF THE CENTER

Aerospace and Ocean Engineering

Raphael T. Haftka
Eric R. Johnson
Rakesh K. Kapania

Chemical Engineering

Donald G. Baird
Richey M. Davis
Garth L. Wilkes

Chemistry

John G. Dillard
James E. McGrath
Thomas C. Ward
James P. Wightman

Civil Engineering

Richard M. Barker
Richard E. Weyers

Electrical Engineering

Ioannis M. Besieris
Richard O. Claus
Douglas K. Lindner

Engineering Fundamentals

Deidre A. Hirschfeld

Engineering Science and Mechanics

David A. Dillard
John C. Duke, Jr.
Daniel Frederick
O. Hayden Griffin, Jr.
Zafer Gürdal

Engineering Science and Mechanics (continued)

Robert A. Heller
Edmund G. Henneke, II
Michael W. Hyer
Robert M. Jones
Ronald D. Kriz
Liviu Librescu
Alfred C. Loos
Don H. Morris
John Morton
Ali H. Nayfeh
J. N. Reddy
Kenneth L. Reifsnider
C. W. Smith
Wayne W. Stinchcomb
Surot Thangjitham

Industrial and Systems Engineering

Joel A. Nachlas

Materials Science & Engineering

Seshu B. Desu
D. P. H. Hasselman
Robert W. Hendricks
Ronald G. Kander

Mathematics

Werner E. Kohler

Mechanical Engineering

Charles J. Hurst
Charles E. Knight
Craig A. Rogers
Curtis H. Stern